METABOLIC PROFILING OF MESENCHYMAL STROMAL CELLS FOR CRITICAL QUALITY ATTRIBUTE IDENTIFICATION

by

TIMOTHY SCOTT MAUGHON JR

(Under the Direction of Steven Stice and Ross Marklein)

ABSTRACT

Mesenchymal stromal cells (MSCs) have been widely used in regenerative medicine applications due to their immunomodulatory properties. However, there are currently no licensed MSC therapies by the Food and Drug Administration (FDA). This can be attributed, in part, to the functional heterogeneity from different MSC donor and tissue sources and lack of critical quality attributes (CQA) for manufacturing MSC therapies. MSC metabolism during the manufacturing process plays a critical role in the potency of these therapies. Metabolites are highly abundant and reflect the cellular phenotype making them ideal candidates for identifying CQAs. This dissertation aims to identify metabolites, both in-process and end of manufacturing, to be used as candidate CQAs that are predictive of MSC immunomodulation. First, three MSC lines were expanded to three passages with metabolic profiling and functional testing ($CD4^+$ and $CD8^+$ T cell proliferation from different two donors and indoleamine-2,3-dehydrogenase (IDO) activity) at the end of each passage. A composite functional score was developed using all five functional metrics for potency prediction. Partial least squares regression identified candidate CQAs predictive of function including several small polar molecules and phosphatidylcholines. Lastly, ten MSC lines were expanded with profiling of non-destructive, in-process media

metabolites and end of expansion intracellular metabolites. Using a robust consensus machine learning approach, metabolites predictive of MSC function were identified. Metabolites found in multiple machine learning models were used to build consensus models. Consensus intracellular metabolites included multiple lipid classes while consensus media metabolites included several amino acids and sugars. Pathway enrichment identified metabolic pathways significantly associated with MSC function such as sphingolipid signaling and metabolism, arginine and proline metabolism, and autophagy. Overall, this work establishes a framework for identifying consensus metabolites that predict MSC function and can be used as candidate CQAs to help guide MSC manufacturing.

INDEX WORDS: mesenchymal stromal cells, metabolomics, critical quality attribute, potency, immunomodulation, t-cell, machine learning, cell manufacturing

METABOLIC PROFILING OF MESENCHYMAL STROMAL CELLS FOR CRITICAL QUALITY ATTRIBUTE IDENTIFICATION

by

TIMOTHY SCOTT MAUGHON JR

BS, University of Georgia, 2018

A Dissertation Submitted to the Graduate Faculty of The University of Georgia in Partial Fulfillment of the Requirements for the Degree

DOCTOR OF PHILOSOPHY

ATHENS, GEORGIA

2023

METABOLIC PROFILING OF MESENCHYMAL STROMAL CELLS FOR CRITICAL QUALITY ATTRIBUTE IDENTIFICATION

by

TIMOTHY SCOTT MAUGHON JR

Major Professor:	Steven Stice
	Ross Marklein
Committee:	Arthur Edison
	Cheryl Gomillion
	Luke Mortensen

Electronic Version Approved:

Ron Walcott
Vice Provost for Graduate Education and Dean of the Graduate School
The University of Georgia
May 2023

ACKNOWLEDGEMENTS

I would first like to thank my advisors Dr. Steve Stice and Dr. Ross Marklein for their encouragement and support over the years. Thank you for constantly being on my side while pushing me to be a better scientist. I would also like to thank my advisors Dr. Cheryl Gomillion, Dr. Art Edison, and Dr. Luke Mortensen for their guidance and support during this entire process.

I have been fortunate enough to meet and work with so many great individuals during my time. Thank you to all the lab members and collaborators over the years including: Seth Andrews, Brian Jurgielewicz, Raymond Swetenburg, Taylor Ellison, Sam Spellicy, Austin Passaro, and Morgane Golan from the Stice; Andrew Larey, Kanupriya Daga, Courtney Campagna, Thomas Spoerer, and Jon McRae from the Marklein lab; Max Colonna and Sara Shen from the Edison lab; Alex Van Grouw and Danning Huang from the Fernandez lab; Adeola Michael and Andrew Shockey from the Platt lab; Annie Bowles-Welch from the Marcus Center. Lastly, I would like to give a special thanks to the Easley lab for always giving me coffee to help keep me going.

Last but not least, I would like to thank all of my friends and family for their love and support over the years. I wouldn't be here without them, and I am blessed to have so many great people in my life. I'd especially like to thank Josh, Morgan, and Lulu Throop for being my extended family here in Athens and for everything you all have done for me. I'd like to thank my sister, Ansley Robertson, and brother-in-law, Colton Robertson, for being the best sister and brother that I could ever ask for and all the laughs over the years. Finally, I would like to

recognize the best parents around, Scott and Laurie Maughon. They have always loved and supported me no matter what and have shaped me into the person I am today. I am so blessed to have you both in my life, and I would like to dedicate this work to you both.

TABLE OF CONTENTS

Page

LIST OF TABLES

Page

LIST OF FIGURES

Page

CHAPTER 1

INTRODUCTION

Mesenchymal stromal cells (MSCs) have been widely studied in both pre-clinical and clinical settings due to their ability to differentiate into various tissue types such as bone, fat, and cartilage and their immunomodulatory properties.[1] MSCs are being used in many clinical trials as allogeneic therapies and have been investigated to treat various inflammatory, autoimmune, and neurodegenerative diseases.[2] MSCs can be derived from a wide range of tissue sources including bone marrow, adipose, umbilical cord, and induced pluripotent stem (iPS) cells.[3] It has been shown that MSCs mediate their immunomodulatory effects through a variety of mechanisms including various secreted factors (i.e. extracellular vesicles, proteins, metabolites), cell mediated contact, and apoptosis.[4]

Despite the promise of MSCs, there are currently no approved therapies for clinical use. The lack of translational therapies can be attributed, in large part, to the heterogeneity of MSCs that arises from donor-donor variability, tissue source, and manufacturing variability.4 Because of this heterogeneity, it has been difficult to establish critical quality attributes (CQAs) to ensure the potency (efficacy) of these therapies. The FDA defines a CQA as "a physical, chemical, biological, or microbiological property or characteristic that should be within an appropriate limit, range, or distribution to ensure the desired product quality. CQAs are generally associated with the drug substance, excipients, intermediates (in-process materials), and drug product."[5] In this work, we are focused on CQAs that predict the potency of MSCs. Cell potency assay standards are lacking making it difficult to predict clinical efficacy and screen for potential MSC

donors for clinical use.[6] Hundreds of millions of MSCs are also needed for therapeutic doses are needed making scaling up of manufacturing an important aspect of translating MSCs to the clinic. Factors such as growth vessel (i.e. type of bioreactor), oxygen diffusion, and nutrient distribution all factor into the heterogeneity that can be found in MSCs during manufacturing.[6–8] Because of these factors, establishing CQAs, whether process dependent or MSC specific, for manufacturing is needed to get MSC therapies approved for clinical use.

Currently, the minimal criteria for the identification of MSCs is based on these three factors; 1. MSCs are adherent to plastic under standard culture conditions, 2. MSCs are CD73, CD90, and CD105 positive while also being CD45, CD34, CD14/CD11b, CD79α/CD19 negative, and human leukocyte antigen (HLA)-DR, 3. MSCs must be able to differentiate into osteoblasts, chondroblasts, and adipocytes.[9] Although important for identification, this criteria does not indicate the capacity of MSCs to modulate immune cells.[10] Therefore, assays that define MSC potency for immunomodulation are necessary for clinical translation. Often these assays involve the co-culture of MSCs with a combination of immune cells such as peripheral blood mononuclear cells (PBMCs) or with individual immune cells such as macrophages, T cells, B cells, and NK cells.[6] Currently there is no consensus potency assay for determining immunomodulation capacity and one assay may not be sufficient enough for ensuring MSC potency in the clinic due to the multiple mechanisms of MSC immunomodulation.[6,11] Researchers are evaluating other molecules expressed or secreted by MSCs either in conjunction with in vitro immune cell assays or as surrogate markers of potency.[11,12] These markers can be used to rapidly assess MSC quality at early timepoints of manufacturing in addition to other potency assays.

Besides established co-culture potency assays, several studies have been conducted looking at proteomics and transcriptomics as surrogate or predictive markers of MSC potency.[13] Two commonly used markers of MSC potency are indolamine 2,3-dioxygenase (IDO) and programmed death ligand 1 (PD-L1).[11,14] Higher intracellular levels of IDO and higher expression of PD-L1 on the cell surface was found to correlate with higher CD4 and CD8 T cell suppression.[14] Knockdown of IDO significantly reduced MSC T cell suppression as well.[11] Recently, a study found that MSCs expressing CD146 suppressed CD4 and CD8 T cell proliferation, showed higher secretion of anti-inflammatory molecules when stimulated with interferon gamma (IFN-γ), and increased T reg formation when compared to CD146 negative MSCs showing its potential as a potency release criterion.[15] Another commonly used marker, Tumor necrosis factor receptor 1 (TNFR1), has been used as a release criterion for MSC potency in several clinical trials, but none of these therapies have gained FDA approval.[16,17] It has been proposed that a multitude of markers may be better for release criterion in order to encompass the multiple ways in which MSCs modulate the immune system. Several secreted factors correlated with T cell suppression both positively and negatively and was confirmed using transcriptomic data when stimulated with IFN-γ.[11] Although these markers are promising for predicting potency, they are all endpoint assays and do not predict potency in-process. Thus, establishing an assay matrix that encompasses both in-process and end of manufacturing product attributes may better ensure MSC quality as compared to a single measurement or assay outcome.

Metabolomics is a growing field due to its close reflection of the cellular phenotype and abundance of measurable metabolites both within the cell and in their culture medium making them ideal candidates for predictive biomarkers.[18,19] Well established tools such as nuclear

magnetic resonance (NMR) and mass spectrometry (MS) are used for measuring metabolites, and metabolic profiling has been used for biomarker and pathway discovery in various aspects of biology.[20,21] Characterization of MSC metabolism in vivo shows a preference towards glycolysis compared to oxidative phosphorylation (OXPHOS).[22] It has been shown that transplanting MSCs from this in vivo environment and expanding them ex vivo in a nutrient rich environment causes a metabolic shift towards OXPHOS.[23,24] MSCs with higher levels of glycolysis are associated with higher levels of IDO and PGE2 along with increased metabolite levels of lactate, citrate, and succinate.[25] Thus, monitoring metabolites both in-process (medium) and at the end of manufacturing (cellular) could be a key component in developing better CQAs for MSC therapies.

The motivation and rationale for using metabolomics to identify predictive markers of MSC potency is highlighted throughout this introduction. The work discussed throughout this dissertation focuses on using metabolomics both during expansion and at the end of expansion to develop robust markers of MSC immunomodulatory potency for improving manufacturing and MSC potency prediction.

Chapter Two and Three are studies that aim to establish a pipeline for discovering CQAs. Chapter Two illustrates the potential of intracellular MSC metabolites for predicting potency based on a combination of potency assays called a composite functional score. Chapter Three builds on Chapter Two by adding an additional six MSC lines with one repeat line. Chapter Three utilizes in-process media metabolites early in the expansion process to predict the composite functional score post thaw. Biomarker discovery was also refined by adding additional modeling techniques to create a “consensus” list of predictive markers rather than

relying on just one predictive machine learning model. These consensus metabolites led to the identification of pathways that may play a significant role in MSC immunomodulation.

Chapter Four provides an overview of the manufacturing challenges associated with MSC extracellular vesicle (EV) therapies. In this review, many of the manufacturing challenges faced by MSCs themselves also apply to the EVs such as heterogeneity and manufacturing conditions (i.e. flask or bioreactor, growth medium). Furthermore, this review discusses the current and emerging methods of characterizing EVs, and how these can be implemented in a manufacturing setting for predicting EV potency.

Chapter 5 is a current opinion article in biomedical engineering on the use of metabolomics for developing robust CQAs for MSC and chimeric antigen receptor T-cell (CAR-T) therapies. MSCs and CAR-T are two of the most widely studied cell therapies, and this chapter discusses how their respective metabolism during manufacturing affects their potency, and discusses current and emerging technologies for measuring metabolites in-process.

Finally, Chapter Six concludes the main work of this dissertation, as well as proposes future directions that build off the work presented in this thesis. Several significant pathways found in Chapter Three are expanded upon in the context of MSC immunomodulation and how to potentially interrogate them based on the CQAs identified. The metabolism of MSCs when interacting with T-cells also illustrates a promising future direction to see how the metabolome of high potency and low potency donors change in response to stimuli. The pipeline developed for identifying CQAs in Chapter Three is discussed in the context of scaling up MSC manufacturing to a bioreactor for predicting MSC EV potency.

REFERENCES

1. Castro-Manrreza, M. E. & Montesinos, J. J. Immunoregulation by mesenchymal stem cells: Biological aspects and clinical applications. J Immunol Res 2015, (2015).
2. Shi, Y. et al. How mesenchymal stem cells interact with tissue immune responses. Trends Immunol 33, 136–143 (2012).
3. Olsen, T. R., Ng, K. S., Lock, L. T., Ahsan, T. & Rowley, J. A. Peak MSC-Are we there yet? Frontiers in Medicine vol. 5 Preprint at https://doi.org/10.3389/fmed.2018.00178 (2018).
4. ROBB, K. P., FITZGERALD, J. C., BARRY, F. & VISWANATHAN, S. Mesenchymal stromal cell therapy: progress in manufacturing and assessments of potency. Cytotherapy 21, 289–306 (2019).
5. Guidance for Industry Q8(R2) Pharmaceutical Development. (2009).
6. Galipeau, J. et al. International Society for Cellular Therapy perspective on immune functional assays for mesenchymal stromal cells as potency release criterion for advanced phase clinical trials. Cytotherapy 18, 151–159 (2015).
7. Brachtl, G. et al. Batch Effects during Human Bone Marrow Stromal Cell Propagation Prevail Donor Variation and Culture Duration: Impact on Genotype, Phenotype and Function. Cells 11, (2022).
8. Stroncek, D. F. et al. Human Mesenchymal Stromal Cell (MSC) Characteristics Vary Among Laboratories When Manufactured From the Same Source Material: A Report by the Cellular Therapy Team of the Biomedical Excellence for Safer Transfusion (BEST) Collaborative. Front Cell Dev Biol 8, (2020).

9. Dominici, M. et al. Minimal criteria for defining multipotent mesenchymal stromal cells. The International Society for Cellular Therapy position statement. Cytotherapy 8, 315–317 (2006).

10. lo Surdo, J. L., Millis, B. A. & Bauer, S. R. Automated microscopy as a quantitative method to measure differences in adipogenic differentiation in preparations of human mesenchymal stromal cells. Cytotherapy 15, 1527–1540 (2013).

11. Chinnadurai, R. et al. Potency Analysis of Mesenchymal Stromal Cells Using a Combinatorial Assay Matrix Approach. Cell Rep 22, 2504–2517 (2018).

12. Spees, J. L., Lee, R. H. & Gregory, C. A. Mechanisms of mesenchymal stem/stromal cell function. Stem Cell Res Ther 7, (2016).

13. de Wolf, C., van de Bovenkamp, M. & Hoefnagel, M. Regulatory perspective on in vitro potency assays for human mesenchymal stromal cells used in immunotherapy. Cytotherapy vol. 19 784–797 Preprint at https://doi.org/10.1016/j.jcyt.2017.03.076 (2017).

14. Guan, Q., Li, Y., Shpiruk, T., Bhagwat, S. & Wall, D. A. Inducible indoleamine 2,3-dioxygenase 1 and programmed death ligand 1 expression as the potency marker for mesenchymal stromal cells. Cytotherapy 20, 639–649 (2018).

15. Bowles, A. C. et al. Signature quality attributes of CD146 + mesenchymal stem/stromal cells correlate with high therapeutic and secretory potency. Stem Cells 38, 1034–1049 (2020).

16. Kebriaei, P. et al. A Phase 3 Randomized Study of Remestemcel-L versus Placebo Added to Second-Line Therapy in Patients with Steroid-Refractory Acute Graft-versus-Host Disease. Biol Blood Marrow Transplant 26, 835 (2020).

17. Kurtzberg, J. et al. A Phase 3, Single-Arm, Prospective Study of Remestemcel-L, Ex Vivo Culture-Expanded Adult Human Mesenchymal Stromal Cells for the Treatment of Pediatric Patients Who Failed to Respond to Steroid Treatment for Acute Graft-versus-Host Disease. Biology of Blood and Marrow Transplantation 26, 845–854 (2020).

18. Liu, Y. & Ma, T. Metabolic regulation of mesenchymal stem cell in expansion and therapeutic application. Biotechnol Prog 31, 468–481 (2015).

19. Steuer, A. E., Brockbals, L. & Kraemer, T. Metabolomic strategies in biomarker research-new approach for indirect identification of drug consumption and sample manipulation in clinical and forensic toxicology? Front Chem 7, 319 (2019).

20. Dunn, W. B., Bailey, N. J. C. & Johnson, H. E. Measuring the metabolome: Current analytical technologies. Analyst vol. 130 606–625 Preprint at https://doi.org/10.1039/b418288j (2005).

21. Goodarzi, P. et al. Metabolomics Analysis of Mesenchymal Stem Cells. Int J Mol Cell Med 8, 30 (2019).

22. Yuan, X., Logan, T. M. & Ma, T. Metabolism in human mesenchymal stromal cells: A missing link between HMSC biomanufacturing and therapy? Frontiers in Immunology vol. 10 977 Preprint at https://doi.org/10.3389/fimmu.2019.00977 (2019).

23. Sherr, C. J. & DePinho, R. A. Cellular senescence: mitotic clock or culture shock? Cell 102, 407–410 (2000).

24. Pattappa, G., Heywood, H. K., de Bruijn, J. D. & Lee, D. A. The metabolism of human mesenchymal stem cells during proliferation and differentiation. J Cell Physiol 226, 2562–2570 (2011).

25. Liu, Y., Yuan, X., Muñoz, N., Logan, T. M. & Ma, T. Commitment to Aerobic Glycolysis Sustains Immunosuppression of Human Mesenchymal Stem Cells. Stem Cells Transl Med 8, 93–106 (2019).

CHAPTER 2

METABOLOMICS AND CYTOKINE PROFILING OF MSCS IDENTIFIES MARKERS PREDICTIVE OF T CELL SUPPRESSION[1]

[1] Ty S Maughon, Xunan Shen, Danning Huang, Adeola O Adebayo Michael, W. Andrew Shockey, Seth H. Andrews, Jon M. McRae III, Manu O Platt, Facundo M. Fernández, Arthur S. Edison, Steven L. Stice, Ross A. Marklein. Accepted by Cytotherapy. Reprinted here with permission of publisher.

Author Contributions:

TM: Conception and study design; Cell expansion, sample collection, cell harvest, and growth characteristics; T cell suppression assay; IDO activity assay; Functional Composite Score; Linear regression; Analysis and interpretation of data; Drafting and revising the manuscript

XS: Conception and study design; all NMR data and analysis; PLSR modeling; Analysis and interpretation of data; Drafting and revising the manuscript

DH: Conception and study design; all MS data and analysis; Analysis and interpretation of data; Drafting and revising the manuscript

AOAM: Cytokine data analysis; Analysis and interpretation of data; Drafting and revising the manuscript

WAS: Conception and study design; Cytokine data analysis

SA: Acquisition of data

JM: Acquisition of data

MOP, FF, AE, RM, SS: Conception and study design; Analysis and interpretation of data; Drafting and revising the manuscript

2.1 ABSTRACT

Background: Mesenchymal stromal cells (MSCs) have shown great promise in the field of regenerative medicine as many studies have shown that MSCs possess immunomodulatory function. Despite this promise, no MSC therapies have been licensed by the FDA. This lack of successful clinical translation is due in part to MSC heterogeneity and a lack of critical quality attributes (CQAs). While MSC Indoleamine 2,3-dioxygnease (IDO) activity has been shown to correlate with MSC function, multiple predictive markers may be needed to better predict MSC function.

Methods: Three MSC lines (two bone marrow, one iPSC) were expanded to three passages. At the time of harvest for each passage, cell pellets were collected for nuclear magnetic resonance (NMR) and ultra-performance liquid chromatography mass spectrometry (UPLC-MS), and media was collected for cytokine profiling. Harvested cells were also cryopreserved for assessing function using T cell proliferation and IDO activity assays. Linear regression was performed on functional data against NMR, MS, and cytokines to reduce the number of important features, and partial least squares regression (PLSR) was used to obtain predictive markers of T cell suppression based on variable importance in projection (VIP) scores.

Results: Significant functional heterogeneity (in terms of T cell suppression and IDO activity) was observed between the three MSC lines, as well as donor-dependent differences based on passage. Omics characterization revealed distinct differences between cell-lines using principal component analysis (PCA). Cell-lines separated along principal component 1 based on tissue source (bone marrow vs. iPSC-derived) for NMR, MS, and cytokine profiles. PLSR modeling of important features predicts MSC functional capacity with NMR (R^2=0.86), MS (R^2=0.83), cytokines (R^2=0.70), and a combination of all features (R^2=0.88).

Discussion: The work described here provides a platform for identifying markers for predicting MSC functional capacity using PLSR modeling that could be used as release criteria and guide future manufacturing strategies for MSCs and other cell therapies.

2.2 INTRODUCTION

Mesenchymal stem/stromal cells (MSCs) have been explored as a cell therapy in clinical trials due to their immunomodulatory properties.[1] Although MSCs have shown great promise in preclinical studies for treatment of immune diseases, there have been challenges translating MSCs into approved therapies. This lack of translation can be attributed to MSC heterogeneity and no well-established critical quality attributes (CQAs i.e. limits or ranges of MSC biological properties) used to monitor MSC functional capacity among cell-lines or even within MSC cultures.[2–4] T cell suppression is one of the most commonly used assays to assess MSC immunomodulatory capacity, but it is not standardized, has low throughput, and there is donor-donor variability among peripheral blood mononuclear cell (PBMC) responses to stimulation.[5]

The International Society for Cell and Gene Therapy (ISCT) has proposed several candidate protein properties to use for predicting MSC functional capacity.[2] Indoleamine 2,3-dioxygenase (IDO) is one indicator of potency that has been proposed that plays a major role in the mechanisms by which MSCs modulate immune cells, such as T cells.6 Although IDO correlates with T cell suppression, there are several other mechanisms through which MSCs exert their potent immunomodulatory effects.[7–9] Therefore, a matrix-based approach (i.e. a combination of predictive markers) is likely needed to ensure a high quality MSC product.[2] Chinnadurai et al. examined the relationship between various RNAs and secreted molecules with T cell proliferation and showed that several secreted factors and RNAs had strong correlations with T cell proliferation.[10] Although these factors correlated with MSC functional capacity,

measurement of these cellular properties require stimulation of sample MSC product acquired at the end of the manufacturing process and thus cannot be performed in-process.

MSCs secrete a broad repertoire of immunomodulatory cytokines that may have therapeutic potential; however, these immunomodulatory functions have not yet been characterized. Several studies have shown that MSC secreted cytokines can be modulated by physiologic conditions such as hypoxia, and pharmacological conditions such as targeted small molecule and growth factor conditioning.[11–13] MSCs from different sources may differ in their immunomodulatory capacities, and the ability to assess cytokine secretion in MSCs using a non-destructive approach such as cytokine assays will allow for a standardized metric for MSC potency during manufacturing;[14] cytokines that are secreted into the media can be measured without interference with cell growth and other conditions. Therefore, combination of specific cytokines secreted by MSCs, together with metrics of T cell suppression and IDO may enable identification of non-destructive, in-process markers for predicting potency.

Measures of cellular metabolism are also promising for assessing MSC quality due to the high abundance of metabolites in cells, and their importance in stem cell fate.[15] Studies have shown that extended in vitro culture of MSCs shifts their metabolism from glycolysis towards oxidative phosphorylation (OXPHOS). MSCs in their native environment have a more glycolytic metabolism, and it has been shown that glycolytic MSCs have improved immunomodulatory effects in vivo.[15–17] Therefore, assessing metabolite profiles in MSCs during expansion could be used as a predictor of their immunomodulatory capacity. Non-targeted metabolomics enables a detailed profiling of therapeutic cells, providing opportunities towards a more precise understanding of cellular therapeutic mechanisms.[18] Nuclear magnetic resonance (NMR) spectroscopy and mass spectrometry (MS) are the two most commonly used techniques in

metabolomics.[19] NMR requires minimal sample preparation, making it highly reproducible. NMR can also provide information in assigning metabolites based on chemical shifts and J-coupling patterns. As an analytical platform, MS also has certain advantages. Its higher sensitivity enables the detection of low abundance metabolites that are below the NMR detection thresholds,[20] whereas its high resolution greatly reduces spectral overlap. When coupled with separation techniques such as gas chromatography (GC) or ultra-performance liquid chromatography (UPLC), spectral complexity is greatly reduced, and metabolic chemical properties can be revealed.[21–23] The combination of NMR and UPLC-MS metabolic profiling provides an even more in-depth measurement of MSC cellular metabolism, potentially leading to the discovery of CQAs. To date, NMR- and MS-based metabolic profiling was used to characterize cellular metabolism, leading to the discovery of biomarkers or pathways different between cell-lines or cellular responses of treatment.[24–26] However, to the best of our knowledge, no studies have been reported where NMR- and/or UPLC-MS- based metabolomics are used to establish predictive markers associated with MSC immunomodulatory potency.

In this study, we measured MSC metabolites and cytokine levels during cell manufacturing that could serve as predictors of MSC immunomodulation and as potential potency assays. These metabolites and cytokines are referred to in this work as predictive markers. Intracellular metabolites and secreted cytokines from three MSC lines at multiple passages were studied to determine their correlation with MSC immunosuppressive capacity post thaw. NMR, UPLC-MS, and cytokine data sets were also merged and filtered to identify predictive markers. Using partial least squares regression (PLSR) and variable importance projection (VIP) scores, we identified a panel of candidate cytokines and metabolites that could be used to predict MSC functional capacity and inform future manufacturing strategies.

2.3 MATERIALS AND METHODS

Cell Culture

Two bone marrow-derived MSC lines (RoosterBio, Frederick MD) lot #0071 (F, 18-30) and #0182 (F, 26) (which the manufacturer has both research and clinical-grade lots available), and one induced pluripotent stem cell derived MSC cell-line (Cellular Dynamics International, Madison WI) (Lot #0003, also prequalified) were used and referred here as BM71, BM182, and iMSC, respectively. MSCs were thawed and allowed to recover for 24 hours in complete medium (MSC-GM) (Alpha-Minimum Essential Medium (Gibco, Waltham MA), 10% fetal bovine serum (Hyclone, Logan UT), 2mM L-glutamine, 50 U/mL penicillin, 50 μg/mL streptomycin (Gibco)) before being seeded at 500 cells/cm2. Cells were expanded in 10 150 mm plates with a negative, media-only control plate and 14 T175 flasks for expansion. After reaching approximately 80% confluency, cells in 150 mm dishes were washed with PBS three times. Cells were then scraped and collected in 80:20 methanol:water solution and stored at -80°C for NMR and MS analysis. Cells grown in T175 flasks for expansion were harvested using 0.05% trypsin (Gibco) and counted using a Cellometer K2 cell counter (Nexcelom, Lawrence MA). Cells were either cryopreserved for functional assays or reseeded in dishes/flasks for continued expansion (3 total passages for each cell-line, 9 total experimental groups). Population doubling level (PDL) for each cell-line/passage was determined using formula 1:

$$PDL = X + 3.322(\log Y - \log I) \quad (1)$$

Where X = initial PDL, I = initial cell seeding number and Y = final number of cells.

T Cell Suppression Assay

MSCs from each cell-line/passage were thawed and allowed to recover for 48 hours with a media change at 24 hours. MSCs were trypsinized (0.05% Trypsin-EDTA, Gibco) then seeded

at three densities (10,000, 5,000 and 2,000 cells/well) in a 96 well plate and cultured for 24 hours. PBMCs (AllCells, Alameda CA) were thawed in Roswell Park Memorial Institute (RPMI) media (RPMI, 20% FBS, 2mM L-glutamine, 50 U/mL penicillin, 50 μg/mL streptomycin) and cultured overnight at 37°C and 5% CO2. Prior to co-culture, PBMCs were labeled with carboxyfluorescein succinimidyl ester (CFSE) (Supplemental Table 2.1, Biolegend, San Diego CA) according to the manufacturer's protocol, and 100,000 PBMCs were added to each well at final MSC:PBMC ratios of 1:10, 1:20, or 1:50 as well as control wells containing only PBMCs. Following PBMC addition, stimulating anti-CD3/CD28 Dynabeads (Thermo Fisher Scientific, Waltham MA) were added at 100,000 beads per well to the appropriate wells (positive controls and all MSC groups). MSCs and PBMCs were co-cultured for 72 hours at 37°C, 5% CO2.

Following co-culture, PBMCs were collected and stained using APC/Fire anti-CD4 and APC anti-CD8 (Supplemental Table 2.1) (Biolegend, San Diego CA). PBMCs were first washed and stained with Zombie Yellow (Supplemental Table 1) (Biolegend, San Diego CA) viability dye and blocked using 2% FBS. PBMCs were then washed again and stained for CD4 and CD8 in the dark at room temperature. Following staining, the antibodies were blocked using 2% FBS and washed. Cells were then fixed with 4% PFA for 30 minutes at 4°C. Cells were then washed and re-suspended in PBS containing 2% FBS. Cells were stored overnight at 4°C in the dark until flow analysis.

Flow Cytometry

All flow cytometry experiments were performed using a CytoFLEX S (Beckman Coulter, Hialeah FL) with 20,000 events collected per sample. All flow cytometry data were analyzed using FlowJo (Treestar, Inc., Ashland OR). Briefly, cell debris, doublets, and Dynabeads were gated out using scatter principles. Then, single stained controls were used for compensation, and

fluorescence minus one controls were used in order to determine positive populations (Supplemental Figure 2.1).

IDO Activity Assay

MSCs from each cell-line/passage experimental group were thawed and cultured for 48 hours with a media change at 24 hours. MSCs were trypsinized then seeded at a density of 40,000 cells/cm2 in a 96 well plate in MSC-GM. After 24 hours, the medium was replaced in each well with MSC-GM containing 10 ng/mL interferon gamma (IFN-γ) (Life Technologies). After an additional 24 hours, conditioned media was collected and frozen at -20°C, and cells were fixed with 4% PFA. Media was thawed and 100 µL was transferred into a 96 well plate. Trichloroacetic acid was used to precipitate excess protein. 75 µL of the supernatant was collected and transferred to a separate 96 well plate. Ehrlich's Reagent was then added to each well to detect L-kynurenine levels using a SpectraMax iD5 (Molecular Devices) plate reader. Levels of L-kynurenine were determined using a standard curve. To normalize L-kynurenine values to cell numbers for each experimental group, we performed automated image analysis to quantify cell nuclei in the wells from which conditioned medium was collected. Following fixation, MSCs were washed with PBS twice, and stained with Hoechst. Cells were then imaged on a Cytation 5 high content imaging system (Biotek, Winooski VT) and cell counts determined using CellProfiler[27] to normalize the amount of L-kynurenine per cell.

Metabolomics Sample Preparation

MSC samples stored in 80:20 methanol:water solution were thawed at 4°C and vortexed three times for 1 min. Then samples were centrifuged at 14,000 x g for 5 min at 4°C. For each sample, 30% (300 µl) and 60% (600 µl) of the supernatant were transferred to pre-labeled Eppendorf tubes for LC-MS and NMR spectroscopy, respectively. For each PDL, 67µl of each

sample was pooled together to generate 2 internal PDL quality control (QC) samples. The remaining 33 µl supernatant of each sample was pooled together to generate 2 internal overall QC samples. In each PDL, the extraction blank sample was added using extraction solvent (methanol: water 80:20). Samples were then evaporated in a Speedvac for 6 hours and stored in -80°C until future analysis. NMR samples with QC controls and 2 buffer blank samples were used for data acquisition. Samples were randomized, with a total 49 samples in each cell-line. The LC-MS sample randomization was identical to NMR.

NMR

The NMR buffer solution was prepared by dissolving 928.6 mg of anhydrous NaH2PO4 and 320.9 mg of Na2HPO4 in 80 ml D2O (Cambridge Isotope Laboratory) in a volumetric flask. Sodium trimethylsilylpropanesulfonate (DSS) was used as a chemical shift and concentration reference standard by adding 333.3 µL of 1.0 M DSS-D6 (Cambridge Isotope Laboratory) stock solution to the buffer for a final DSS concentration of 1/3 mM. The pH was adjusted to 7.4 (uncorrected for isotope effects) and was brought to a volume of 100 ml with D2O and mixed well. The pH was rechecked, and the buffer stored at 4°C until use.

The NMR samples were reconstituted in 80 µL of the NMR buffer and vortexed thoroughly. Sixty µL of each sample was transferred to racks of 96 1.7-mm NMR tubes for data acquisition using a SamplePro Tube robotic system (Bruker Biospin, Billerica, MA, USA). Samples were run on a Bruker NEO 800 MHz NMR spectrometer equipped with a 1.7-mm cryoprobe and Bruker SampleJet cooled to 5.6°C. One dimensional nuclear Overhauser enhancement spectroscopy with water suppression (1D-NOESY PR) was collected on all samples. The spectra were processed using NMRPipe[28] and in-house MATLAB metabolomics toolbox (https://github.com/artedison/Edison_Lab_Shared_Metabolomics_UGA). The spectra

were aligned using Correlation Optimized Wrapping (COW) algorithm[29] and normalized with a Probabilistic quotient normalization (PQN)[30] algorithm. The non-overlapped peaks were manually binned, and the area under curve was calculated for each non-overlapped feature.

Two-dimensional 1H-13C Heteronuclear Single Quantum Coherence (HSQC) and 1H-13C HSQC-Total Correlated Spectroscopy (HSQC-TOCSY) spectra on internal pooled samples were collected for metabolite identification. The spectra were processed using NMRPipe, and the in-house MATLAB metabolomics toolbox. The 2D NMR spectra were matched to a metabolite database using the COLMARm.[31] The metabolites were assigned a confidence level ranging from 1 to 5 according to published criteria.[32]

After metabolite identification, peaks were further normalized by the number of protons in each functional group corresponding to a given peak. A total of 28 metabolites were obtained from binning of the whole spectra. The unknown binned features were used to perform correlation analysis. The features with correlation coefficient values greater or equal to 0.8 were then grouped together as tentative unknown metabolites. A total of 29 tentative unknown features were extracted from 100 features (Supplemental Figure 2.2).

UPLC-MS

Cell extract samples and a sample blank were resuspended in 50 µL methanol/water (80:20 v/v), and a pooled quality control (QC) sample was created by mixing a 10 µL aliquot of each cell extract sample. Both the sample blank and the pooled sample were processed with the same procedure, and were analyzed together with the cell extract samples. All samples were run in randomized order on consecutive days. QC samples were analyzed every 10 runs to assess UPLC−MS system stability and correct time-dependent batch effects with a QC-based regression curve.

UPLC-MS analyses were performed using a Vanquish Horizon UPLC (Thermo Fisher Scientific, Inc., Waltham, MA) system coupled to an Orbitrap ID-X Tribrid mass spectrometer (Thermo Fisher Scientific, Inc., Waltham, MA). Hydrophilic interaction (HILIC) chromatography was performed with a Waters ACQUITY UPLC BEH HILIC, 2.1 × 75 mm, 1.7 μm particle column. Mobile phase A was water/acetonitrile (95:5 v/v), 10 mM ammonium acetate, and 0.05% ammonium hydroxide. Mobile phase B was acetonitrile with 0.05% ammonium hydroxide. Chromatographic gradients can be found in Supplemental Information (Supplemental Table 2.2). The column temperature was 55 °C, while samples were maintained at 5 °C in the autosampler. Two μL of each sample were injected, and the mass spectrometer was operated in positive ion mode. For metabolite identification purposes, data-dependent acquisition (DDA) experiments were used to collect MS/MS spectra at stepped normalized collision energy (NCE) of 10, 30, and 50.

Cytokine Profiling

Conditioned media from each cell-line/passage (at the time of cell harvest) were collected and prepared for cytokine profiling using the Human Premixed Multi-Analyte Magnetic Luminex Assay (R&D Systems, Minneapolis MN) that was customized for this study quantifying cathepsin S, cystatin C, GCSF, angiopoietin 1, VEGF, PDGF-AA, bFGF, osteopontin, IL-8, IL-6, CCL12/MCP-1, and CCL5/RANTES (Supplemental Table 3). Cytokine profiling was performed following a standard protocol. Briefly, 50 μL standard or media sample was added to a 96-well plate, followed by 50 μL diluted microparticle cocktail and incubated for 2-hours at room temperature on an orbital microplate shaker. Using a magnetic device attached to the bottom of the microplate, each well was washed with 50 μL of wash buffer. Then 50 μL diluted biotin-antibody cocktail was added to wells and incubated for 1-hour at room temperature

on an orbital microplate shaker. After washing, 50 µL of streptavidin-PE was added to each well and incubated for 30 min. 100 µL of wash buffer was added to wells to resuspend microparticles and samples were then loaded into a BioPlex 200 Luminex system (Bio-Rad) and analyzed. The assay measures the intensity of PE emission, which is correlated to cytokine concentration standards.

Data Analysis and Statistical Methods

Principal component analysis (PCA) was conducted using JMP (version 15). All suppression assays, linear regression models, and IDO assays were analyzed using Prism (GraphPad, San Diego CA). Comparison of T cell proliferation to the positive control, comparison of T cell proliferation among all groups at the 1:10 dilution, and IDO activity were analyzed using one-way ANOVA with Tukey's post-hoc test. Comparisons of T cell suppression against passage 1 and against the 1:10 dilution were analyzed using a two-way ANOVA with Tukey's post hoc test. Error bars represent standard error on all bar graphs.

NMR and MS features were mapped to CD4+ and CD8+ proliferation rates using simple linear regression. The top 20 metabolites of each dataset with the lowest p-values ($p<0.05$) were selected for downstream analysis. The selected 20 NMR metabolites, 20 MS metabolites and all cytokine data were used to train a partial least square regression (PLSR) model. The response was the PCA loading score generated by using principal component 1 of all five functional measures termed, composite functional score. The predictors with variable importance in projection (VIP) scores greater or equal to 1 were selected as predictive markers.

2.4 RESULTS

Cell-line and passage-dependent differences in T cell suppression

PDL was used to assess MSC age and growth characteristics for each cell-line throughout expansion (Supplemental Table 2.4). PDL, doublings per day, and log growth of cell expansions were recorded (Figure 2.1B-D). Following expansion, MSC cell-lines at three different passages were co-cultured with anti-CD3/CD28 stimulated PBMCs in order to assess their immunosuppressive capacity with two PBMC donors. MSCs were cultured at three different MSC:PBMC ratios as well as positive (no MSCs with stimulation) and negative (no MSCs, no stimulation) controls. After 3 days, CD4+ and CD8+ T cell proliferation was assessed based on CFSE dilution (Figure 2.2A-F). A dose response was observed when increasing the MSC:PBMC ratio on the ability of the iMSC and BM182 cells to suppress CD4+ and CD8+ proliferation ($p<0.05$). CD4+ and CD8+ T cell proliferation decreased at the 1:50 dilution compared to the 1:10 dilution ($p<0.05$) in BM71 except for P3. The 1:10 MSC:PBMC ratio had the greatest variation in function across all cell-lines and passages and was used for comparison and predictive function. All passages of the iMSCs and BM182 lines suppressed CD4+ and CD8+ T cell proliferation when compared to the positive control ($p<0.05$) (Figure 2.2A, C, D, F). BM71 increased CD4+ proliferation at all passages and increased CD8+ proliferation at P1 ($p<0.05$) and had no significant differences at P2 and P3 when compared to the positive control (Figure 2.2B, E). For BM182, CD4+ and CD8+ T cell proliferation ($p<0.05$) was suppressed at P3 compared to earlier passages and had similar suppression as the iMSCs (Figure 2.2G). These studies were repeated using PBMCs harvested from a second donor (Supplemental Figure 2.2). Similarly, there was an MSC dose dependent response, as the 1:10 MSC:PBMC ratio had significantly lower ($p<0.05$) CD4+ and CD8+ proliferation when compared with 1:20 and 1:50

ratios (Supplemental Figure 2.2 A-F). Although BM71 did suppress both CD4+ (except P1) and CD8+ T cells when compared to the positive control ($p<0.05$), they possessed different immunomodulatory capacities than the iMSCs and BM182 (CD4+ and CD8+ $p<0.05$) at the 1:10 ratio (Supplemental Figure 2.2G,H). Again, iMSCs consistently suppressed both CD4+ and CD8+ proliferation across all passages. BM182 P3 had significantly less CD4+ proliferation compared to P1 ($p<0.05$) and P2 ($p<0.05$). BM182 P3 also had significantly less CD8+ proliferation compared to P1 ($p<0.05$), was less than P2 although not technically significant ($p=0.06$) (Supplemental Figure 2.2G, H).

MSC IDO activity correlates with T cell proliferation

IDO activity for each cell-line/passage group was quantified as another functional readout of MSC immunomodulatory capacity (Figure 2.2I). Similar to the T cell suppression results, iMSCs displayed high IDO activity (indicated by high levels of L-kynurenine) for all passages and BM71 had the lowest IDO activity for all cell-lines at each passage. IDO activity of BM182 increased from P1 to P2 ($p<0.05$) with P3 displaying the highest levels of L-kynurenine ($p<0.05$) compared to all other cell-lines. Linear regression was performed to determine the relationship between IDO activity and CD4+/CD8+ T cell proliferation (Figure 2.2J, K). IDO activity correlated with both CD4+ and CD8+ T cell proliferation ($R2=0.75$ and $R2=0.79$, respectively) for the 1:10 MSC:PBMC ratio. The second PBMC donor was consistent with the first PBMC donor, IDO activity and MSC suppression of CD4+/CD8+ T cells ($R2=0.85$ and $R2=0.81$, respectively) were positively correlated (i.e higher IDO activity means higher T cell suppression) (Supplemental Figure 2.3).

NMR-based identification of MSC metabolic signatures

For each cell-line/passage, the intracellular products were analyzed using NMR metabolomics profiling. The heat map of all detected metabolites shows that the overall metabolite signature was cell-line specific with some passage differences observed within cell-lines (Figure 2.3A). It provides intuitive visualization of a data table. Each colored cell on the map corresponds to a concentration value in our data table, with samples in rows and features/compounds in columns. The data was auto scaled and normalized. As an unbiased way of looking at the metabolic signature of MSCs, we used unsupervised PCA to examine differences in the cell-lines. Unsupervised PCA revealed distinct metabolic differences between the cell-lines (Figure 2.3B). Different tissue donor sources clearly separated along PC1 with iMSC samples grouped together on the positive side of PC1 and the both BM cell-lines on the negative side. iMSCs were significantly different ($p<0.05$) from BM71 and BM182 along PC1, but there were no observable differences between BM71 and BM182 (Figure 2.3C). BM182 separated from BM71 along PC2 at P3 ($p<0.05$), which is the passage at which BM182 showed significant functional improvement (Figure 2.3D).

UPLC-MS-based identification of MSC metabolic signatures

Additional cell pellet samples collected at the time of cell harvest for each cell-line/passage were analyzed using UPLC-MS. As with NMR metabolic profiling results, the heat map for the 1368 metabolite features showed clear differences in the metabolic profile between BM and iMSC cell-lines, and between different passages within a given cell-line (Figure 2.4A). Similar to what was observed in NMR, PCA of the 1368 UPLC-MS metabolites displayed a clear separation of all cell-lines (Figure 2.4B). iMSCs separated from both BM71 and BM182 ($p<0.05$) along the PC1 axis, with no differences between BM71 and BM182 (Figure 2.4C). All

cell-lines were significantly different ($p<0.05$) from one another along PC2 (Figure 2.4D). There were no metabolomic profile differences between passages within a cell-line.

Secreted cytokine profile of MSC conditioned media

Conditioned media collected at the time of MSC harvest for each cell-line/passage were analyzed using Multi-Analyte Magnetic Luminex assay. The heatmap revealed variable cytokine expression from all cell-lines (Figure 2.5A). Cytokines with similar functions clustered together, for example, CCL5 and CCL2, both chemotactic cytokines for T-cells are clustered. Similarly, VEGF and angiopoietin, angiogenic growth factors, are clustered on the heat map. Cathepsin S, a protease expressed and secreted by cells during angiogenesis clustered with these cytokines.[33,34] IL-8, IL-6 and cystatin C clustered closely with the chemotactic cytokines (Figure 2.5A). To examine cytokine signature differences among the cell-lines using an unbiased approach, we performed PCA. The scores plot showed a distinct separation of cytokine profiles among cell-lines (Figure 5B). The cytokine profiles of the iMSCs grouped together at PC1 on the positive side, while the two BM cell-lines were clustered on the negative side ($p<0.05$) (Figure 2.5C). Differences were also observed within the iMSC line (P2 vs. P1/P3) and BM71 line (P1 vs. P2/P3) ($p<0.05$) (Figure 2.5C). The first passage of iMSCs and BM71 were significantly different ($p<0.05$) from the later passages within their respective cell-line along PC2 (Figure 2.5D). BM182 showed no significant differences along PC2 (Figure 2.5D).

Regression of identified metabolites to determine markers for predictive function

Metabolites identified from NMR and MS were regressed with CD4+ and CD8+ T cell proliferation (Figure 2.6). Metabolites with strong positive or negative correlations ($R2>0.50$) were then used in order to reduce the data set and ordered based on the strongest correlation. Regression with PBMC Donor 1 revealed strong correlations with multiple NMR metabolites.

Myo-inositol had the highest R2 values for both CD4+ (R2=0.84) and CD8+ (R2=0.84) T cell proliferation as followed by unknown NMR metabolite 2 (ukNMR-2) (R2=0.82 and R2=0.77, respectively) (Figure 2.6A-C). To confirm these results, NMR metabolites were then regressed with PBMC Donor 2. Myo-inositol and ukNMR-2 correlated (R2=0.54 and R2=0.74, respectively) with CD4+ proliferation (Supplemental Figure 2.5). Regression with CD8+ proliferation showed very similar results to PBMC Donor 1 with myo-inositol and ukNMR-2 having strong correlations (R2=0.81 and R2=0.88, respectively). Linear Regression with UPLC-MS metabolites also revealed multiple metabolites that correlated with function. From PBMC donor 1, the top two correlated metabolites for CD4+ and CD8+ proliferation were unknown MS metabolite 1349 (ukM-1349) (R2=0.88 and R2=0.85, respectively) and phosphatidylcholine, PC(O-38:4) (R2=0.81 and R2=0.88, respectively) (Figure 2.6E-H). ukM-1349 and PC(O-38:4) both correlated with PBMC donor 2 CD4+ (R2=0.64 and R2=0.55, respectively) and CD8+ (R2=0.87 and R2=0.83, respectively) T cell proliferation as well (Supplemental Figure 2.5 and Supplemental Table 2.6).

PLSR modeling of predictive markers enables prediction of MSC functional capacity

A composite functional score was created in order to assess each cell-line's overall functional capacity due to varying levels of T cell activation from different PBMC donors (Figure 2.7A). All five functional outputs were plotted using PCA, and PC1 was then used as the composite functional score which accounted for 92.1% of the variance (Figure 2.7 B, C). The top 20 correlated metabolites from linear regression analyses were then used to train the PLSR model. Features with VIP scores greater than 1 were selected: 6 NMR metabolites (Figure 2.7D), 7 MS metabolites (Figure 2.7E), 4 cytokines (Figure 2.7F), and 10 total predictive markers when combining all data sets (Figure 2.7G) from each model respectively. PLSR was then retrained on

each omics data set. NMR had the greatest R2 value (R2=0.86) followed by MS (R2=0.83) and cytokines (R2=0.70) (Figure 2.7 H-J). Combining these data sets showed high predictability (R2=0.88), but not higher than NMR or MS alone. Furthermore, we used a leave-one-out cross validation approach to perform some additional level of validation. In this approach, one of the samples is removed from the dataset and used as a "known unknown". A new model is then built and used to predict the removed sample. This process is repeated for all samples and then the average error computed.

2.5 DISCUSSION

MSC therapies are currently being investigated due to their immunomodulatory properties, but translation to the clinic has been a challenge because of the heterogeneity of MSCs and a lack of CQAs that predict potency.[4,35] Combinatorial, matrix-based approaches may help overcome these challenges by encompassing more than one functional metric since MSCs modulate the immune system using different mechanisms.[10] In this study, we combined comprehensive metabolomics profiling with non-destructive cytokine profiling to determine several predictive markers for assessing MSC immunosuppressive capacity. Using a composite functional score, these markers were strongly correlated with MSC functional capacity. The approach outlined in this study takes large data sets that sample distinct cellular functions and identifies important features for MSC potency prediction.

Cellular metabolism is a key regulator of MSC fate and immunomodulatory potency.[15] Using an NMR based metabolomics approach, dynamic changes between cell lines and passages were observed. BM182 at P3 was functionally better than P1 and P2. Several intracellular metabolites were positively and negatively correlated with MSC functional capacity. The amino acids serine and asparagine were significant based on a PLSR model with VIP selection. Serine

levels have been shown to control the self-renewal of epidermal stem cells (EpdSCs) as decreased extracellular serine activates de novo serine synthesis and promotes epidermal differentiation of EpdSCs. It has also been shown that blocking serine synthesis facilitates malignant progression.[36] Asparagine has been shown to regulate stem cell proliferation.[37] Additionally, depletion of asparagine in cell culture medium results in diminished cell growth.[38] NN-dimethylglycine, a derivative of the amino acid glycine, is also positively correlated with MSC function. It is also a byproduct of the metabolism of choline. To our knowledge, there are no studies that demonstrate a relationship between NN-dimethylglycine and stem cell biology and thus further investigation is warranted. Phosphocreatine has been shown to reduce reactive oxygen species and protect against diabetes-induced kidney injury.[39,40] Myo-inositol is an important growth-promoting factor of mammalian cells, and possibly acts as an osmolyte.[41,42] Myo-inositol constitutes a component of membrane phospholipids and mediates osmoregulation.[43] All the identified metabolites play essential roles in cell growth and facilitate cell proliferation although their role in MSC immunomodulatory capacity needs to be further investigated.

MS-based metabolic profiling revealed 7 metabolites that were associated with MSC immunomodulatory potency. Four of these were annotated as phosphatidylcholines (PCs), including PC(O-36:4), PC(O-38:4), and PC(O-32:0), and PC(O-34:0). PC constitutes a major portion of the cell membrane and play an important role in cellular reprogramming and signaling.[44] The intermediate of PC synthesis or hydrolysis, lysophosphatidylcholines (LPCs), have been reported as markers for discriminating different MSC sources and could be related to differences in MSC differentiation capacity and immunomodulatory properties.[26] The PCs in our study were negatively correlated with MSC immunomodulatory capacity. Lower levels of PCs

were detected in iMSCs at all passages and BM 182 at passage 3, which were the MSC groups that demonstrated higher immunosuppressive capacity. Furthermore, we discovered that the 4 PCs group into 2 pairs (PC(O-38:4)/PC(O-36:4) and PC(O-34:0)/ PC(O-32:0)) sharing the same unsaturation degree and a difference of 2 carbons in their fatty acid chain composition, suggesting an underlying, yet unexplained, connection of those PC in their biosynthesis pathway. Increases in unsaturation levels of polyunsaturated PCs may alter membrane fluidity and hence can contribute to changes in MSC morphology, which has also been shown to predict MSC function.[45,46,47] However, to date, the biological role of PCs in stem cell metabolism at the fatty acid chain level is still poorly understood.

MSCs have also been shown to have beneficial effects by secreting proteins to modulate cell behavior in regenerative medicine and health applications.[48–50] For this study, cytokines that span multiple MSC functions of angiogenesis, tissue repair, and recruitment of immune cells were quantified.[51] The amount of each secreted cytokine/growth factor was investigated in a non-destructive manner to enable monitoring of temporal changes due to cell secretion, media changes during expansion and passaging, as well as cell uptake through autocrine or paracrine signaling. Cytokine profiling in MSCs has been described in the literature as a metric of MSC functionality, with certain secreted cytokines upregulated in MSCs, and other cytokines unchanged or reduced, and secreted in multiple cell-lines and donors.[10,52] By investigating levels of cytokines in MSC culture media in conjunction with metabolites and T cell suppression, we have developed an assay matrix for predicting MSC potency for immunomodulation. Besides serving as potential effectors of MSC immunomodulatory function, the cytokines profiled in this study have also been shown to directly impact MSC behavior.[53,54] A potential function is priming of MSCs, where MSCs are conditioned with specific cytokines to increase their

immunomodulatory properties.[10] Priming may be efficacious in instances where there is low MSC survival potential ex vivo or differences in sources and donor reduces effectiveness of MSC for use in regenerative and immunomodulatory applications. MSC priming using our in-process cytokines and culture conditions can be used to develop substrates or engineered tissue for regenerative medicine.[55] Also, non-destructive monitoring of secreted factors in spent media could potentially serve as predictive markers for large scale MSC manufacturing (in bioreactors, for example). MSC-secreted cytokines can regulate MSC function both in an autocrine and paracrine manner. For example, the binding of secreted IL-8 to its receptor CXCR1 or CXCR2 can activate intracellular PI3K, MAPK, Akt phosphorylation and initiate functions of cell survival, angiogenesis and cell migration.[56] In contrast, targeted ablation of secreted cytokines such as IL-6, either by gene silencing or inhibition, led to reduced MSC proliferation and reduced capacity of MSCs to suppress T cell proliferation.[57] Ultimately, studying this crosstalk between MSCs and secreted cytokine may be a relevant aspect of MSC expansion for manufacturing.

It is well documented that MSC functional heterogeneity is derived from differences in donor/tissue source, MSC doubling level, and manufacturing conditions.[35,58] Being able to understand and predict these differences is a challenge that needs to be addressed in order to advance MSC therapies. Knowing what to measure can help screen for high potency MSCs and assess when these MSCs begin to lose potency due to senescence.[46,59,60] Metabolomics and cytokine profiling elucidated several correlated features that, when used alone or in combination, were indicative of MSC potency and were able to predict an increase in potency in the BM182 line. IL-6 and IL-8 are both inflammatory cytokines that recruit immune cells such as T cells, neutrophils, and macrophages. They have also been shown to inhibit T cell apoptosis and

regulatory T cell differentiation.[61–63] Higher levels of these cytokines were secreted by less potent lines (BM71). Although the role of PCs in MSCs on immunomodulatory capacity is largely unknown, studies have shown that oxidized phospholipids, such as PCs, play a role in preventing the activation of T cells and dendritic cells as well as mediate apoptosis.[64–67] Apoptosis of MSCs by cytotoxic T cells has been shown to play an important role in their immunomodulatory capacity.[68] Myo-inositol and serine's role in MSC immune suppression has not been investigated to this point, but soluble myo-inositol has been shown to be effective in treating autoimmune diseases such as thyroiditis and hypothyroidism.[69] Further investigation into the pathways involving these metabolites will improve our understanding of how MSCs modulate the immune system.

Effective prediction of MSC potency is an important factor in manufacturing high quality therapies. Predicting MSC functional capacity has been a major challenge because MSCs can exert their immunomodulatory effects through a number of different mechanisms and immune cells. Therefore, using a combination of cell metabolites and secreted cytokines can help better predict MSC potency and set specific markers to aid in process by design cell manufacturing systems.[2,4,10,70] Our study used a combination of metabolites and cytokines in order to better predict MSC potency. These are easy to target and measure for manufacturing and understanding how these metabolites affect cell function can help refine and improve the manufacturing process. This approach of predictive marker discovery and understanding can also be translated into other cell therapies such as chimeric antigen receptor T-cell (CAR-T), iPSCs, neural stem cells, and even MSC-derived extracellular vesicles. Moving forward, interrogating pathways that involve these metabolites will be important for assay development and better understanding the relationship of MSC metabolism with immunomodulation. Non-destructive, in-process

monitoring of MSC metabolism using conditioned medium will also enable on-demand, precise control of MSC manufacturing. Finally, this discovery platform can be used to establish MSC predictive markers for other therapeutic applications involving differentiation (e.g. osteo-, adipo-, and chondrogenesis), tissue engineering, cancer treatment, and angiogenesis.

2.6 REFERENCES

1. Castro-Manrreza, M. E. & Montesinos, J. J. Immunoregulation by mesenchymal stem cells: Biological aspects and clinical applications. J. Immunol. Res. 2015, (2015).
2. Galipeau, J. et al. International Society for Cellular Therapy perspective on immune functional assays for mesenchymal stromal cells as potency release criterion for advanced phase clinical trials. Cytotherapy 18, 151–159 (2015).
3. Olsen, T. R., Ng, K. S., Lock, L. T., Ahsan, T. & Rowley, J. A. Peak MSC-Are we there yet? Frontiers in Medicine vol. 5 (2018).
4. ROBB, K. P., FITZGERALD, J. C., BARRY, F. & VISWANATHAN, S. Mesenchymal stromal cell therapy: progress in manufacturing and assessments of potency. Cytotherapy 21, 289–306 (2019).
5. de Wolf, C., van de Bovenkamp, M. & Hoefnagel, M. Regulatory perspective on in vitro potency assays for human mesenchymal stromal cells used in immunotherapy. Cytotherapy vol. 19 784–797 (2017).
6. Guan, Q., Li, Y., Shpiruk, T., Bhagwat, S. & Wall, D. A. Inducible indoleamine 2,3-dioxygenase 1 and programmed death ligand 1 expression as the potency marker for mesenchymal stromal cells. Cytotherapy 20, 639–649 (2018).
7. Bernardo, M. E. & Fibbe, W. E. Mesenchymal stromal cells: Sensors and switchers of inflammation. Cell Stem Cell vol. 13 392–402 (2013).

8. Shi, Y. et al. How mesenchymal stem cells interact with tissue immune responses. Trends in Immunology vol. 33 136–143 (2012).

9. Keating, A. Mesenchymal stromal cells: New directions. Cell Stem Cell vol. 10 709–716 (2012).

10. Chinnadurai, R. et al. Potency Analysis of Mesenchymal Stromal Cells Using a Combinatorial Assay Matrix Approach. Cell Rep. 22, 2504–2517 (2018).

11. Kamota, T. et al. Ischemic Pre-Conditioning Enhances the Mobilization and Recruitment of Bone Marrow Stem Cells to Protect Against Ischemia/Reperfusion Injury in the Late Phase. J. Am. Coll. Cardiol. 53, 1814–1822 (2009).

12. Afzal, M. R. et al. Preconditioning Promotes Survival and Angiomyogenic Potential of Mesenchymal Stem Cells in the Infarcted Heart via NF-kB Signaling. www.liebertonline.com=ars.

13. Shi, R. Z., Wang, J. C., Huang, S. H., Wang, X. J. & Li, Q. P. Angiotensin II induces vascular endothelial growth factor synthesis in mesenchymal stem cells. Exp. Cell Res. 315, 10–15 (2009).

14. Mattar, P. & Bieback, K. Comparing the immunomodulatory properties of bone marrow, adipose tissue, and birth-associated tissue mesenchymal stromal cells. Frontiers in Immunology vol. 6 (2015).

15. Liu, Y. & Ma, T. Metabolic regulation of mesenchymal stem cell in expansion and therapeutic application. Biotechnol. Prog. 31, 468–481 (2015).

16. Liu, Y., Yuan, X., Muñoz, N., Logan, T. M. & Ma, T. Commitment to Aerobic Glycolysis Sustains Immunosuppression of Human Mesenchymal Stem Cells. Stem Cells Transl. Med. 8, 93–106 (2019).

17. Yuan, X., Logan, T. M. & Ma, T. Metabolism in human mesenchymal stromal cells: A missing link between HMSC biomanufacturing and therapy? Frontiers in Immunology vol. 10 977 (2019).

18. Goodarzi, P. et al. I IJ JM MC CM M Metabolomics Analysis of Mesenchymal Stem Cells. (2019).

19. Dunn, W. B., Bailey, N. J. C. & Johnson, H. E. Measuring the metabolome: Current analytical technologies. Analyst vol. 130 606–625 (2005).

20. Theodoridis, G. A., Gika, H. G., Want, E. J. & Wilson, I. D. Liquid chromatography-mass spectrometry based global metabolite profiling: A review. Anal. Chim. Acta 711, 7–16 (2012).

21. Jiye, A. et al. Extraction and GC/MS analysis of the human blood plasma metabolome. Anal. Chem. 77, 8086–8094 (2005).

22. Vorkas, P. A. et al. Untargeted UPLC-MS profiling pipeline to expand tissue metabolome coverage: Application to cardiovascular disease. Anal. Chem. 87, 4184–4193 (2015).

23. Want, E. J. et al. Global metabolic profiling procedures for urine using UPLC-MS. Nat. Protoc. 5, 1005–1018 (2010).

24. Fei, F., Bowdish, D. M. E. & McCarry, B. E. Comprehensive and simultaneous coverage of lipid and polar metabolites for endogenous cellular metabolomics using HILIC-TOF-MS. Anal. Bioanal. Chem. 406, 3723–3733 (2014).

25. Abdul-Hamid, N. A. et al. NMR metabolomics for evaluating passage number and harvesting effects on mammalian cell metabolome. Anal. Biochem. 576, 20–32 (2019).

26. Lee, S. J. et al. Comparative study on metabolite level in tissue-specific human mesenchymal stem cells by an ultra-performance liquid chromatography quadrupole time of flight mass spectrometry. Anal. Chim. Acta 1024, 112–122 (2018).

27. Carpenter, A. E. et al. CellProfiler: Image analysis software for identifying and quantifying cell phenotypes. Genome Biol. 7, (2006).

28. Delaglio, F. et al. NMRPipe: A multidimensional spectral processing system based on UNIX pipes. J. Biomol. NMR 6, 277–293 (1995).

29. Kumar, K., Schweiggert, R. & Patz, C.-D. Introducing a novel procedure for peak alignment in one-dimensional 1 H-NMR spectroscopy: a prerequisite for chemometric analyses of wine samples . Anal. Methods 12, 3626–3636 (2020).

30. Dieterle, F., Ross, A., Schlotterbeck, G. & Senn, H. Probabilistic quotient normalization as robust method to account for dilution of complex biological mixtures. Application in1H NMR metabonomics. Anal. Chem. 78, 4281–4290 (2006).

31. Bingol, K., Li, D. W., Zhang, B. & Brüschweiler, R. Comprehensive metabolite identification strategy using multiple two-dimensional NMR spectra of a complex mixture implemented in the COLMARm web server. Anal. Chem. 88, 12411–12418 (2016).

32. Walejko, J. M., Chelliah, A., Keller-Wood, M., Gregg, A. & Edison, A. S. Global metabolomics of the placenta reveals distinct metabolic profiles between maternal and fetal placental tissues following delivery in non-labored women. Metabolites 8, (2018).

33. Shi, G.-P. et al. Deficiency of the Cysteine Protease Cathepsin S Impairs Microvessel Growth. Circ. Res. 92, 493–500 (2003).

34. Ward, C. et al. Antibody Targeting of Cathepsin S Inhibits Angiogenesis and Synergistically Enhances Anti-VEGF. PLoS One 5, e12543 (2010).

35. Wilson, A., Hodgson-Garms, M., Frith, J. E. & Genever, P. Multiplicity of mesenchymal stromal cells: Finding the right route to therapy. Frontiers in Immunology vol. 10 1112 (2019).

36. Baksh, S. C. et al. Extracellular serine controls epidermal stem cell fate and tumour initiation. Nat. Cell Biol. 22, 779–790 (2020).

37. Luo, M., Brooks, M. & Wicha, M. S. Asparagine and Glutamine: Co-conspirators Fueling Metastasis. Cell Metabolism vol. 27 947–949 (2018).

38. Palmer, E. E. et al. Asparagine Synthetase Deficiency causes reduced proliferation of cells under conditions of limited asparagine. Mol. Genet. Metab. 116, 178–186 (2015).

39. Jing, Z. et al. Phosphocreatine Promotes Osteoblastic Activities in H2O2-Induced MC3T3-E1 Cells by Regulating SIRT1/FOXO1/PGC-1α Signaling Pathway. Curr. Pharm. Biotechnol. 22, 609–621 (2020).

40. Shopit, A. et al. Protection of diabetes-induced kidney injury by phosphocreatine via the regulation of ERK/Nrf2/HO-1 signaling pathway. Life Sci. 242, 117248 (2020).

41. Polito, L., Laganà, A. S. & Chhetri, D. R. Myo-Inositol and Its Derivatives: Their Emerging Role in the Treatment of Human Diseases. (2019) doi:10.3389/fphar.2019.01172.

42. Jansen, J. F. A. et al. Stem cell profiling by nuclear magnetic resonance spectroscopy. Magn. Reson. Med. 56, 666–670 (2006).

43. Biology of Inositols and Phosphoinositides. vol. 39 (Springer US, 2006).

44. Ridgway, N. D. The role of phosphatidylcholine and choline metabolites to cell proliferation and survival. Critical Reviews in Biochemistry and Molecular Biology vol. 48 20–38 (Taylor & Francis, 2013).

45. Meissen, J. K. et al. Induced Pluripotent Stem Cells Show Metabolomic Differences to Embryonic Stem Cells in Polyunsaturated Phosphatidylcholines and Primary Metabolism. PLoS One 7, (2012).

46. Klinker, M. W., Marklein, R. A., Lo Surdo, J. L., Wei, C. H. & Bauer, S. R. Morphological features of IFN-γ-stimulated mesenchymal stromal cells predict overall immunosuppressive capacity. Proc. Natl. Acad. Sci. U. S. A. 114, E2598–E2607 (2017).

47. Sohn, J., Lin, H., Fritch, M. R. & Tuan, R. S. Influence of cholesterol/caveolin-1/caveolae homeostasis on membrane properties and substrate adhesion characteristics of adult human mesenchymal stem cells. Stem Cell Res. Ther. 9, 86 (2018).

48. Pittenger, M. F. et al. Mesenchymal stem cell perspective: cell biology to clinical progress. npj Regenerative Medicine vol. 4 1–15 (2019).

49. Musiał-Wysocka, A., Kot, M. & Majka, M. The Pros and Cons of Mesenchymal Stem Cell-Based Therapies. doi:10.1177/0963689719837897.

50. Parekkadan, B. & Milwid, J. M. Mesenchymal Stem Cells as Therapeutics. (2010) doi:10.1146/annurev-bioeng-070909-105309.

51. Samsonraj, R. M. et al. Concise Review: Multifaceted Characterization of Human Mesenchymal Stem Cells for Use in Regenerative Medicine. Stem Cells Transl. Med. 6, 2173–2185 (2017).

52. Park, C. W. et al. Cytokine secretion profiling of human mesenchymal stem cells by antibody array. Int. J. Stem Cells 2, 59–68 (2009).

53. Lacey, D. C., Simmons, P. J., Graves, S. E. & Hamilton, J. A. Proinflammatory cytokines inhibit osteogenic differentiation from stem cells: implications for bone repair during inflammation. Osteoarthr. Cartil. 17, 735–742 (2009).

54. Leuning, D. G. et al. The cytokine secretion profile of mesenchymal stromal cells is determined by surface structure of the microenvironment. Sci. Rep. 8, 1–9 (2018).

55. Noronha Nc, N. D. C. et al. Priming approaches to improve the efficacy of mesenchymal stromal cell-based therapies. Stem Cell Research and Therapy vol. 10 (2019).

56. Yang, A. et al. IL-8 Enhances Therapeutic Effects of BMSCs on Bone Regeneration via CXCR2-Mediated PI3k/Akt Signaling Pathway. Cell. Physiol. Biochem. 48, 361–370 (2018).

57. Dorronsoro, A. et al. Intracellular role of IL-6 in mesenchymal stromal cell immunosuppression and proliferation. Sci. Rep. 10, 21853 (2020).

58. Kern, S., Eichler, H., Stoeve, J., Klüter, H. & Bieback, K. Comparative Analysis of Mesenchymal Stem Cells from Bone Marrow, Umbilical Cord Blood, or Adipose Tissue. Stem Cells 24, 1294–1301 (2006).

59. Killer, M. C. et al. Immunosuppressive capacity of mesenchymal stem cells correlates with metabolic activity and can be enhanced by valproic acid. Stem Cell Res. Ther. 8, 100 (2017).

60. Turinetto, V., Vitale, E. & Giachino, C. Senescence in human mesenchymal stem cells: Functional changes and implications in stem cell-based therapy. International Journal of Molecular Sciences vol. 17 1164 (2016).

61. Anton, K., Banerjee, D. & Glod, J. Macrophage-Associated Mesenchymal Stem Cells Assume an Activated, Migratory, Pro-Inflammatory Phenotype with Increased IL-6 and CXCL10 Secretion. PLoS One 7, e35036 (2012).

62. Rose-John, S. Il-6 trans-signaling via the soluble IL-6 receptor: Importance for the proinflammatory activities of IL-6. International Journal of Biological Sciences vol. 8 1237–1247 (2012).

63. Harada, A. et al. Essential involvement of interleukin-8 (IL-8) in acute inflammation. in Journal of Leukocyte Biology vol. 56 559–564 (Federation of American Societies for Experimental Biology, 1994).

64. Seyerl, M. et al. Oxidized phospholipids induce anergy in human peripheral blood T cells. Eur. J. Immunol. 38, 778–787 (2008).

65. Serbulea, V., DeWeese, D. & Leitinger, N. The effect of oxidized phospholipids on phenotypic polarization and function of macrophages. Free Radical Biology and Medicine vol. 111 156–168 (2017).

66. Blüml, S. et al. Oxidized Phospholipids Negatively Regulate Dendritic Cell Maturation Induced by TLRs and CD40. J. Immunol. 175, 501–508 (2005).

67. Sareen, N. et al. Early passaging of mesenchymal stem cells does not instigate significant modifications in their immunological behavior. Stem Cell Res. Ther. 9, 121 (2018).

68. Galleu, A. et al. Apoptosis in mesenchymal stromal cells induces in vivo recipient-mediated immunomodulation. Sci. Transl. Med. 9, (2017).

69. Fallahi, P. et al. Myo-inositol in autoimmune thyroiditis, and hypothyroidism. Reviews in Endocrine and Metabolic Disorders vol. 19 349–354 (2018).

70. Galipeau, J. & Sensébé, L. Mesenchymal Stromal Cells: Clinical Challenges and Therapeutic Opportunities. Cell Stem Cell 22, 824–833 (2018).

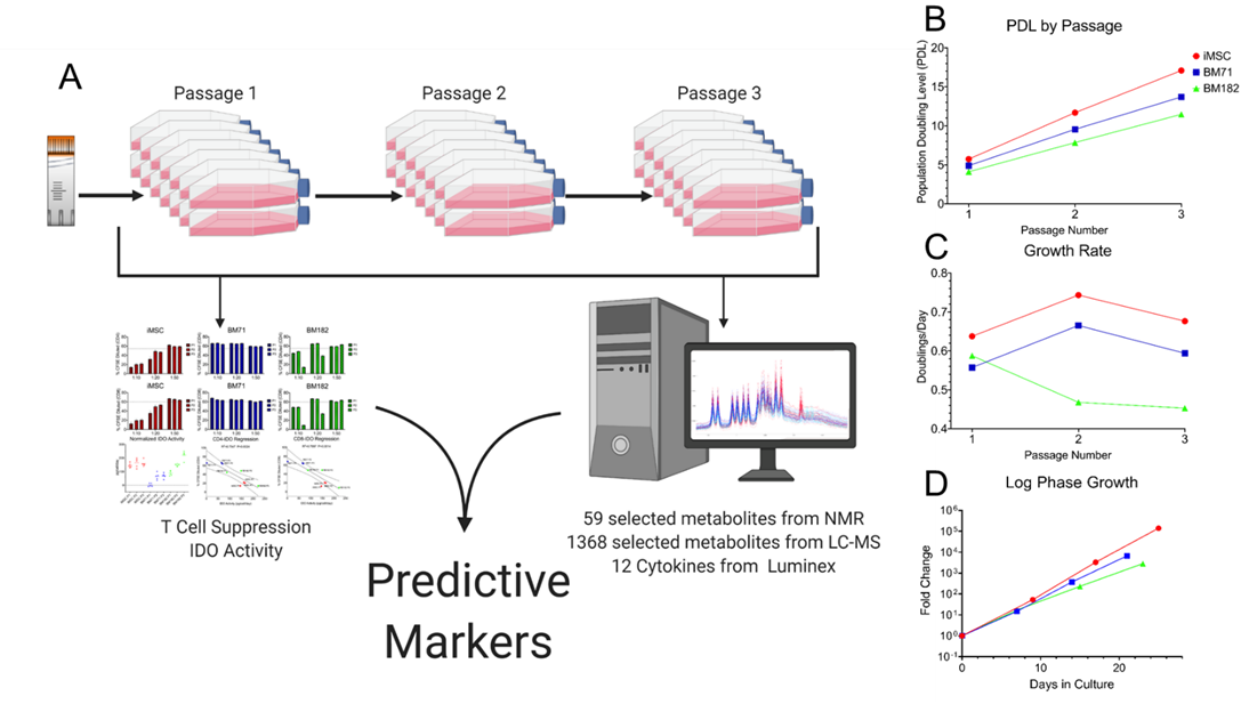

Figure 2.1. MSC expansion workflow and growth characteristics. (A) MSC characterization workflow from expanded cells to discover predictive markers. (B) Population doubling level changes of three MSC lines over three passages. (C) MSC growth rate in doublings per day over three passages. (D) Log phase growth characteristics of each MSC line over the number of days in culture.

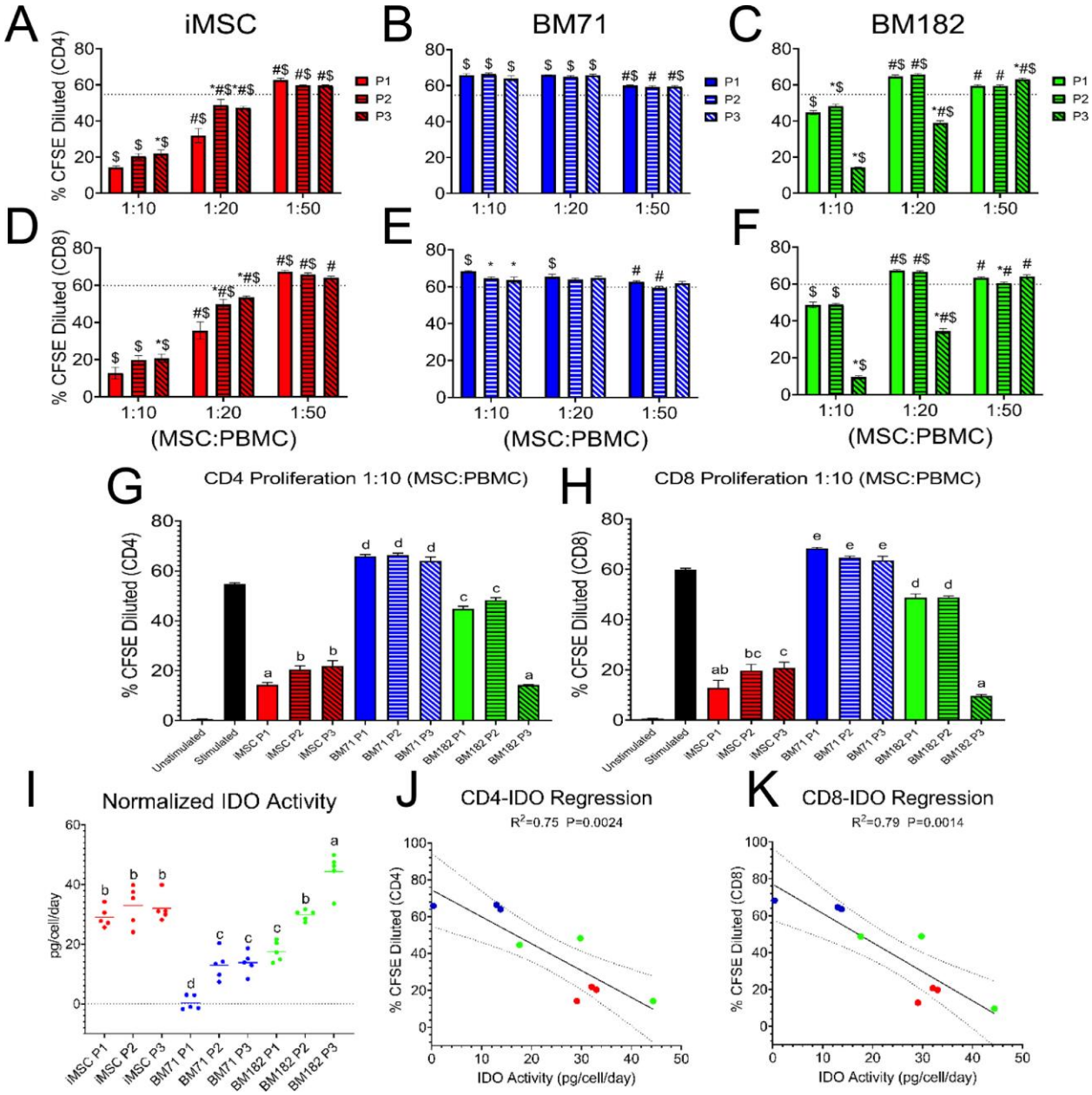

Figure 2.2. MSC functional capacity characterized by T-cell proliferation and IDO activity. MSCs were co-cultured with stimulated PBMCs at three different MSC:PBMC ratios (1:10, 1:20, 1:50). (A–C) CD4+ and (D–F) CD8+ T-cell proliferation was assessed at each passage and ratio by % CFSE dilution. A two-way ANOVA was used to determine whether there was a significant difference from P1 within a ratio (*), a significant difference from the 1:10 ratio within a passage (#) or a significant difference from the stimulated control ($). (G) CD4+ and

(H) CD8+ T-cell proliferation comparing all cell lines and passages at the 1:10 ratio and (I) IDO activity measured by L-kynurenine levels normalized to cell number and days in culture were analyzed using one-way ANOVA with Tukey's post-hoc test to determine significance. Linear regression was performed to determine the relationship between IDO activity and (J) CD4+ and (K) CD8+ T-cell proliferation. Groups not sharing the same lettering in G, H and I represent a statistical difference. $P < 0.05$. ANOVA, analysis of variance; CFSE, carboxyfluorescein succinimidyl ester.

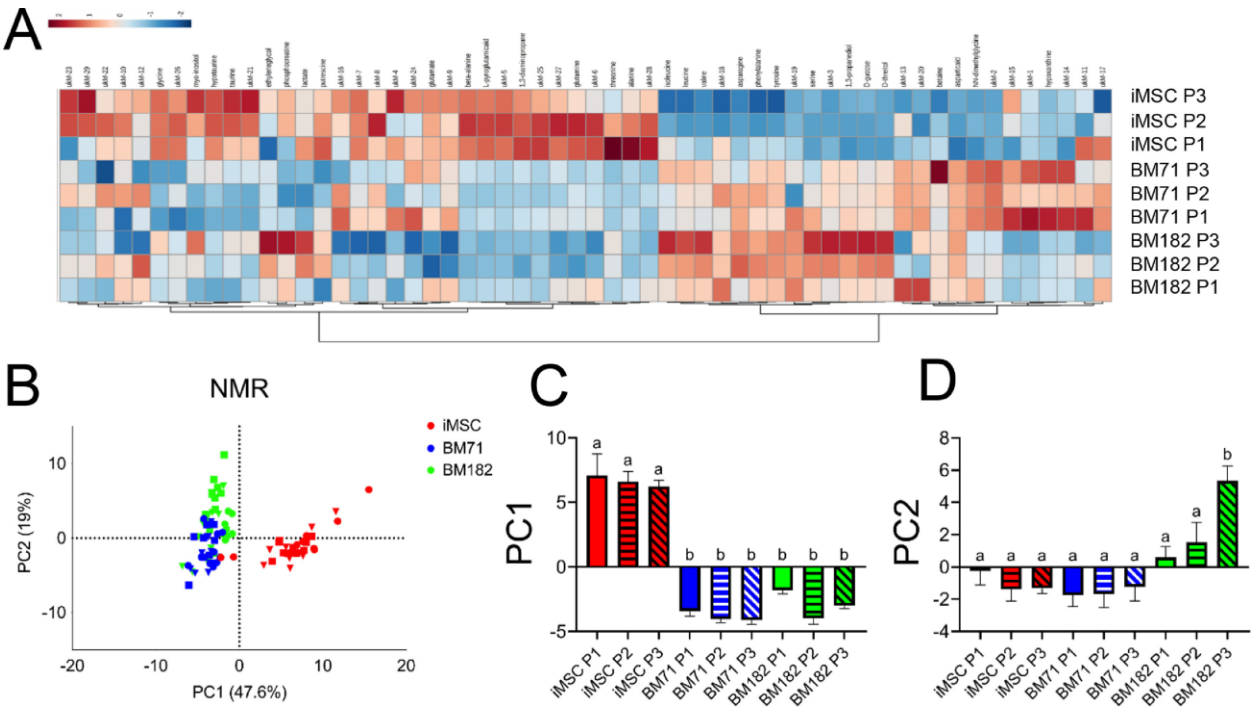

Figure 2.3. MSC metabolic profile from NMR analysis. (A) Heat map of all 58 metabolites using Euclidian distance measure and Ward clustering method. (B) Unsupervised PCA of all metabolites for each cell line at three passages (P1 = circle, P2 = triangle, P3 = square). (C) One-way ANOVA comparison of average PC1 value. (D) One-way ANOVA comparison of average PC2 value. Groups not sharing the same lettering in C and D represent a statistical difference. $P < 0.05$. ANOVA, analysis of variance.

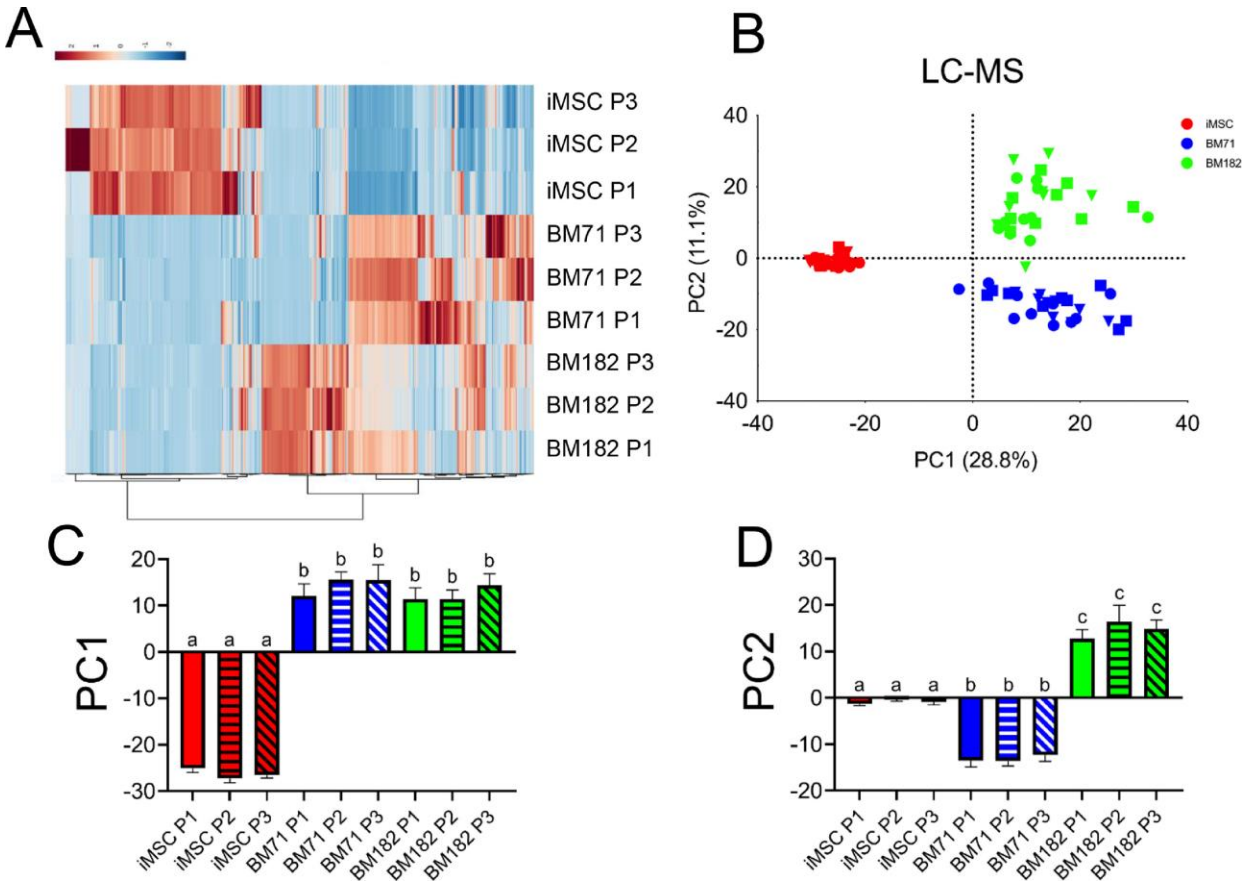

Figure 2.4. MSC metabolic profile from MS analysis. (A) Heat map of 1386 metabolites using Euclidian distance measure and Ward clustering method. (B) Unsupervised PCA of all metabolites for each cell line at three passages (P1 = circle, P2 = triangle, P3 = square). (C) One-way ANOVA comparison of average PC1 value. (D) One-way ANOVA comparison of average PC2 value. Groups not sharing the same lettering in C and D represent a statistical difference. $P < 0.05$. ANOVA, analysis of variance.

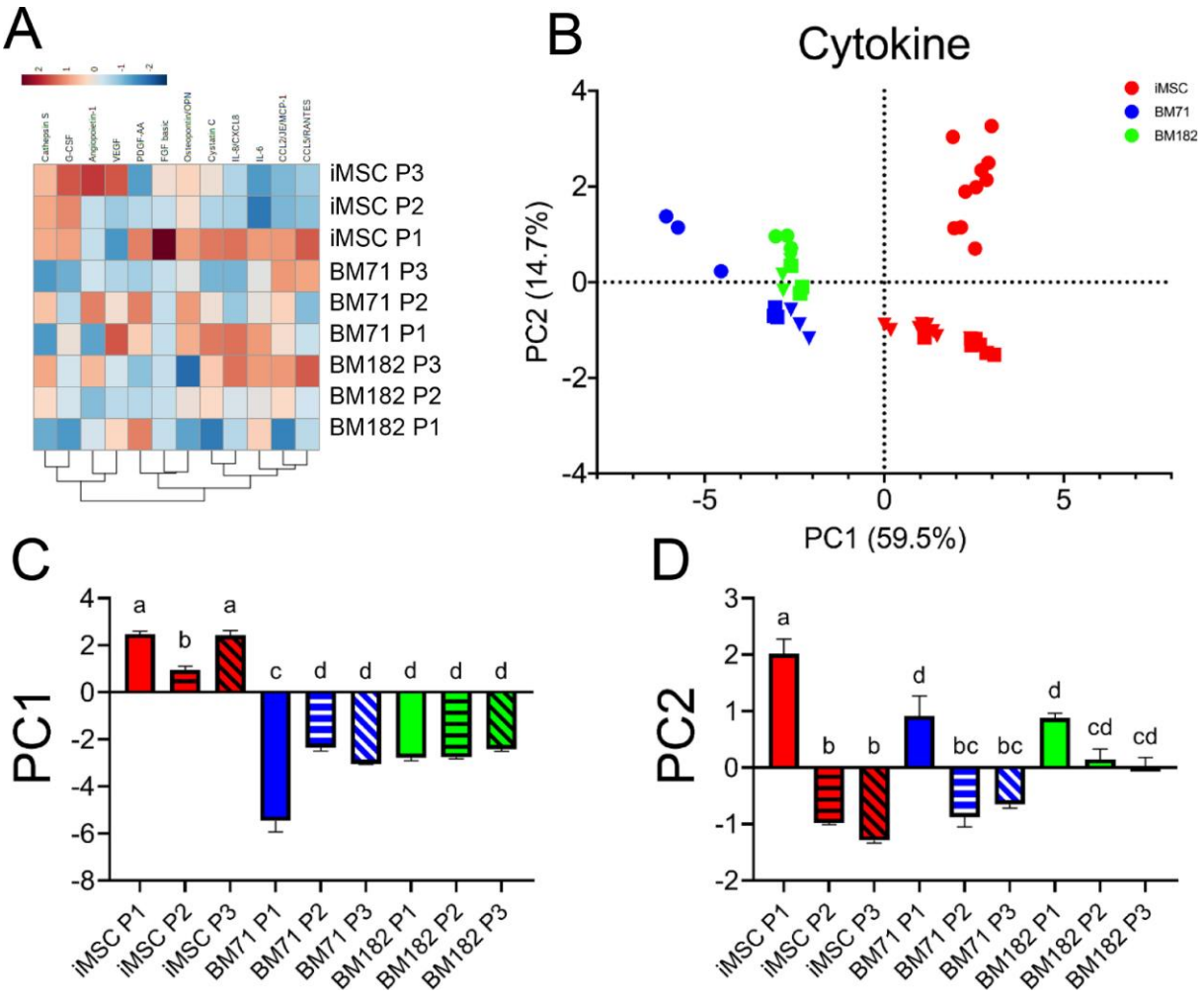

Figure 2.5. MSC cytokine profile. (A) Heat map of all 12 measured cytokines using Euclidian distance measure and Ward clustering method. (B) Unsupervised PCA of all cytokines for each cell line at three passages (P1 = circle, P2 = triangle, P3 = square). (C) One-way ANOVA comparison of average PC1 value. (D) One-way ANOVA comparison of average PC2 value. Groups not sharing the same lettering in C and D represent a statistical difference. $P < 0.05$. ANOVA, analysis of variance.

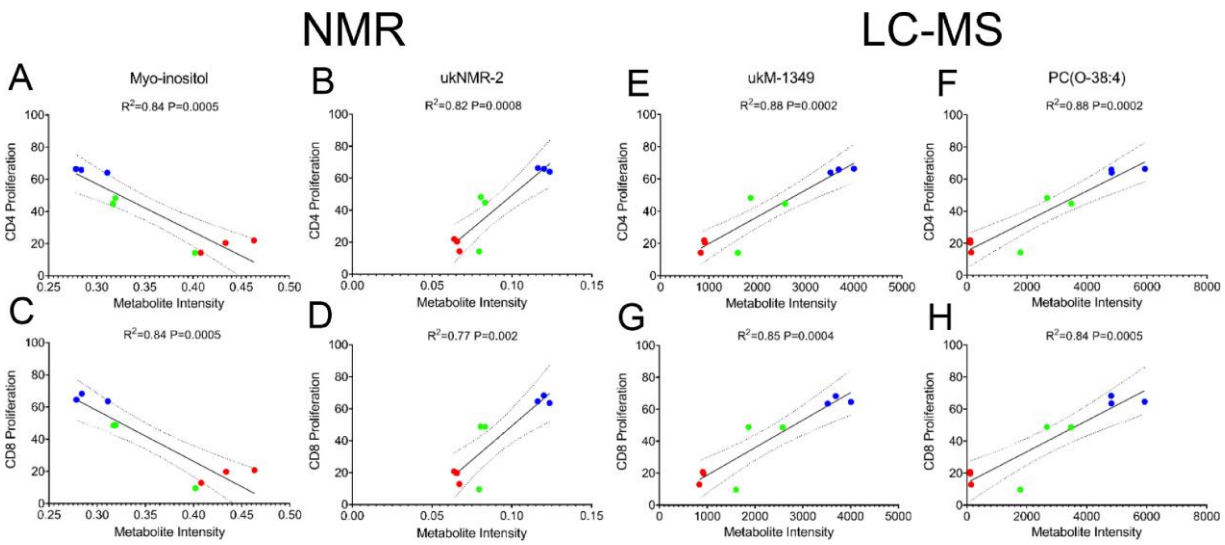

Figure 2.6. Linear regression analysis of the top correlated metabolites. (A,C) Myo-inositol and (B,D) ukNMR-2 had the highest R2 values for CD4+ and CD8+ T-cell proliferation from NMR metabolites. (E,G) ukM-1349 and (F,H) PC(O-38:4) had the highest R2 values for CD4+ and CD8+ T-cell proliferation from MS metabolites. The top 20 metabolites with the highest R2 values were then chosen for further modeling to discover predictive markers. Red = iMSCs, blue = BM71, green = BM182. LC-MS, liquid chromatography MS.

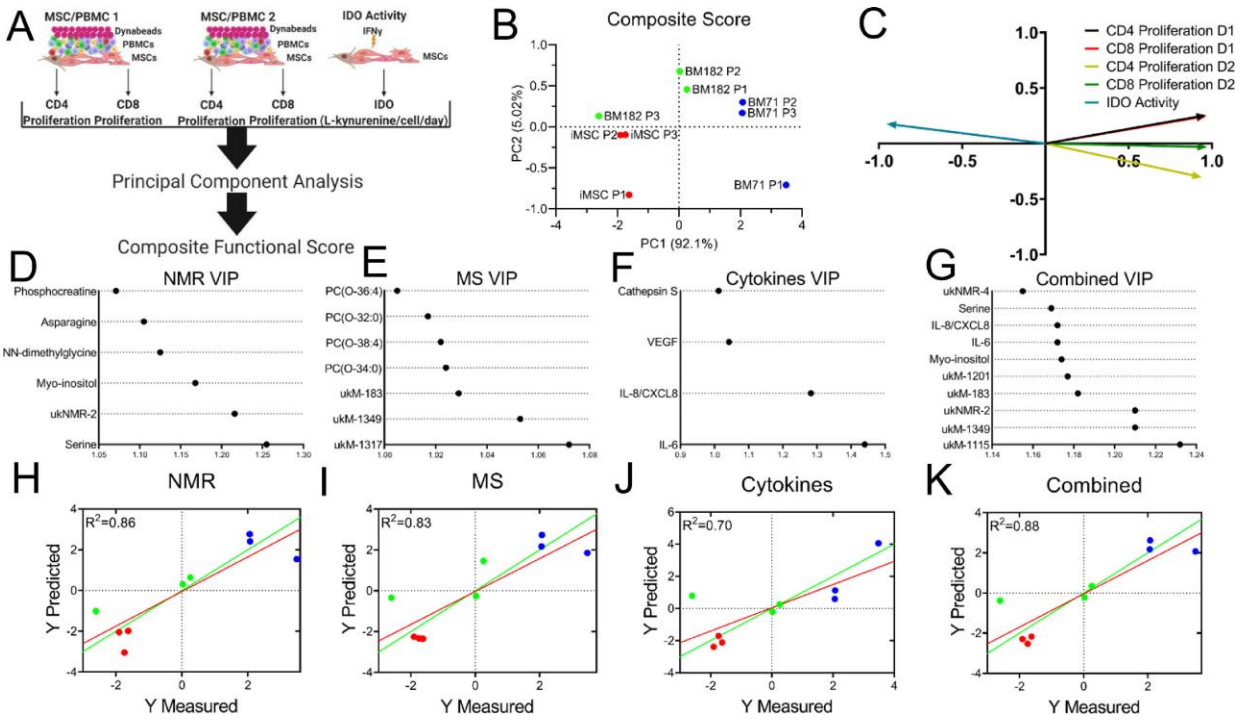

Figure 2.7. PLSR modeling of important features elucidates predictive markers. (A–C) CD4+ and CD8+ T-cell proliferation from two donors and IDO activity (five total functional outputs) were analyzed using PCA. PC1 accounted for 92.1% of the variance and was then taken and used as a composite functional score for further predictive modeling. VIP scores were assigned to the top (D) NMR, (E) MS, (F) cytokine and (G) combined features based on (H–K) PLSR modeling. The VIP molecules chosen are considered predictive markers. IFNγ, interferon gamma.

Laser	EM Filter	Marker	Color / Format	Host / Target	Isotype	Clone	Company	Catalog
638	780/30	CD4	APC/Fire	Mouse anti-Human	IgG1 κ	RPA-T4	BioLegend	67-0047-T025
638	660/20	CD8	APC	Mouse anti-Human	IgG1	CN9V1	BioLegend	orb248718
488	525/40	CFSE	CFSE	N/A	N/A	N/A	BioLegend	423801
405	610/20	Zombie Yellow	Zombie Yellow	N/A anti-All Species	N/A	N/A	BioLegend	423104

Supplemental Table 2.1. PBMC co-culture assay antibodies and flow cytometer information.

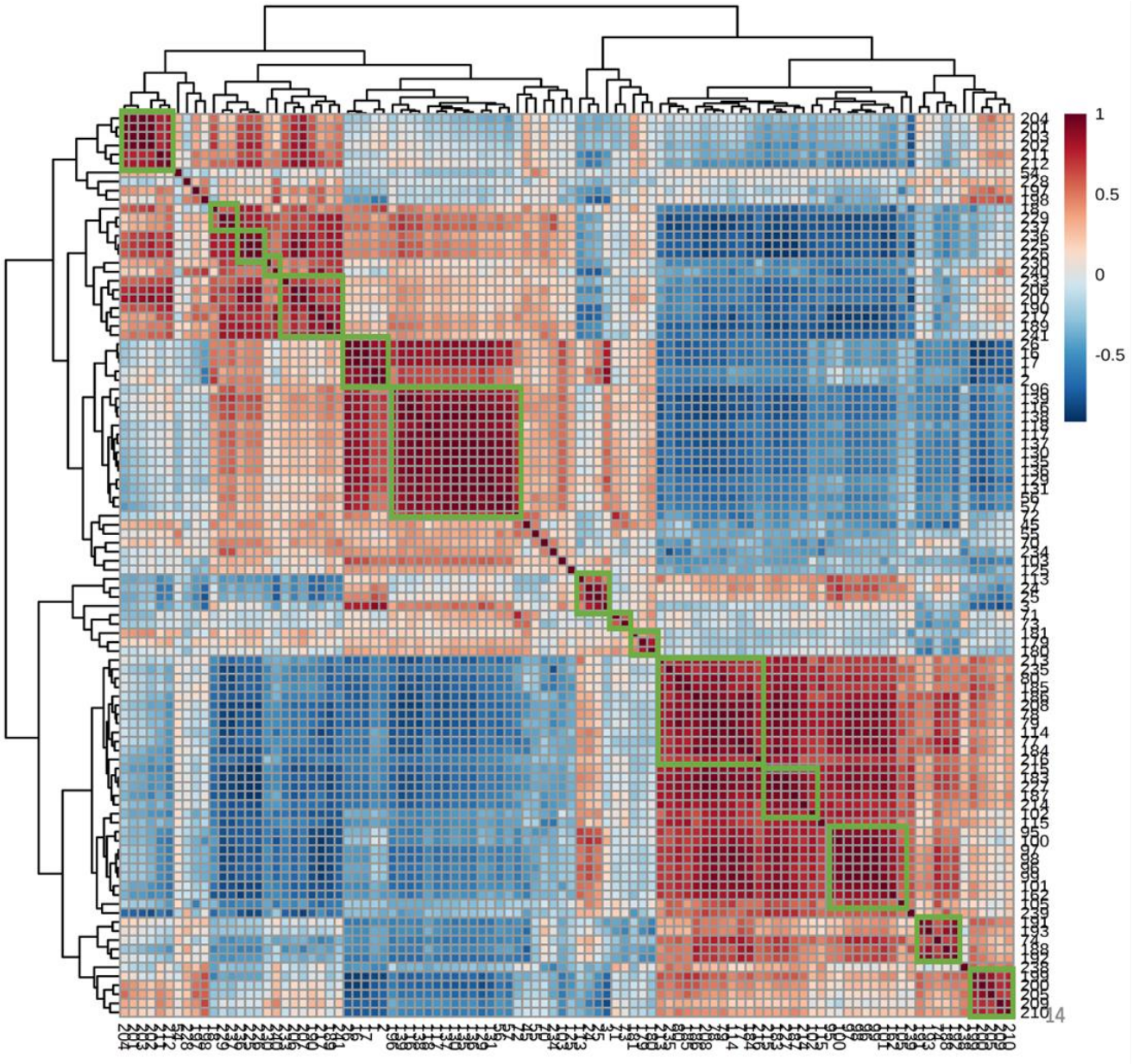

Supplemental Figure 2.1. The correlation map of 100 unknown NMR features. We assume that correlation coefficient values greater or equal to 0.8 indicating those features are from same metabolite and grouped together as Indicated by green box in the figure. The features with correlation coefficient value less than 0.8, we considered them as individual metabolites. Total

100 unknown features were grouped to 29 unknown metabolites. The color bar indicating correlation coefficient values calculated using Z score.

HILIC Separation Method				
Time (min)	**A**	**B**	**Flow rate (ml/min)**	**Curve**
0	5	95	0.4	5
0.5	5	95	0.4	6
9	70	30	0.4	6
9.4	70	30	0.4	6
9.5	5	95	0.4	6
11	5	95	0.4	6
12	5	95	0.4	6

Supplemental Table 2.2. Methods information. Chromatographic gradient for HILIC method: mobile phase A was water/acetonitrile (95:5 v/v), with 10 mM ammonium acetate and 0.05% ammonium hydroxide, and B was acetonitrile with 0.05% ammonium hydroxide. Both ionization modes utilized identical mobile phases and identical chromatographic gradients.

Analyte	Function
Angiopoietin-1	Promote angiogenesis and vascular growth
CCL2/MCP-1	Recruits immune cells to sites of inflammation
Cystatin C	Inhibitor of cysteine cathepsin proteases
IL-8/CXCL8	Stimulates neutrophil migration and phagocytosis
PDGF-AA	Cell growth, differentiation and survival
Cathepsin S	Proteolysis, antigen presentation, extracellular functions
CCL5/RANTES	Recruits immune cells to sites of inflammation
FGF basic	Numerous, cell growth and development, embryonic development
IL-6	Numerous, pro-inflammatory signaling
Osteopontin/OPN	Cell migration, adhesion and survival
VEGF	Encourages formation of blood vessels
G-CSF	Stimulates granulocyte and stem cell production and release

Supplemental Table 2.3. List of all cytokines measured and their corresponding function.

Cell-Line/Passage	Population Doubling Level (PDL)	Doublings per Day
iMSC P1	5.7	0.63
iMSC P2	11.7	0.74
iMSC P3	17.1	0.68
BM71 P1	3.9	0.56
BM71 P2	8.6	0.67

Supplemental Table 2.4. PDL and doublings per day values of each cell-line at each passage.

Metabolite	Confidence Score	$CD4^+$ Proliferation PBMC D1 p value	$CD8^+$ Proliferation PBMC D1 p value	$CD4^+$ Proliferation PBMC D2 p value	$CD8^+$ Proliferation PBMC D2 p value
1,3-diaminopropane	3	0.0455	0.0554	0.3778	0.0565
1,3-propanediol	3	0.7056	0.7567	0.7913	0.5208
alanine	4	0.0304	0.0389	0.3416	0.0535
asparagine	4	0.0021	0.0026	0.0963	0.029
aspartic acid	4	0.4647	0.5197	0.9916	0.3624
beta-alanine	4	0.0243	0.0293	0.2331	0.0225
betaine	4	0.5911	0.616	0.7034	0.6191
glucose	4	0.5637	0.6228	0.8347	0.4985
threitol	3	0.044	0.0572	0.3073	0.0579
glutamate	4	0.039	0.0496	0.3276	0.0542
glutamine	4	0.0016	0.0024	0.0612	0.0019
glycine	4	0.0205	0.023	0.1952	0.0152
hypotaurine	4	0.0162	0.0177	0.1662	0.0106
hypoxanthine	4	0.4121	0.3892	0.2808	0.6632
isoleucine	4	0.1163	0.1265	0.5603	0.2372
L-pyroglutamic acid	3	0.156	0.1464	0.1692	0.3623
lactate	4	0.048	0.0597	0.346	0.0472
leucine	4	0.0005	0.0005	0.0238	0.001
myo-inositol	4	0.0028	0.0027	0.0394	0.003
NN-dimethylglycine	4	0.0895	0.0929	0.1941	0.2148
phenylalanine	4	0.0043	0.0068	0.0359	0.0033
phosphocreatine	4	0.0061	0.0077	0.1935	0.0173
putrescine	3	0.0169	0.0193	0.0434	0.103
serine	4	0.0124	0.0133	0.1136	0.0066
taurine	4	0.5886	0.6509	0.8277	0.5039
threonine	4	0.0102	0.0129	0.2188	0.0264
tyrosine	4	0.1816	0.1779	0.203	0.3715
valine	4	0.1328	0.1206	0.0546	0.2482
ukNMR-1	/	0.0751	0.0736	0.0017	0.0282
ukNMR-2	/	0.0008	0.002	0.003	0.0002
ukNMR-3	/	0.6171	0.5474	0.3233	0.8212
ukNMR-4	/	0.0389	0.0484	0.3705	0.0662
ukNMR-5	/	0.0422	0.0524	0.2953	0.0353
ukNMR-6	/	0.1612	0.1993	0.597	0.1639
ukNMR-7	/	0.2288	0.2586	0.7817	0.2074
ukNMR-8	/	0.245	0.2823	0.6771	0.1873
ukNMR-9	/	0.1499	0.1824	0.6002	0.1693
ukNMR-10	/	0.0442	0.055	0.1646	0.0148
ukNMR-11	/	0.9659	0.9898	0.2329	0.6817

ukNMR-12	/	0.1519	0.1857	0.3297	0.0739
ukNMR-13	/	0.6154	0.7216	0.9032	0.536
ukNMR-14	/	0.1316	0.1298	0.0288	0.0916
ukNMR-15	/	0.2037	0.2246	0.7016	0.2187
ukNMR-16	/	0.0748	0.094	0.3894	0.08
ukNMR-17	/	0.1686	0.2018	0.7266	0.2693
ukNMR-18	/	0.5793	0.5728	0.831	0.4587
ukNMR-19	/	0.0916	0.1357	0.229	0.2903
ukNMR-20	/	0.9493	0.9817	0.8399	0.7014
ukNMR-21	/	0.0133	0.0159	0.099	0.0076
ukNMR-22	/	0.0219	0.0259	0.1993	0.0209
ukNMR-23	/	0.0699	0.078	0.1697	0.0222
ukNMR-24	/	0.1738	0.2047	0.7233	0.2166
ukNMR-25	/	0.035	0.0434	0.358	0.0482
ukNMR-26	/	0.0083	0.0106	0.0621	0.0019
ukNMR-27	/	0.0821	0.1035	0.4364	0.0831
ukNMR-28	/	0.0397	0.0516	0.2819	0.0379
ukNMR-29	/	0.0638	0.0706	0.1925	0.0244

Supplemental Table 2.5. NMR identified metabolites, confidence scores and p- values from linear regression model. The metabolites were assigned a confidence level ranging from 1 to 5 according to published criteria.[32]

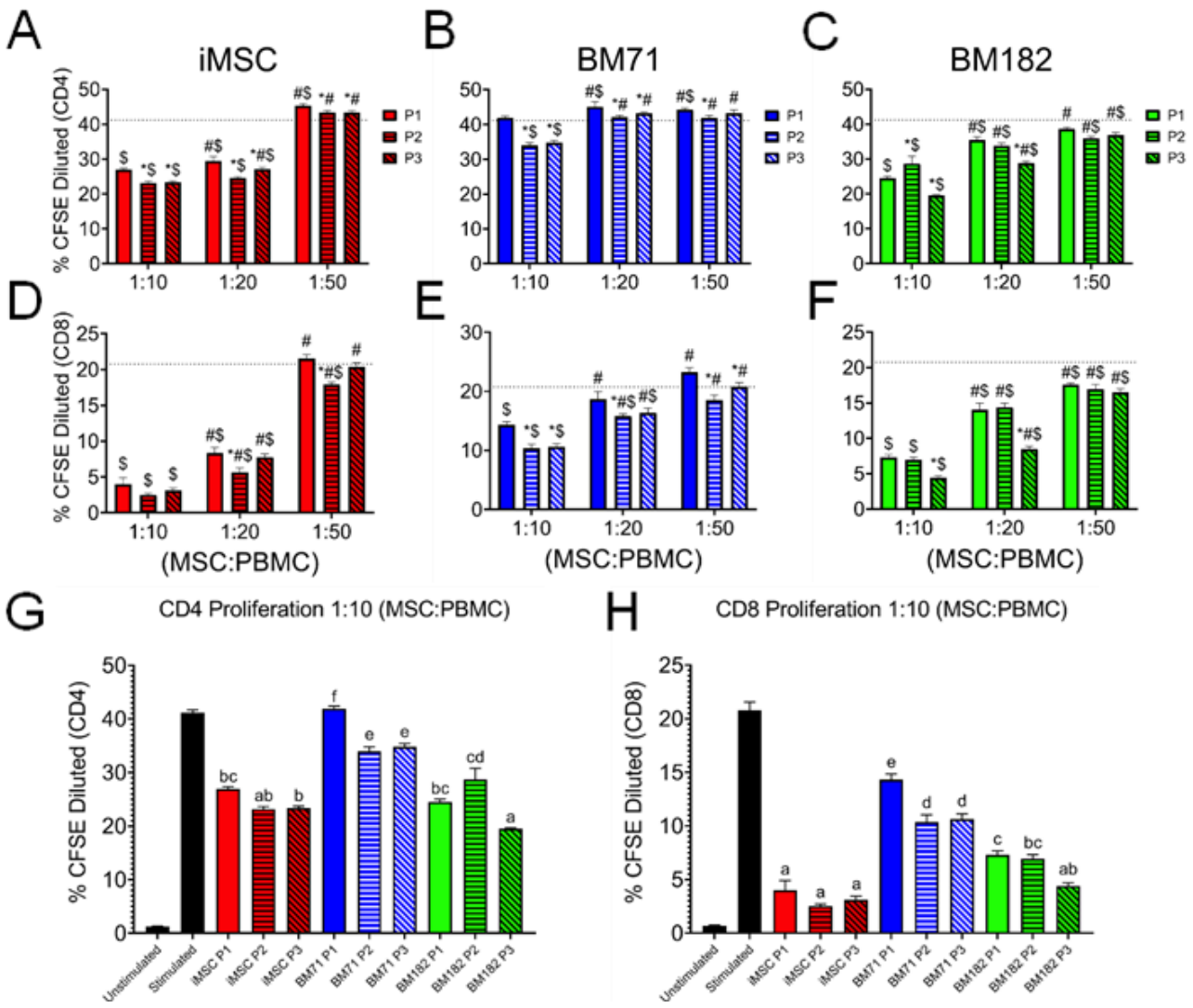

Supplemental Figure 2.2. T cell proliferation assay using a second PBMC donor. MSCs were co-cultured with stimulated PBMCs at three different MSC:PBMC ratios (1:10, 1:20, 1:50). (A-C) CD4+ and (D-F) CD8+ T cell proliferation was assessed at each passage and ratio by % CFSE dilution. A 2-way ANOVA was used in order to determine if there was a significant difference from P1 within a ratio (*), a significant difference from the 1:10 ratio within a passage (#), or a significant difference from the stimulated control ($) with $p<0.05$ considered significant. (G) CD4+ and (H) CD8+ T cell proliferation comparing all cell-lines and passages at the 1:10 ratio. Groups not sharing the same lettering in G and H represents a statistical difference ($p<0.05$).

Metabolite	$CD4^+$ Proliferation PBMC D1 R^2 value	$CD8^+$ Proliferation PBMC D1 R^2 value	$CD4^+$ Proliferation PBMC D2 R^2 value	$CD8^+$ Proliferation PBMC D2 R^2 value	Increasing (+) or Decreasing (-) levels with higher potency
Phosphocreatine	0.71	0.67	0.49	0.73	+
Asparagine	0.76	0.75	0.35	0.52	+
NN-dimethylglycine	0.74	0.75	0.48	0.74	-
Myo-inositol	0.84	0.84	0.54	0.81	-
Serine	0.58	0.57	0.46	0.33	+
PC(O-36:4)	0.84	0.81	0.52	0.84	-
PC(O-32:0)	0.85	0.81	0.55	0.85	-
PC(O-38:4)	0.88	0.84	0.55	0.83	-
PC(O-34:0)	0.87	0.83	0.58	0.84	-

Supplemental Table 2.6. NMR and MS important identified metabolites with R2 values from the linear regression model for both CD4+ and CD8+ proliferation of two PBMC donors, and indication of whether metabolite intensity increases or decreases with higher potency.

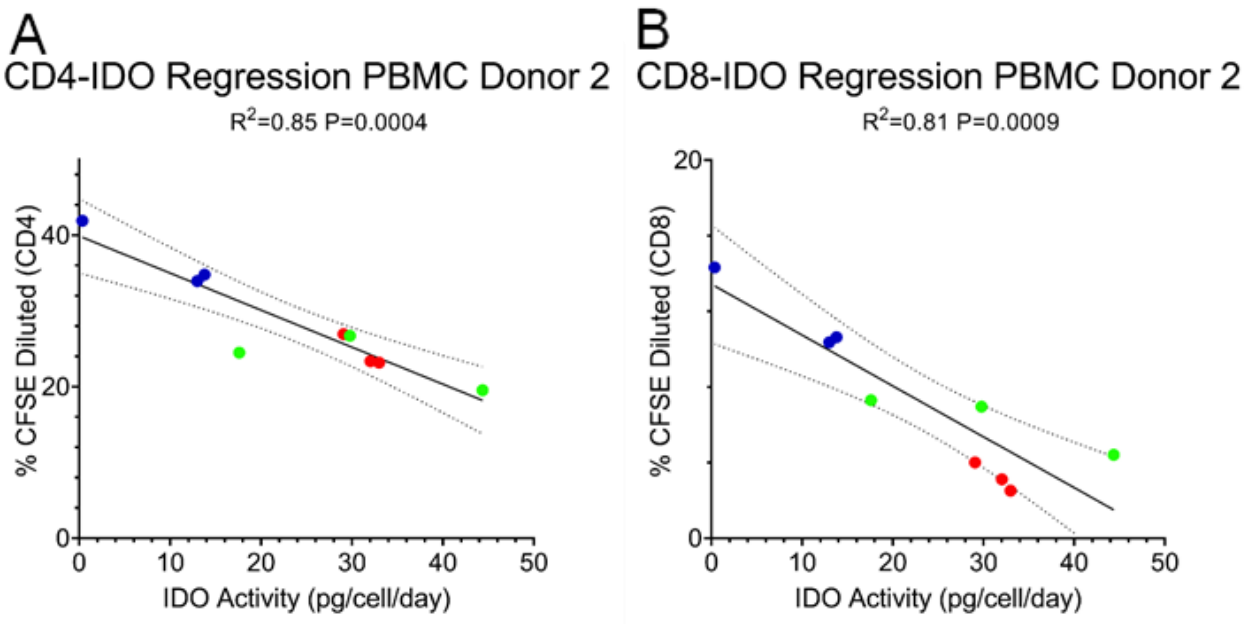

Supplemental Figure 2.3. Regression of IDO activity and T cell proliferation with a second PBMC donor. Linear regression of the relationship between IDO activity and (A) CD4+ and (B) CD8+ T cell proliferation.

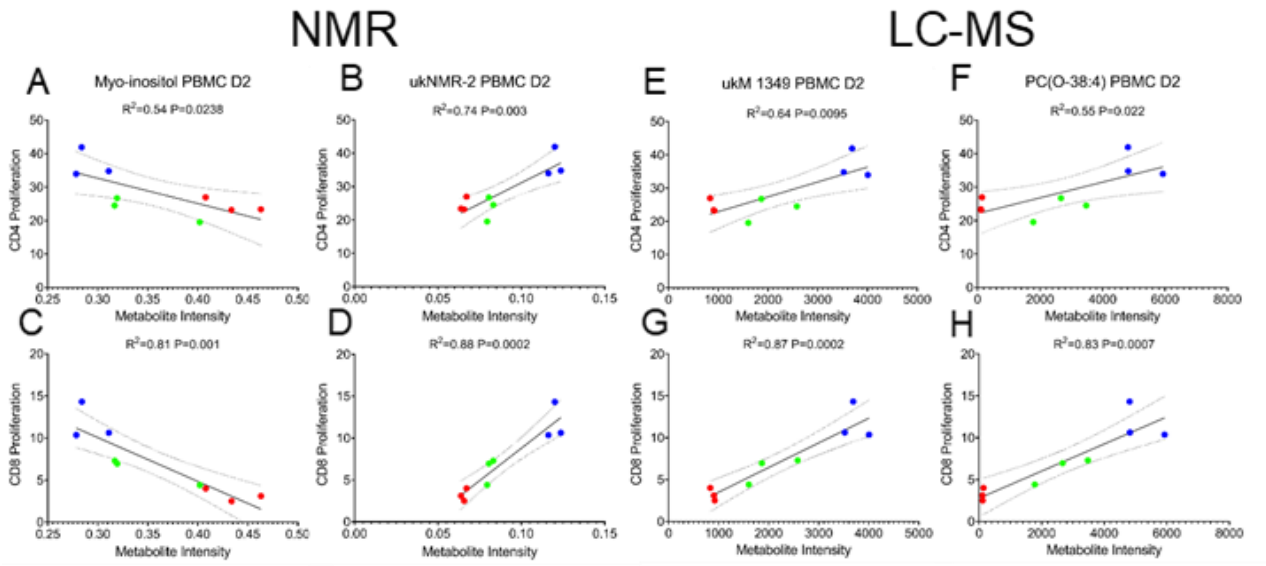

Supplemental Figure 2.4. Linear regression analysis of the top correlated metabolites with PBMC donor 2. (A,C) Myo-inositol, (B,D) ukNMR-2, (E,G) ukM-1349, and (F,H) PC(O-38:4) all correlated with CD4+ and CD8+ T cell proliferation for both PBMC donors.

CHAPTER 3

DEVELOPMENT OF A ROBUST CONSENSUS MODELING APPROACH FOR IDENTIFYING CELLULAR AND MEDIA METABOLITES PREDICTIVE OF MESENCHYMAL STROMAL CELL POTENCY[2]

[2]Ty S. Maughon, Alexandria Van Grouw, Maxwell B. Colonna, Xunan Shen, Andrew M. Larey, Samuel G. Moore, Carolyn Yeago, Facundo M. Fernández, Arthur S. Edison, Steven L. Stice, Annie C. Bowles-Welch, Ross A. Marklein. Submitted to Stem Cells on 2/16/2023.

Author Contributions:

TM: Conception and design; T cell suppression assay; IDO activity assay; Composite functional score; data analysis and interpretation; manuscript writing

AVG: Collection and assembly of MS data; MS data analysis and interpretation; ML modeling; data analysis and interpretation; manuscript writing

MBC: Collection and assembly of NMR data; NMR data analysis and interpretation; ML modeling; data analysis and interpretation; manuscript writing

XS: Collection and assembly of data

AML: Collection and assembly of data

SGM: Collection and assembly of data

CY: Conception and design; financial support

FMF, ASE, SLS: Conception and design; financial support; manuscript writing and final approval of manuscript

ABW: Conception and design; collection and assembly of data; data analysis and interpretation; manuscript writing; final approval of manuscript

RAM: Conception and design; data analysis and interpretation; financial support; manuscript writing and final approval of manuscript

3.1 ABSTRACT

Mesenchymal stromal cells (MSCs) have shown promise in regenerative medicine applications due in part to their ability to modulate immune cells. However, MSCs demonstrate significant functional heterogeneity in terms of their immunomodulatory function because of differences in MSC donor/tissue source, as well as non-standardized manufacturing approaches. As MSC metabolism plays a critical role in their ability to expand to therapeutic numbers ex vivo, we comprehensively profiled intracellular and extracellular metabolites throughout the expansion process to identify predictors of immunomodulatory function (T cell modulation and indoleamine-2,3-dehydrogenase (IDO) activity). Here, we profiled media metabolites in a non-destructive manner through daily sampling and nuclear magnetic resonance (NMR), as well as MSC intracellular metabolites at the end of expansion using mass spectrometry (MS). Using a robust consensus machine learning approach, we were able to identify panels of metabolites predictive of MSC immunomodulatory function for 10 independent MSC lines. This approach consisted of identifying metabolites in 2 or more machine learning models and then building consensus models based on these consensus metabolite panels. Consensus intracellular metabolites with high predictive value included multiple lipid classes (such as phosphatidylcholines, phosphatidylethanolamines, and sphingomyelins) while consensus media metabolites included proline, phenylalanine, and pyruvate. Pathway enrichment identified metabolic pathways significantly associated with MSC function such as sphingolipid signaling and metabolism, arginine and proline metabolism, and autophagy. Overall, this work establishes a generalizable framework for identifying consensus predictive metabolites that predict MSC function, as well as guiding future MSC manufacturing efforts through identification of high potency MSC lines and metabolic engineering.

3.2 INTRODUCTION

Preclinical and clinical studies have demonstrated evidence of promising therapeutic effects from the use of mesenchymal stromal cells (MSCs) for a broad range of applications including autoimmune, neurodegenerative, and inflammatory diseases.[1–3] MSCs are derived from various tissues of the body, most commonly bone marrow, adipose, and umbilical cord,[4–7] and can be administered directly as cell therapies or used to create cell-derived products (e.g., secretome and extracellular vesicles).[8–10] The secretory repertoire of MSCs is rich in cytokines, chemokines and growth factors that, combined with the fact that MSCs lack or possess low expression of self-antigens (thus permitting allogeneic use), renders MSCs a potential cell therapy for a large patient population with life-altering conditions.[9,10] However, efficacy outcomes from clinical trials are inconsistent and pose a major roadblock to the approval of MSCs as cell therapies despite a well-established safety record.[11] One major challenge that must be addressed to facilitate clinical translation is MSC functional heterogeneity, which can be attributed to different donors, tissue sources and culture conditions (i.e., 'manufacturing') introduced during MSC ex vivo expansion.[1,12,13] MSCs require ex vivo expansion to yield a sufficient cell supply to meet the needs for clinical dosages, which are typically on the order of hundreds of millions of cells.[14] Relatedly, a lack of standard cell culture practices and processes is another challenge that contributes to poor reproducibility and inconsistent clinical outcomes.[15] Better understanding of MSC functional heterogeneity will lead to critical quality attributes (CQAs), which are part of a comprehensive analytical assay suite to be used for MSC selection and release criteria, ultimately improving their clinical translation.

CQAs predictive of MSC immunomodulatory potency serve as a quantitative and reproducible measure for assessing MSC quality, thus enabling rational approaches to both

identify high quality MSC lines (donors), as well as optimize culture conditions that facilitate scaling to larger manufacturing formats such as bioreactors. Several approaches to identify CQAs correlative to MSC functional potency have been reported.[16,17] Based on previous work[10,18], MSC potency assays often assess MSC immunomodulatory functions such as indoleamine 2.3-dioxygenase (IDO) activity, as well as MSC modulation of activated immune cells (e.g. T cells and macrophages). These functions are relevant to a broad range of diseases and have been associated with MSC secretion of anti-inflammatory, mitogenic, and tissue reparative factors.[19,20] Priming MSCs with stimulatory molecules (e.g., interferon-γ (IFN- γ) or tumor necrosis factor-α (TNF- α)) promotes the increased secretion of paracrine mediators such as IDO and anti-inflammatory molecules (e.g., interleukin-10) that are relevant in the context of MSC immunomodulation (e.g., suppress T cell proliferation, induce regulatory phenotypes of T cells and macrophages).[21,22] Not only can these MSC-mediated effects related to immunomodulatory potency establish a set of CQAs, they shed light on metabolic activities that are vital to the basic understanding of MSC functions that can be leveraged for therapeutic use.[23] However, the reproducibility and robustness of these potency assay formats reduce their appeal for assessing CQAs in a manufacturing setting.

Robust multi-omic approaches coupled with computational modeling to identify correlations to functional potency have been leveraged to identify predictive markers in cell therapies.[24–26] Metabolomics is an emerging field due to the abundance of metabolites and their reflection of the cellular phenotype which allows for non-targeted approaches for important biomarker discovery.[27,28] Well established techniques such as nuclear magnetic resonance (NMR) and mass spectrometry (MS) are often used to measure both cellular and extracellular metabolites.[29,30] In terms of MSC metabolism, it has been shown that MSCs preferentially utilize

glycolysis over oxidative phosphorylation (OXPHOS) in vivo, but shift towards OXPHOS from extended culture and expansion.[30] Greater OXPHOS metabolism has also been shown to lead to a decrease in T cell suppression by MSCs.[23] Previously, our group assessed end of expansion intracellular metabolites as candidate predictive markers, and putative CQAs, using three independent MSC lines at three passages. Partial least squares regression (PLSR) was used to determine predictive markers based on their variable importance projection (VIP) score.[26] Several amino acids, small molecule metabolites (e.g. myo-inositol), and phosphatidylcholines (PCs) were shown to be correlative to MSC functional potency (measured in terms of both T cell modulation and IDO activity).

In this study, we expanded on our previous work by applying a novel CQA discovery framework whereby metabolomic data generated both in-process (during the first three days of MSC expansions) and at end of production (intracellular metabolites from harvested MSCs) were input into a suite of models to predict MSC immunomodulatory potency. For this study, we generated ten MSC lines consisting of the following: the same three cell lines as our previous study, six additional MSC lines, and a repeat expansion of one of the MSC lines.[26] For each MSC line, unsupervised analysis of media metabolites and intracellular metabolome of MSCs were correlated to a functional composite score (based off T cell suppression and IDO activity) using several machine learning (ML) models. CQAs were resolved across a total of 7 models (for both extracellular and intracellular inputs) to identify consensus metabolites that were subsequently related using metabolic pathway analysis. Top consensus media metabolites predictive of MSC potency include several amino acids (proline, arginine, aspartate), pyruvate and fructose. Top consensus intracellular metabolites predictive of MSC potency include several lipid classes such as PCs, phosphatidylethanolamines (PEs), and sphingomyelins (SMs). These

were then mapped to several metabolic pathways to infer their potential biological roles as they relate to MSC immunomodulation. This study establishes a generalizable framework for identifying predictive markers from early stage culture media and intracellular metabolomic analyses that can ultimately be used to select for MSC lines with desired properties and guide future MSC manufacturing strategies.

3.3 MATERIALS AND METHODS

MSC Expansion and MSC/MSC-Conditioned Medium Sample Preparation

Bone marrow-derived MSCs (BMMSCs) were purchased from RoosterBio, Inc. (Frederick, MD), and iMSCs were purchased from Fujifilm Cellular Dynamics Inc (Madison, WI). Prior to this study's expansion, MSCs were previously expanded to an initial population doubling level (PDL0) reported in Supplemental Table 3.1. Additional information for each MSC cell line including final PDL, donor demographic information, and final cell yield is also reported in this table. Cryopreserved vials from each donor were thawed, and 10^6 MSCs were seeded into an initial T-150 tissue culture flask in complete media containing Gibco™ Minimum Essential Media α with nucleosides (Thermo Fisher Scientific, Waltham, MA), 10% fetal bovine serum (FBS; HyClone Laboratories, Logan, UT), and 1% penicillin-streptomycin solution (10,000 U/mL; Sigma-Aldrich, St. Louis, MO) for a culture rescue period of 48 hr. The same lot of FBS was used throughout the study. MSCs were then washed with endotoxin-free Dulbecco's phosphate buffered saline (PBS) without calcium and magnesium (Millipore Sigma), harvested using 1X TrypLE™ Express Enzyme (Thermo Fisher Scientific), neutralized with complete media, and centrifuged 300g to create a cell pellet. MSCs were then resuspended in complete media and counted. Next, MSCs from each donor were seeded at 500 cells/cm2 into 10 T-75 flasks containing 10 mL complete media. Control flasks containing 10 mL complete media only

were also prepared. All flasks were then transferred to a humidified incubator set to 37° C and 5% CO2.

MSC conditioned medium (CM) sample collection of 300 µl was performed for each flask at approximately the same time each day (±1 hr) and total complete media exchange was performed every 3 days until MSCs achieved 70-80% confluence. All media samples were placed directly into –80° C storage until further analysis by NMR. MSCs were then harvested using the same procedure described above. Cell pellets were split for cryopreservation (and functional analysis, see below) or preparation for intracellular lipidomic/metabolic analysis. Cell pellets designated for cryopreservation were prepared into cryovials containing 10^6 MSCs in 1 mL CryoStor® CS 10 (Sigma-Aldrich) and stored at –80° C for 24 hr using controlled rate freezing containers. Vials were then transferred to the vapor phase in a liquid nitrogen cryogenic freezer until further analysis. For intracellular lipidomic/metabolomic analysis, cell pellets were washed twice by resuspending in PBS and centrifuged at 10,000 rpm. All supernatant was removed and cell pellets were then stored at –80° C.

MSC Functional Analysis - T cell Suppression Assay

MSCs from each cell-line were thawed and allowed to recover for 48 hours with a media change at 24 hours. MSCs were harvested using TrypLE then seeded at a density of 10,000 cells/well in a 96 well plate and cultured for 24 hours. Previously frozen peripheral blood mononuclear cells (PBMCs, AllCells, Alameda CA) were thawed in RPMI media (RPMI, 20% FBS, 2mM L-glutamine, 50 U/mL penicillin, 50 µg/mL streptomycin) and cultured overnight at 37°C and 5% CO2. Prior to co-culture, PBMCs were labeled with CFSE (Supplemental Table 3.2, Biolegend, San Diego CA) according to the manufacturer's protocol, and 100,000 PBMCs were added to each well at a final MSC:PBMC ratio of 1:10 as well as control wells containing

only PBMCs. Following PBMC addition, stimulating anti-CD3/CD28 Dynabeads (Thermo Fisher Scientific, Waltham MA) were added at 100,000 beads per well to the appropriate wells (positive controls and all MSC groups). MSCs and PBMCs were co-cultured for 72 hours at 37°C, 5% CO2.

Following co-culture, PBMCs were collected and stained using Brilliant Violet 711 anti-CD4 and APC anti-CD8 (Supplemental Table 3.2) (Biolegend, San Diego CA). PBMCs were first washed and stained with Zombie Yellow (Supplemental Table 3.2) (Biolegend, San Diego CA) viability dye and blocked using 2% FBS. PBMCs were then washed again and stained for CD4 and CD8 in the dark at room temperature. Following staining, the antibodies were blocked using 2% FBS and washed. PBMCs were then fixed with 4% PFA for 30 minutes at 4°C, washed and re-suspended in PBS containing 2% FBS, and finally stored overnight at 4°C in the dark until flow analysis.

All flow cytometry experiments were performed using a Novocyte Quanteon flow cytometer (Agilent, Santa Clara CA) with 20,000 events collected per sample. All flow cytometry data were analyzed using FlowJo (Treestar, Inc., Ashland OR). Briefly, cell debris, doublets, and Dynabeads were gated out using scatter principles. Then, single stained controls were used for compensation, and fluorescence minus one controls were used to determine positive populations (Supplemental Figure 3.1).

MSC Functional Analysis - Indoleamine 2,3 Dioxygenase (IDO) Activity Assay

MSCs from each cell-line were thawed and cultured for 48 hours with a media change at 24 hours. MSCs were harvested using TryplE then seeded at a density of 40,000 cells/cm2 in a 96 well plate. After 24 hours, the medium was replaced in each well with complete medium containing 10 ng/mL IFN-γ (Life Technologies). After an additional 24 hours, conditioned

medium was collected and frozen at -20°C, and cells were fixed with 4% PFA. Each medium sample was thawed and 100 µL transferred into a 96 well plate. Trichloroacetic acid was used to precipitate excess protein. 75 µL of the supernatant was collected and transferred to a separate 96 well plate. Ehrlich's Reagent was then added to each well to detect L-kynurenine levels using a SpectraMax iD5 (Molecular Devices) plate reader. Levels of L-kynurenine were determined using a standard curve. To normalize L-kynurenine values to cell numbers for each replicate well (n=5 wells) within an experimental group, we performed automated image analysis to quantify cell nuclei in the wells from which conditioned medium was collected. Following fixation, MSCs were washed with PBS twice, and stained with Hoechst (10µg/mL) in 0.1% Tween20 PBS solution for 1hr. Cells were then imaged on a Cytation 5 high content imaging system (Biotek, Winooski VT) and cell counts determined using CellProfiler to normalize the amount of L-kynurenine per cell.

Generation of a Composite Score of MSC Potency

Using the results from functional assays, a composite functional score was generated to use as an overall potency metric. The averages of the percentage of CFSE dilution of CD4 and CD8 T cells from two PBMC donors and IDO activity were subject to principal component analysis (PCA) using JMP software (V9.2). The first principal component (PC1) value of each cell line was taken as the respective composite functional score and represented 74.5% of the total variance of the data.

NMR Media Analysis of MSC Culture

Frozen media samples were transported on dry ice for NMR analysis. Samples were prepared in batches for each rack of 96 1.7 mm SampleJet NMR tubes (Bruker BioSpin). Briefly, samples were pulled and sorted on dry ice, then thawed at 4°C. A solution of 3.33 mM DSS-D6

in deuterium oxide (Cambridge Isotope Laboratories) were mixed into media samples to a final concentration of 10% deuterium oxide. Samples were then centrifuged @ 2990 g for 20 min at 4°C to pellet any debris that may have been collected with the media. 60 µl were transferred from each sample tube to NMR tubes using Bruker SamplePro liquid handling system (Bruker BioSpin). Ten µl of remaining volume from each sample in the rack was combined to create an internal pool used within each rack. These internal pooled samples were placed throughout the rack as quality control during data acquisition.

NMR spectra were collected on a Bruker Avance NEO spectrometer at 800 MHz using a 1.7 mm TCI cryogenic probe and TopSpin software (Bruker BioSpin). One-dimensional spectra were collected on all samples using the noesypr1d pulse sequence under automation using IconNMR software. After one-dimensional data acquisition of all samples, 10 samples of each media type were selected at random, material collected from the NMR tubes, and combined to form a media specific pool used for two-dimensional (2D) spectral acquisition. 2D HSQC and TOCSY spectra were collected on pooled samples for metabolite annotation. One-dimensional spectra were automatically phase and baseline corrected using a batch script executed in MestreNova software (MestreLab Research). 2D spectra were processed in NMRpipe.31

One dimensional spectra were referenced, water/end regions removed, aligned and normalized using an in-house MATLAB (The MathWorks, Inc.) toolbox established by Robinette, et. al and implemented within NMRbox.[32,33] Spectral features that were sufficiently well aligned across spectra were semi-automatically integrated using an interactive MATLAB function to obtain feature intensity values. These feature intensity values were batch corrected across the two batches of data collection using the ComBat algorithm34 implemented in Metaboanalyst.[35] The feature values for the first timepoint of each replicate was subtracted from

the values of the second and third timepoints, to produce features representing the differences between them. To reduce the total number of feature differences used for machine learning analyses, a variance filter was applied to select a subset of spectral features with highest variance as previously described.[25] For each timepoint differences being assessed, the top percentage of variable features was determined by the subset which provided the best partial least squares regression R2 when used as input. This resulted in 69 features used for the features for Day 3 minus Day 1 values, and 21 features for Day 2 minus Day 1 values.

Intracellular Metabolite Analysis of MSCs Using LC-MS

Approximately one million MSCs were analyzed for each sample. Frozen cell pellets were thawed and washed prior to undergoing a modified Bligh-Dyer extraction to yield two phases. Extraction solvent (2:2:1 chloroform:methanol:water) and glass beads (400-600 µm) were added to cell pellets for extraction and homogenization in a TissueLyser II to 30 Hz for 6 minutes. Samples were then sonicated and centrifuged. Following extraction, 300 µL aliquots from each layer were transferred to new microcentrifuge tubes and solvent was dried using vacuum centrifugation. Dried organic phase samples were re-constituted in isopropyl alcohol, while dried aqueous phase samples were re-constituted in 80% methanol. Re-constitution was followed by sonication, centrifugation, and transfer to liquid chromatography (LC) vials for ultrahigh performance liquid chromatography mass spectrometry (UHPLC-MS) analysis (Supplemental Table 3.3). Media samples without cells were also analyzed as blanks to remove any features corresponding to remaining media components on the cells. Ten µL of media was subject to the same Bligh-Dyer extraction as above and extracts were run according to the instrumental methods listed above. A quality control (QC) sample for hydrophilic interaction chromatography (HILIC) and reverse phase datasets was created by pooling 20 µL from each

experimental sample. The pooled QC injections were used for drift correction of peak areas. Sample queue was randomized with a mix of samples, QCs, and blanks.

Metabolomic analysis was performed on all aqueous extracts using UHPLC-MS on an Orbitrap ID-X Tribrid mass spectrometer (ThermoFisher Scientific). HILIC separation was employed with a Waters ACQUITY UPLC BEH amide column (2.1×150 mm, 1.7 µm particle size) on a Vanquish (ThermoFisher Scientific) chromatograph. Lipidomic analysis was performed on all organic extracts using UHPLC-MS on a Q Exactive HF Hybrid Quadrupole-Orbitrap mass spectrometer system (ThermoFisher Scientific). Reverse Phase separation was employed with an AccucoreTM C30 column (2.1 × 150 mm, 2.6 µm particle size) on a Vanquish (ThermoFisher Scientific) chromatograph. Data dependent acquisition (DDA) was employed in both instrument methods to yield fragmentation information for detected metabolites and lipids. DDA methods collected full scan data at resolution of 120,000 in the orbitrap. This was followed by collection of fragmentation spectra (MS2) of selected precursors collected in the ion trap with an isolation window of 0.4 m/z with a cycle time of 1.25 s. Dynamic exclusion was set to exclude MS2 collection of precursors within a 6 s window with a 10 ppm mass tolerance for the precursor ion. Stepped normalized collision energies of 15%, 30%, and 45% were employed with HCD and CID 35% to collect MS2 spectra.

Data was preprocessed in Compound Discoverer 3.2 (Thermo Fisher Scientific). This included drift correction and blank removal. All features with at least 5x the signal in the blanks and were present in at least 50% of all pooled QC injections were kept for analysis. This resulted in a dataset with a total of 8,388 features. Further data filtering was used to remove features with relative standard deviations lower than 25% between all samples, features with poor chromatographic peak shape, and features with no MS2 spectral data. Because the experimental

samples were prepared at two distinct times, a batch correction (Supplemental Figure 3.2) was employed to harmonize the data. Feature peak areas were corrected across the two batches using the ComBat algorithm[34] implemented in Metaboanalyst[35]. Annotations were performed based on exact mass matches, MS2 spectra fragmentation patterns, and MS2 spectral library database matches. The final datasets used for machine learning included 436 annotated lipids and 43 annotated small polar analytes. The peak areas in these datasets were median normalized and autoscaled prior to machine learning workflow.

Computational Analysis and Statistical Methods

Identification of features predictive of the functional composite score across MSC donors was based on methods described previously25 using multiple machine learning methods. In brief, the ML regression methods utilized were random forest (RF), gradient boosted regression (GBR), decision tree regression (DTR), least absolute shrinkage and selection operator (LASSO), partial-least squares regression (PLSR), support vector regression (SVR), and symbolic regression (SR). These models were used to extract predictive variables (or variable combinations). SR was performed using Evolved Analytics' Data Modeler software (Evolved Analytics LLC). All other models were generated with the LinearSVR, PLSRegression, RandomForestRegressor, DecisionTreeRegressor, Lasso, and GradientBoostingRegressor functions as part of the sklearn software package implemented in Python.[36] Parameter tuning was done for all sklearn models in a grid search manner using the GridSearchCV function with 5-fold cross validation (CV) and using R2 as the scoring criteria. For each regression model, feature selection was performed using the same regression type (i.e., LASSO). Final prediction performance was measured by calculating leave-one-out R2 (LOO-R2) values on final models

with CV-optimized parameters. Model specific parameters and parameter ranges that were used are available in code.

Consensus analysis of the relevant variables extracted from each ML model was done to identify consistent predictive features of function using both in-process media features (measured by NMR) and end-product cellular lipids and metabolites (measured by LC-MS). For RF, GBR, DTR, LASSO, PLSR, SVR models, features that ranked in the top 20% of feature importance were selected, while for SR variables present in ≥10% of the top-performing SR models from Data Modeler ($R2 \geq 90\%$, complexity ≤300) were chosen to investigate consensus. Those variables that appeared as important in 2 or more ML methods were deemed consensus features and included for further annotation (NMR) and pathway analysis (NMR and MS).

Because the iMSC sample was the only non-bone marrow derived line, this could be an outlier. To determine the importance of the iMSC sample on the models, the final metabolite panels in the consensus models were used to create models without the iMSC sample. All modeling parameters were kept the same with the exception of changing the 5-fold cross validation to 3-fold to accommodate 9 samples. The success of these models was evaluated using LOO-R2. All statistics were performed in Python or Prism (GraphPad Software, San Diego CA).

Metabolite Pathway Analysis

Enrichment analysis of consensus metabolites from both NMR and MS was performed using Metaboanalyst. Specifically, the list of consensus metabolites was submitted to perform over representation analysis by mapping to all pathways in the small molecule pathway database (SMPDB) From the list of consensus NMR metabolites, 6 out of 7 consensus metabolites were able to be mapped by Metaboanalyst, while all 16 MS consensus metabolites were mapped. Lipid pathway enrichment was performed with LIPEA, using the default background for Homo

sapiens. 16 out of 33 submitted consensus lipid species were mapped to KEGG lipids used by the LIPEA program. Final lists of mapped metabolites/lipids used for pathway enrichment are included in Supplemental Table 3.4.[37]

3.4 RESULTS

Cell-line Dependent Differences in MSC Potency

Following expansion and cryopreservation of all MSC lines, MSCs were thawed to determine their functional capacity. Proliferation of CD4+ and CD8+ T cells (based on %CFSE dilution) from two PBMC donors and IDO activity (L-kynurenine production) were used to evaluate each MSC functional capacity between MSC lines and create a functional composite score (Figure 3.1A). Similar trends were observed for CD4+ (Figure 3.1B, D) and CD8+ (Figure 3.1C, E) proliferation for both PBMC donors with MSCs suppressing T cells in a broad range from 46.8-67.4% (CD4+) and 54.2-77.0% (CD8+) for PBMC Donor 1 and 10.7-46.2% (CD4+) and 14.8-38.1% (CD8+) for PBMC Donor 2. This observation was evident by regressing CD4+ vs CD8+ T cell proliferation results for both PBMC Donor 1 and PBMC Donor 2 (R2=0.86 and R2=0.90, respectively) (Supplemental Figure 3.3). The iMSC line had the highest suppression of CD4+ and CD8+ T cell proliferation in both PBMC donors. RB182 was not significantly different from the iMSCs for CD4+ and CD8+ T cell proliferation in PBMC donor 1 but was for PBMC donor 2. RB71 consistently had the least amount of CD4+ and CD8+ T cell suppression from both donors. All MSC lines were significantly different from the positive control (dotted line). The MSC lines with the highest T cell suppression function (iMSC, RB177, and RB182) were also high in IDO activity (Figure 3.1F). While MSC line RB71 had the lowest observed T cell suppression, its IDO activity was not the lowest of the 10 MSC lines as its activity was approximately in the middle range (46.3 pg/cell/day) of all observed IDO activity values (20.5-

80.6 pg/cell/day). During cell expansion, a repeat line, derived from RB174, was used to compare different expansion dates (i.e. batches). Functional comparison between these two expansions (termed RB174_1 and RB174_2 for batch 1 and 2, respectively) showed no significant difference within any assay. A functional composite score was generated with PCA using all the functional assay results. As PC1 comprised 74.5% of the variance in the dataset, we used PC1 values for the composite score (Figure 3.1G). This functional composite score displays a wide range of immunomodulatory function between all MSC lines with lower PC1 scores indicating MSC lines with the highest potency i.e. high T cell suppression and IDO activity.

Cell-line Differences in Intracellular MSC Metabolome

UHPLC-MS analysis by reverse phase and HILIC chromatography high-resolution mass spectrometry (Supplemental Table 3.3) of MSC cell pellets yielded a rich metabolomic dataset with a total of 479 annotated features. Annotations were assigned using exact mass and MS2 spectral library matches. This feature list and the corresponding abundances were used to conduct unsupervised clustering to observe metabolic differences in the 10 MSC lines examined in this study. Sample clustering with the metabolites measured in this dataset showed that the iMSC sample had significant metabolic differences from all the bone-marrow derived cell lines using both Ward clustering (Figure 3.2A) and PCA (Figure 3.2B). Little clustering was observed according to potency except in the case of the middle performing cell lines, which have more metabolic similarity. However, the MSC lines with highest potency (iMSC) and lowest potency (RB71) were maximally separated based on their metabolic signatures using both Ward clustering and PCA.

We initially sought to find single metabolites that could predict MSC potency by examining linear correlations of metabolite abundances with the composite score. Simple linear

regressions were made for each analyte in the dataset and ordered according to R2 (Supplemental Table 3.4C). There were 18 annotated metabolites with R2 above 0.5 in the dataset. Two of these, PI (18:1/18:1) and PE (O-18:1/22:6), are shown in Figure 3.2C and 3.2D, respectively. As few of the individual metabolites were predictive of MSC potency after multiple testing correction it was determined that a panel of metabolites identified through machine learning (ML) based regressive methods would yield higher predictive power, as well as elucidate possible pathways involved in the regulation of these metabolites.

Media samples collected at daily intervals during cell expansions were analyzed by 1D 1H-NMR. In addition, 2D NMR spectra were collected on pooled material to aid in annotation of spectral features in the 1D spectrum. After spectral processing and alignments, a total of 138 spectral features were semi-automatically selected and quantified across all samples. These spectral features correspond to a smaller number of metabolites, each metabolite having one too many spectral features based upon its chemical structure. These features were initially left unannotated in order to not exclude features corresponding to unknown metabolites that may have useful value in downstream analyses. To avoid the assumptions of linear or monotonic relationships of feature intensity over time in downstream analyses, feature values at Day 1 were subtracted from Days 2 and 3 to create two datasets representing the net change in feature intensity over each time period (1 and 2 days, respectively). Notably, clustering analyses of these values do not show any clear patterns between donors or potency measures. (Figure 3.3A). PCA of all samples from expansion days 1, 2 and 3 also showed no strong clustering corresponding to donor, but rather a pattern of samples clustering by the day of culture (Figure 3.3B). Similar to the MS data analysis, linear regression was performed between each average spectral feature intensity and composite score for each MSC line. The top performing features (in terms of R2)

are shown in Figure 3.3C, D. Again, the changes in these individual spectral features showed reasonable correlation to the potency score, but after false discovery rate correction, these correlations were not significant. Particularly given the observed non-linear dynamics of many of these spectral features, it was hypothesized that identifying a panel of spectral features predictive of potency would be aided using diverse ML methods.

Modeling Approach and Identification of Consensus Predictive Metabolites

Evaluation of machine learning models

To find potency-related patterns in the data, several ML regression types were used for potency modeling (Table 3.1). Most models had comparable performance in both NMR and MS datasets based on LOO-R2, which indicates there are potency-related metabolic differences. This is reflected in metabolite abundances both intracellularly and in the cell media. Because the annotated metabolites and metabolite features identified in each model were not identical, we sought to develop a consensus modeling strategy to ensure metabolites of interest were robust and not unique to a particular ML approach. This strategy consisted of selecting only metabolites or features present in more than one of the initial models within a particular dataset – MS lipids, MS small polars (MS metabolite panel in Supplemental Table 3.4A, B), NMR Day 2, or NMR Day 3 models were included in the consensus models. Most of the consensus models have comparable performance to the initial non-consensus models (in terms of LOO-R2), which underscores the robustness and predictive value of our consensus metabolite panels. To confirm these consensus models were not highly dependent on the iMSC sample, the final consensus metabolite panels were used to create another set of consensus models built and cross-validated on only the nine bone-marrow derived lines. The performance of these models, evaluated using LOO-R2, was comparable for MS models (LOO-R2 range from 0.72 to 0.99) while removal of

iMSC from NMR consensus models resulted in lower LOO-R2 for most models (PLSR, SVM, GBR, LASSO, RF and DT). However, the NMR consensus model constructed using symbolic regression was highly predictive of MSC potency (LOO-R2=0.96).

Intracellular Metabolite Class Patterns in Modeling Results

Phosphatidylcholines (PC), phosphatidylethanolamines (PE) and sphingomyelins (SM) make up a large portion of the annotated dataset and show high importance in the models (Figure 3.4 A, B). Interestingly, ether-linked phosphatidylethanolamines (PE-O) made up a smaller portion of the overall dataset compared to other lipid classes but were still among the top contributors to the models. Based on the weights applied to these lipid abundances in the regression models, they were highly important for model building. The over-representation of them in the models compared to the overall dataset is evidence that their abundances are related to MSC potency as measured by the composite score. This indicates a possible role in MSC functionality for members of this lipid class.

Amino acids and their analogues make up the majority of the small polar annotated dataset and showed importance in regression models (Figure 3.4 C, D). Similar to PC in the lipid dataset, as they make up the largest portion of the data and contribute the most significantly to the models, no strong conclusions based on over-representation can be made. A hexose was detected in this dataset that was in the final panel for several of the models. However, there was only one sugar in the final annotated dataset meaning that class coverage for sugars was low. Given this finding, no strong conclusions about biological role or over-representation should be made.

The consensus metabolite list was made up of all metabolites that were in the final panel, following variable selection, of more than one initial model – lipid or small polar. This

consensus list (Supplemental Table 3.4A,B) was primarily composed of PC, amino acids and analogues, PE-O, and phosphatidylserines (PS) (Figure 3.4E). These 41 metabolites from 15 classes (Figure 3.4E) all showed importance in the models and were later investigated in pathway analysis. The variable presence plots for SR (Supplemental Figure 3.4) indicate the following metabolites as having high occurrence in the final suite of models used for SR: acetyllysine, glucose isomer, hydroxykynurenamine, PE (O-32:1), PC (31:0), PE (O-38:2), and PI (36:2). In terms of the decision tree (DT) model, there was one ceramide (Cer(d33:1)) that was the sole contributor (Figure 3.4F). Small changes in the data can cause large differences in DT models, making them relatively unstable compared to other types of models. It was also observed in this workflow that the DT regression models often selected a small number of predictive features. Since this particular lipid was not significantly important in other models as well, the large importance in the DT regression model may or may not be significant.

*Different Consensus Media Metabolites Exhibit Distinct Change*s

A total of 23 unique spectral features were selected as consensus features from both NMR timepoint datasets having been in top important features for at least two ML methods (Figure 3.5A, B). Two features were common to both timepoint datasets (5.53 ppm and 5.30 ppm). The average trajectory over time for each of these consensus features is shown in Figure 3.5C. As noted previously, many of these features show non-linear and non-monotonic behavior over time, and different changes between Day 1 and Day 2 or Day 3, accounting for some of the different features that were selected as consensus between the two datasets. Of the selected consensus features from both Day 3 and Day 2 NMR features, several were annotated to metabolites including proline, arginine, fructose, phenylalanine, pyruvate and an unknown uridine diphosphate-sugar (Figure 3.5D). Of these metabolites, pyruvate and proline had some of

the highest variable presence scores in the SR suite of models (Supplemental Figure 3.4) as well as several unknown, unannotated metabolites. Several features that appeared as important in some ML methods were not matched to spectral databases and may require further experimentation to confidently annotate. Particularly, two of these unknown features at 5.53 ppm and 5.30 ppm appeared as consensus features in both timepoint datasets, suggesting that whatever metabolite(s) these features correspond to may be a robust predictor of potency across time.

Interpretation of Consensus Metabolites Through Pathway Analysis

The consensus list from each modeling set (Supplemental Table 3.4A, B for MS and Figure 3.5D for NMR) was used to search for potency-associated changes in metabolism on the pathway level. Of the top enriched pathways, there were 7 with significant p-values ($p<0.05$) for the NMR consensus metabolites (Figure 3.6A), 12 with significant p-values ($p<0.05$) for MS lipidomic analysis (Figure 3.6B), and none for MS small polar analysis (Figure 3.6C). Top lipid enriched pathways included sphingolipid signaling pathway, autophagy, and necroptosis, indicating that these lipids could be important in MSCs based on their role in cell cycle. Approximately 10% of the small polar dataset was able to be annotated, compared to the lipid dataset which was 45% annotated. Because enrichment analysis relies on over-representation of metabolites in particular pathways, the lower metabolite coverage of the small polar dataset was likely a contributing factor to the lack of significance of the pathways identified. Additionally, some of the identified metabolites in this dataset were not found in pathways in the Small Molecule Pathway Database used for pathway enrichment. Despite the lack of significantly enriched pathways in the MS metabolite data, interestingly there was some agreement between top resulting pathways in the NMR and MS small polar analyses. In particular, aspartate

metabolism, arginine-proline metabolism, glycine-serine metabolism, and glucose-alanine metabolism appeared in the top enriched pathways for both datasets. This points to some potential consistency in similar metabolic pathways responsible for predicting MSC potency both early in-process and at end-process. This points to some potential consistency in similar metabolic pathways responsible for predicting MSC potency both early in-process and at end-process.

3.5 DISCUSSION

The identification of CQAs correlative to immunomodulatory potency would enable predictive approaches to address some of the grand challenges that hinder the approval and clinical use of MSCs as cell therapies.[16,17] Donor-donor variability and different ex vivo manufacturing procedures create inconsistencies in the therapeutic potency of MSCs, and ultimately efficacy outcomes when evaluated in clinical trials.[12,13] In this study, we greatly expanded on our previous work26 through incorporation of additional cell-lines, assessment of in-process and end-process metabolites, and development of comprehensive ML modeling approach to identify predictive markers. The in-process media analysis might inform decisions made early in cell expansion phase that if translated to a manufacturing setting would reduce manufacturing cost due to identification of failed batches early in manufacturing. For the broad-spectrum analysis of intracellular metabolomics, the discovery of small molecules and lipids correlative to MSC immunomodulation, as a panel of CQAs, is of great interest and a means to distinguish biological heterogeneity and predict the in vivo therapeutic potency of the MSC product. Moreover, a composite score indicative of immunomodulatory potency was developed based on cumulative results from multiple in vitro potency assays to enable correlations of top features from media and intracellular metabolome. This robust approach accounts for the

variability in MSC functional responses and identifying consensus top features, i.e. potential CQAs, using ML models.

An inherent limitation of relying on a single ML model to inform decisions or hypotheses about data can be intrinsic bias based on the specific framework and assumptions that go into using a specific method.[38,39] By using a diverse array of ML regression methods, we avoid being biased too strongly by a single method in identifying features and metabolites predictive of MSC potency. Our consensus approach to identifying potential CQAs reduces the possibility of model specific results by ensuring that they are deemed important by multiple ML methods as illustrated previously.[25] Ultimately the biggest limitation to this method is the size of our dataset, which is limited by the amount of cell material needed for both functional assays and analytical measurements. However, we attempt to mitigate the impact of overfitting on the interpretation of our results using cross-validated model tuning and leave-one-out model performance calculations, in addition to performing our ML analysis without our "outlier" iMSC donor to assess that unique group's impact on our results.

Lipid classes such as phosphatidylcholines (PC), phosphatidylethanolamines (PE), phosphatidylinositols (PI), and phosphatidylserines (PS) are all glycerophospholipids that were found as predictors in our ML models.[40,41] Differences in MSC glycerophospholipid composition has been shown between young and old MSC donors as well as early and late passage MSCs.[41,42] PC and PE were two of the most abundant lipid classes found in the ML models and are two of the most abundant glycerophospholipids found in mammalian cells.[40] PC account for roughly 50% of all cellular phospholipids, and have been shown to be predictive of MSC immunomodulation.[26,42,43] The majority of PE are found in the mitochondrial membrane, and MSC mitochondrial fitness is associated with its glycolytic potential.[23,43,44] Greater glycolytic

potential has been shown to be associated with greater MSC immunomodulation.[23,44] PE have also been shown to positively regulate autophagy, which helps prevent cellular ageing.[45] Several studies have shown that increased autophagy in MSCs can help prevent senescence, increase survival and engraftment, and increase immunomodulatory function.[46,47] As mentioned previously, PI were also predictors of MSC immunomodulation and are precursors for the biosynthesis of glycosylphosphatidylinositol (GPI) anchors.[48] GPI anchored markers such as CD157, which aids in immunomodulation, is involved in migration, self-renewal, osteogenic differentiation, and mitochondrial transfer in MSCs.[49–51] Another glycerophospholipid, PS, is an important molecule in apoptosis signaling, and in vivo studies have suggested that MSC apoptosis may be crucial for their therapeutic efficacy.[52–54] Two other lipid classes found as predictors, sphingomyelins (SM) and ceramides (Cer), are closely related to one another via the sphingolipid metabolic pathway.[55] Increases in sphingomyelin from ceramide treatment has been shown to increase senescence in bone marrow MSC (BMMSC)s.[56] Increased levels of acyl chain ceramides are also associated with decreased levels of IDO activity in BMMSCs.[55] The sphingolipid signaling pathway, a significant pathway found in our results, also plays an important role in MSC migration and osteogenic differentiation.[57,58]

Similarly, we sought to identify metabolites in the media during expansion that relate to immunomodulatory function as this represents a non-destructive, in-process approach for monitoring cell quality. In-process monitoring allows for greater control and quality assurance of cell therapies throughout the expansion process.[59,60] In-process monitoring of parameters such oxygen diffusion, CO2, pH, temperature, and glucose and lactate consumption/production are well established in biomanufacturing.[61] New methods such as gas chromatography mass spectrometry have been used to measure biomarkers predictive of MSC immunomodulation.[62]

Here, we profiled media metabolites from the first three days of expansion to predict MSC function at the end of manufacturing. The amino acids proline, arginine, phenylalanine, and aspartate were all predictive of MSC immunomodulation. Arginine and proline metabolism has been associated with autophagy of MSCs, which was found as a significant pathway from our lipid analysis.[63] Increased ammonia is a by-product of protein and amino acid catabolism and is converted to urea through the urea cycle with arginine and aspartate being key amino acids in the urea cycle.[64,65] Aspartate metabolism is also associated with the TCA cycle which is increased from cellular OXPHOS with pyruvate being an intermediate of both OXPHOS and glycolysis.[30] As mentioned previously, metabolic shifts in MSCs from glycolysis to OXPHOS is associated with a decrease in MSC immunomodulation.[23] Similarly, IFN-γ and hypoxic conditioning increases glycolysis in MSCs and increases the capacity for glucose and fructose uptake.[66] Additionally, arginine and proline metabolism, amino sugar metabolism, and galactose metabolism showed significant differences when comparing adipose-derived MSCs (ADMSCs) and BMMSCs.[67] Upregulation of genes associated with galactose metabolism has also been associated with higher immunomodulation of MSCs.[68] These results further emphasize the critical role of metabolism during MSC manufacturing and how our robust machine learning approach can identify pathways relevant to MSC therapeutic potential.

Conclusion

Overall, this study establishes a comprehensive framework for future studies to interrogate metabolites as predictive markers for MSCs when changing manufacturing parameters. A major example of a significant manufacturing change would be increasing manufacturing scale for clinical trials as the average dose for MSC based therapies is on the order of 10^8 cells for a single patient.[14] Because of this, scaling up to bioreactors is necessary to

produce enough cells for the clinic. Scaling up MSC manufacturing has a significant effect on parameters such as nutrient transport and MSC metabolism.30 Another parameter is the type of media used for the expansion of MSCs. Priming MSCs with inflammatory factors such as IFN-γ or TNF-α, as well as hypoxia, are also being explored for MSC therapies due to the potential of increasing their therapeutic potential.[23,66,69] Priming conditions have significant effects on MSC metabolism and could potentially lead to greater therapeutic outcomes through a more homogeneous, potent MSC product.[23,30,66] Lastly, MSC metabolism could further predict MSC engraftment and survivability in vivo, which together have been linked to clinical outcomes.[70] By using multiple MSC lines and ML models, this study sets the framework for rigorous predictive marker identification that can be used in future studies to help address potential manufacturing process hurdles for MSC therapeutics. Based on the metabolite classes identified in this work (both in-process and at the end of expansion), targeted assays can be developed for better MSC potency assessment and release/selection criteria for immunomodulatory therapeutics.

3.6 REFERENCES

1. Galipeau, J. & Sensébé, L. Mesenchymal Stromal Cells: Clinical Challenges and Therapeutic Opportunities. Cell Stem Cell 22, 824–833 (2018).
2. Ball, L. M. et al. Multiple infusions of mesenchymal stromal cells induce sustained remission in children with steroid-refractory, grade III–IV acute graft-versus-host disease. Br J Haematol 163, 501–509 (2013).
3. Lanzoni, G. et al. Umbilical cord mesenchymal stem cells for COVID-19 acute respiratory distress syndrome: A double-blind, phase 1/2a, randomized controlled trial. Stem Cells Transl Med 10, 660 (2021).

4. Pittenger, M. F. et al. Mesenchymal stem cell perspective: cell biology to clinical progress. npj Regenerative Medicine vol. 4 1–15 Preprint at https://doi.org/10.1038/s41536-019-0083-6 (2019).
5. Dominici, M. et al. Minimal criteria for defining multipotent mesenchymal stromal cells. The International Society for Cellular Therapy position statement. Cytotherapy 8, 315–317 (2006).
6. Zuk, P. A. et al. Multilineage cells from human adipose tissue: implications for cell-based therapies. Tissue Eng 7, 211–228 (2001).
7. T, N.-I. & H, H. Umbilical cord-derived mesenchymal stem cells: Their advantages and potential clinical utility. World J Stem Cells 6, 195 (2014).
8. van Balkom, B. W. M., Gremmels, H., Giebel, B. & Lim, S. K. Proteomic Signature of Mesenchymal Stromal Cell-Derived Small Extracellular Vesicles. Proteomics 19, (2019).
9. Vizoso, F. J., Eiro, N., Cid, S., Schneider, J. & Perez-Fernandez, R. Mesenchymal Stem Cell Secretome: Toward Cell-Free Therapeutic Strategies in Regenerative Medicine. Int J Mol Sci 18, (2017).
10. Spees, J. L., Lee, R. H. & Gregory, C. A. Mechanisms of mesenchymal stem/stromal cell function. Stem Cell Res Ther 7, (2016).
11. Kebriaei, P. et al. A Phase 3 Randomized Study of Remestemcel-L versus Placebo Added to Second-Line Therapy in Patients with Steroid-Refractory Acute Graft-versus-Host Disease. Biol Blood Marrow Transplant 26, 835 (2020).
12. Brachtl, G. et al. Batch Effects during Human Bone Marrow Stromal Cell Propagation Prevail Donor Variation and Culture Duration: Impact on Genotype, Phenotype and Function. Cells 11, (2022).

13. Stroncek, D. F. et al. Human Mesenchymal Stromal Cell (MSC) Characteristics Vary Among Laboratories When Manufactured From the Same Source Material: A Report by the Cellular Therapy Team of the Biomedical Excellence for Safer Transfusion (BEST) Collaborative. Front Cell Dev Biol 8, (2020).

14. Olsen, T. R., Ng, K. S., Lock, L. T., Ahsan, T. & Rowley, J. A. Peak MSC-Are we there yet? Frontiers in Medicine vol. 5 Preprint at https://doi.org/10.3389/fmed.2018.00178 (2018).

15. Wuchter, P. et al. Standardization of Good Manufacturing Practice-compliant production of bone marrow-derived human mesenchymal stromal cells for immunotherapeutic applications. Cytotherapy 17, 128–139 (2015).

16. ROBB, K. P., FITZGERALD, J. C., BARRY, F. & VISWANATHAN, S. Mesenchymal stromal cell therapy: progress in manufacturing and assessments of potency. Cytotherapy 21, 289–306 (2019).

17. de Wolf, C., van de Bovenkamp, M. & Hoefnagel, M. Regulatory perspective on in vitro potency assays for human mesenchymal stromal cells used in immunotherapy. Cytotherapy vol. 19 784–797 Preprint at https://doi.org/10.1016/j.jcyt.2017.03.076 (2017).

18. Shi, Y. et al. How mesenchymal stem cells interact with tissue immune responses. Trends Immunol 33, 136–143 (2012).

19. Gieseke, F. et al. Human multipotent mesenchymal stromal cells use galectin-1 to inhibit immune effector cells. Blood 116, 3770–3779 (2010).

20. Gonçalves, F. D. C. et al. Membrane particles generated from mesenchymal stromal cells modulate immune responses by selective targeting of pro-inflammatory monocytes. Sci Rep 7, (2017).

21. Bowles, A. C. et al. Signature quality attributes of CD146 + mesenchymal stem/stromal cells correlate with high therapeutic and secretory potency. Stem Cells 38, 1034–1049 (2020).

22. Saparov, A., Ogay, V., Nurgozhin, T., Jumabay, M. & Chen, W. C. W. Preconditioning of Human Mesenchymal Stem Cells to Enhance Their Regulation of the Immune Response. Stem Cells Int 2016, (2016).

23. Liu, Y., Yuan, X., Muñoz, N., Logan, T. M. & Ma, T. Commitment to Aerobic Glycolysis Sustains Immunosuppression of Human Mesenchymal Stem Cells. Stem Cells Transl Med 8, 93–106 (2019).

24. Jimenez, A. C., Heist, C. A., Navaei, M., Yeago, C. & Roy, K. Longitudinal two-dimensional gas chromatography mass spectrometry as a non-destructive at-line monitoring tool during cell manufacturing identifies volatile features correlative to cell product quality. Cytotherapy (2022) doi:10.1016/J.JCYT.2022.06.001.

25. Odeh-Couvertier, V. Y. et al. Predicting T-cell quality during manufacturing through an artificial intelligence-based integrative multiomics analytical platform. Bioeng Transl Med 7, (2022).

26. Maughon, T. S. et al. Metabolomics and cytokine profiling of mesenchymal stromal cells identify markers predictive of T-cell suppression. Cytotherapy 24, 137–148 (2022).

27. Goodarzi, P. et al. I IJ JM MC CM M Metabolomics Analysis of Mesenchymal Stem Cells. (2019).

28. Rinschen, M. M., Ivanisevic, J., Giera, M. & Siuzdak, G. Identification of bioactive metabolites using activity metabolomics. Nature Reviews Molecular Cell Biology vol. 20 353–367 Preprint at https://doi.org/10.1038/s41580-019-0108-4 (2019).

29. Dunn, W. B., Bailey, N. J. C. & Johnson, H. E. Measuring the metabolome: Current analytical technologies. Analyst vol. 130 606–625 Preprint at https://doi.org/10.1039/b418288j (2005).

30. Yuan, X., Logan, T. M. & Ma, T. Metabolism in human mesenchymal stromal cells: A missing link between HMSC biomanufacturing and therapy? Frontiers in Immunology vol. 10 977 Preprint at https://doi.org/10.3389/fimmu.2019.00977 (2019).

31. Delaglio, F. et al. NMRPipe: A multidimensional spectral processing system based on UNIX pipes. Journal of Biomolecular NMR 1995 6:3 6, 277–293 (1995).

32. Robinette, S. L. et al. Hierarchical alignment and full resolution pattern recognition of 2D NMR Spectra: Application to nematode chemical ecology. Anal Chem 83, 1649–1657 (2011).

33. Maciejewski, M. W. et al. NMRbox: A Resource for Biomolecular NMR Computation. Biophys J 112, 1529–1534 (2017).

34. Johnson, W. E., Li, C. & Rabinovic, A. Adjusting batch effects in microarray expression data using empirical Bayes methods. Biostatistics 8, 118–127 (2007).

35. Pang, Z. et al. Using MetaboAnalyst 5.0 for LC–HRMS spectra processing, multi-omics integration and covariate adjustment of global metabolomics data. Nature Protocols 2022 17:8 17, 1735–1761 (2022).

36. Pedregosa, F. et al. Scikit-learn: Machine Learning in Python. Journal of Machine Learning Research 12, 2825–2830 (2012).

37. Acevedo, A., Durán, C., Ciucci, S., Gerl, M. & Cannistraci, C. V. LIPEA: Lipid Pathway Enrichment Analysis. bioRxiv 274969 (2018) doi:10.1101/274969.

38. Koza, J. R. Genetic programming as a means for programming computers by natural selection. Statistics and Computing 1994 4:2 4, 87–112 (1994).

39. Mendez, K. M., Reinke, S. N. & Broadhurst, D. I. A comparative evaluation of the generalised predictive ability of eight machine learning algorithms across ten clinical metabolomics data sets for binary classification. Metabolomics 15, 1–15 (2019).

40. Hishikawa, D., Hashidate, T., Shimizu, T. & Shindou, H. Diversity and function of membrane glycerophospholipids generated by the remodeling pathway in mammalian cells. J Lipid Res 55, 799–807 (2014).

41. Lu, X. et al. Integrated Lipidomics and Transcriptomics Characterization upon Aging-Related Changes of Lipid Species and Pathways in Human Bone Marrow Mesenchymal Stem Cells. J Proteome Res 18, 2065–2077 (2019).

42. Kilpinen, L. et al. Aging bone marrow mesenchymal stromal cells have altered membrane glycerophospholipid composition and functionality. J Lipid Res 54, 622–635 (2013).

43. van der Veen, J. N. et al. The critical role of phosphatidylcholine and phosphatidylethanolamine metabolism in health and disease. Biochimica et Biophysica Acta (BBA) - Biomembranes 1859, 1558–1572 (2017).

44. Killer, M. C. et al. Immunosuppressive capacity of mesenchymal stem cells correlates with metabolic activity and can be enhanced by valproic acid. Stem Cell Res Ther 8, 1–8 (2017).

45. Rockenfeller, P. et al. Phosphatidylethanolamine positively regulates autophagy and longevity. Cell Death & Differentiation 2015 22:3 22, 499–508 (2015).

46. Jakovljevic, J. et al. Modulation of autophagy as new approach in mesenchymal stem cell-based therapy. Biomedicine & Pharmacotherapy 104, 404–410 (2018).

47. Rastaldo, R., Vitale, E. & Giachino, C. Dual Role of Autophagy in Regulation of Mesenchymal Stem Cell Senescence. Front Cell Dev Biol 8, 276 (2020).

48. Hooper, N. M. Glycosyl-phosphatidylinositol anchored membrane enzymes. Clinica Chimica Acta 266, 3–12 (1997).

49. Katoh, M. & Katoh, M. CD157 and CD200 at the crossroads of endothelial remodeling and immune regulation. Stem Cell Investig 6, (2019).

50. Li, J. et al. CD157 in bone marrow mesenchymal stem cells mediates mitochondrial production and transfer to improve neuronal apoptosis and functional recovery after spinal cord injury. Stem Cell Res Ther 12, 1–14 (2021).

51. Ortolan, E., Augeri, S., Fissolo, G., Musso, I. & Funaro, A. CD157: From immunoregulatory protein to potential therapeutic target. Immunol Lett 205, 59–64 (2019).

52. Segawa, K. & Nagata, S. An Apoptotic ‘Eat Me’ Signal: Phosphatidylserine Exposure. Trends Cell Biol 25, 639–650 (2015).

53. Galleu, A. et al. Apoptosis in mesenchymal stromal cells induces in vivo recipient-mediated immunomodulation. Sci Transl Med 9, (2017).

54. Pang, S. H. M. et al. Mesenchymal stromal cell apoptosis is required for their therapeutic function. Nature Communications 2021 12:1 12, 1–19 (2021).

55. DeVeaux, S. A. et al. Characterizing human mesenchymal stromal cells' immune-modulatory potency using targeted lipidomic profiling of sphingolipids. Cytotherapy 24, 608–618 (2022).

56. Khayrullin, A. et al. Very Long-Chain C24:1 Ceramide Is Increased in Serum Extracellular Vesicles with Aging and Can Induce Senescence in Bone-Derived Mesenchymal Stem Cells. Cells 8, (2019).

57. Price, S. T. et al. Sphingosine 1-Phosphate Receptor 2 Regulates the Migration, Proliferation, and Differentiation of Mesenchymal Stem Cells. Int J Stem Cell Res Ther 2, (2015).

58. Marycz, K. et al. The effect of the bioactive sphingolipids S1P and C1P on multipotent stromal cells-new opportunities in regenerative medicine. Cell Mol Biol Lett 20, 510–533 (2015).

59. Lipsitz, Y. Y., Timmins, N. E. & Zandstra, P. W. Quality cell therapy manufacturing by design. Nature Biotechnology 2016 34:4 34, 393–400 (2016).

60. Baradez, M. O., Biziato, D., Hassan, E. & Marshall, D. Application of Raman spectroscopy and univariate modelling as a process analytical technology for cell therapy bioprocessing. Front Med (Lausanne) 5, 47 (2018).

61. O'Brien, S. A. & Hu, W. S. Cell culture bioprocessing — the road taken and the path forward. Curr Opin Chem Eng 30, 128–134 (2020).

62. Jimenez, A. C., Heist, C. A., Navaei, M., Yeago, C. & Roy, K. Longitudinal two-dimensional gas chromatography mass spectrometry as a non-destructive at-line monitoring tool during cell manufacturing identifies volatile features correlative to cell product quality. Cytotherapy 24, 1136–1147 (2022).

63. Sun, Y. et al. Metabolic profiling associated with autophagy of human placenta-derived mesenchymal stem cells by chemical isotope labeling LC−MS. Exp Cell Res 372, 52–60 (2018).

64. Soria, L. R. et al. Enhancement of hepatic autophagy increases ureagenesis and protects against hyperammonemia. Proc Natl Acad Sci U S A 115, 391–396 (2018).

65. Tapiero, H., Mathé, G., Couvreur, P. & Tew, K. D. I. Arginine. Biomedicine & Pharmacotherapy 56, 439–445 (2002).

66. Wobma, H. M. et al. The influence of hypoxia and IFN-γ on the proteome and metabolome of therapeutic mesenchymal stem cells. Biomaterials 167, 226–234 (2018).

67. Li, J. Z. et al. Metabolic profiles of adipose-derived and bone marrow-derived stromal cells from elderly coronary heart disease patients by capillary liquid chromatography quadrupole time-of-flight mass spectrometry. Int J Mol Med 41, 184–194 (2018).

68. Zhuang, Y. et al. Comparison of biological properties of umbilical cord.derived mesenchymal stem cells from early and late passages: Immunomodulatory ability is enhanced in aged cells. Mol Med Rep 11, 166–174 (2015).

69. Klinker, M. W., Marklein, R. A., lo Surdo, J. L., Wei, C. H. & Bauer, S. R. Morphological features of IFN-γ-stimulated mesenchymal stromal cells predict overall immunosuppressive capacity. Proc Natl Acad Sci U S A 114, E2598–E2607 (2017).

70. Salazar-Noratto, G. E. et al. Understanding and leveraging cell metabolism to enhance mesenchymal stem cell transplantation survival in tissue engineering and regenerative medicine applications. Stem Cells 38, 22–33 (2020).

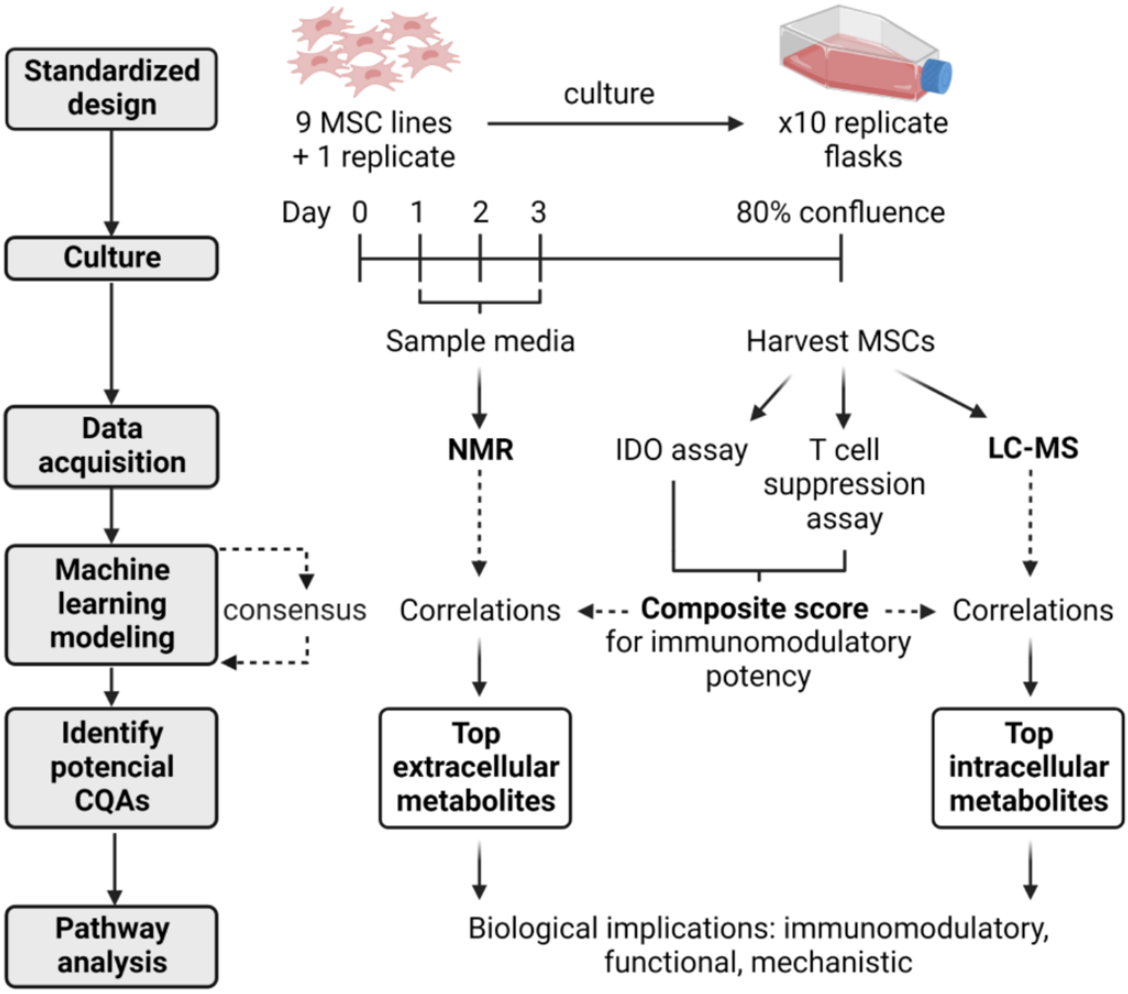

Graphical Abstract Figure 3.1. Graphical Abstract Methodology

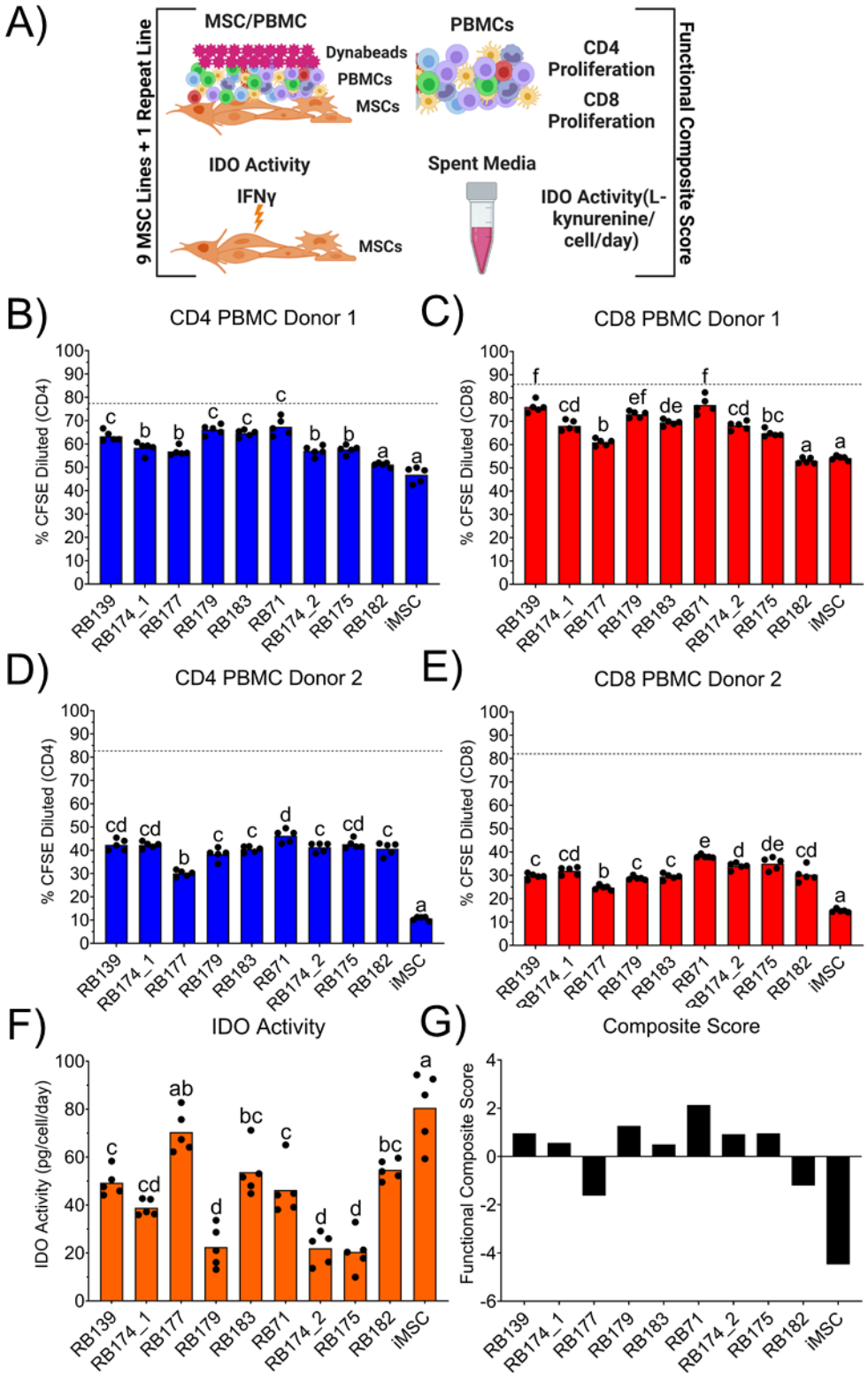
A)
9 MSC Lines + 1 Repeat Line
MSC/PBMC
Dynabeads
PBMCs
MSCs
IDO Activity
IFNγ
MSCs
PBMCs
Spent Media
CD4 Proliferation
CD8 Proliferation
IDO Activity(L-kynurenine/cell/day)
Functional Composite Score
B)
CD4 PBMC Donor 1
% CFSE Diluted (CD4)
C)
CD8 PBMC Donor 1
% CFSE Diluted (CD8)
D)
CD4 PBMC Donor 2
% CFSE Diluted (CD4)
E)
CD8 PBMC Donor 2
% CFSE Diluted (CD8)
F)
IDO Activity
IDO Activity (pg/cell/day)
G)
Composite Score
Functional Composite Score
RB139
RB174_1
RB177
RB179
RB183
RB71
RB174_2
RB175
RB182
iMSC

Figure 3.1. Functional analysis of MSCs at the end of expansion. (A) Schematic of functional assays used to generate functional composite score. CD4 (B) and CD8 (C) T cell proliferation of PBMC donor 1 and CD4 (D) and CD8 (E) T cell proliferation of PBMC donor 2 based on %CFSE dilution. (F) IDO activity measured by levels of L-kynurenine in terms of pg/cell/day. (G) Functional composite score based on results of all assays (B-F). All statistics were calculated using a one-way ANOVA with Tukey's post hoc test. Differences in letters indicate a significant difference ($P<0.05$) between MSC lines.

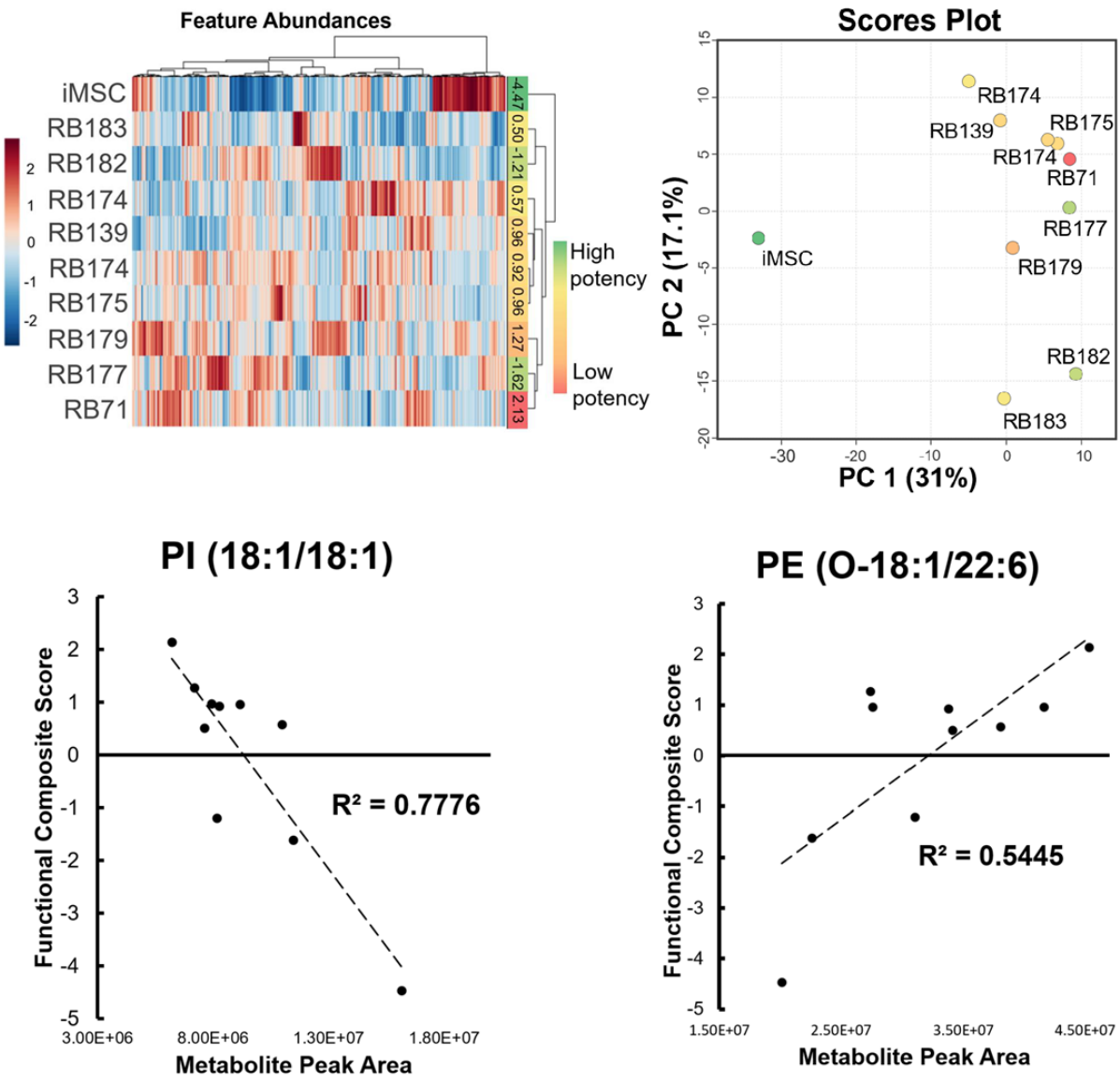

Figure 3.2. Mass spectrometry metabolomics analysis of MSC lines. Heatmap (A) and PCA scores plot (B) of ten MSC pellet samples with all 479 annotated features in the UHPLC-MS dataset that fed into the ML regression workflow. Samples are color coded according to the composite functional score determined from the functional assay results (Figure 1G). Red indicates a higher score (i.e. lower function) in immunomodulatory assays. Green indicates a lower score (i.e. higher function). Heatmap uses Euclidean distance measure and Ward

clustering. Simple linear regressions of the abundances of lipids PI (18:1/18:1) (C) and PE (O-18:1/22:6) (D) against the functional composite score for 10 MSC samples.

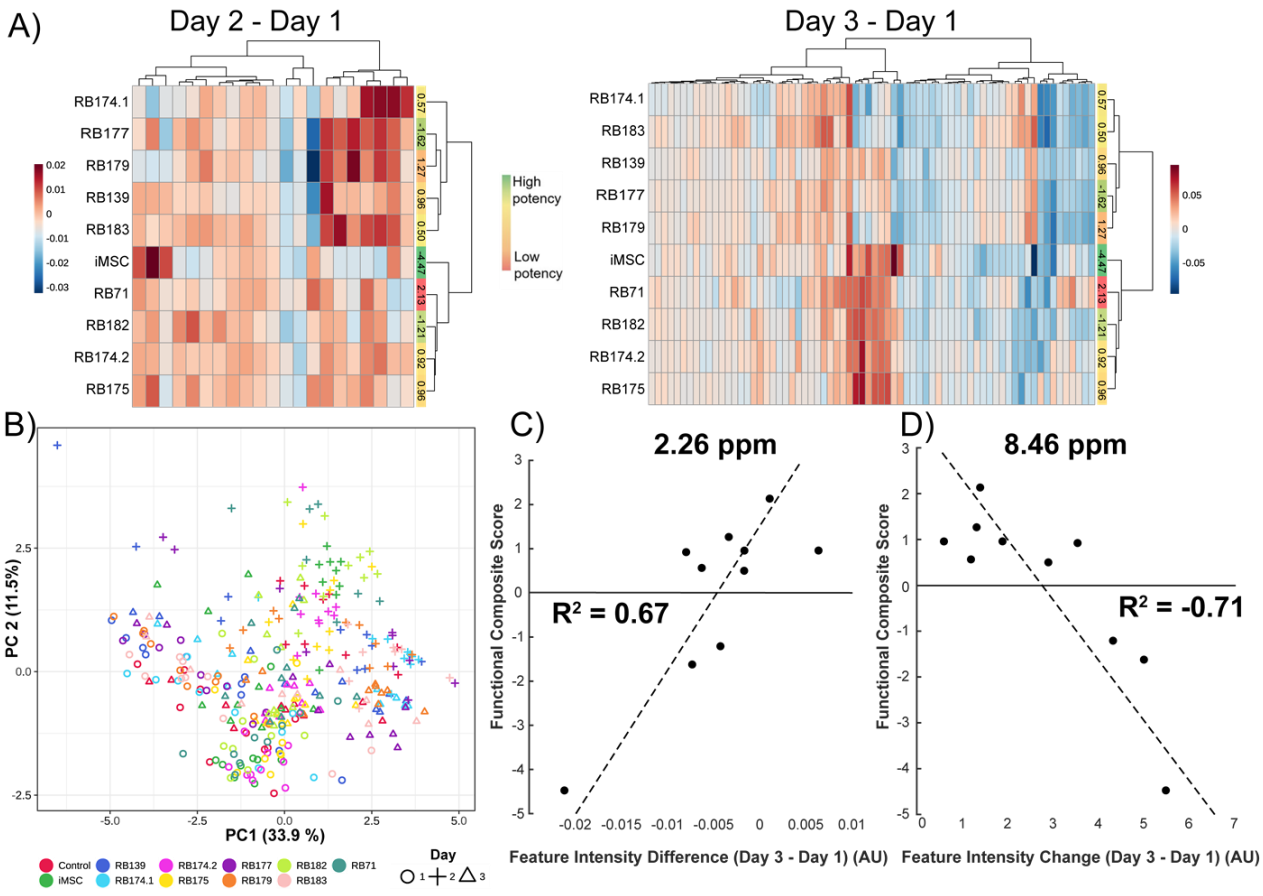

Figure 3.3. NMR analysis on daily media samples. A) Heatmap clustergram of Day 2-Day 1 highly variable feature intensities (21) and Day 3-Day 1 highly variable feature intensities (69). B) PCA scores plot of all samples from days 1-3, using all spectral features (138) as input. n=10 datapoints for each cell-line/timepoint with each cell-line represented by different color and each day by different shape. C) Regression of average donor Day 3 – Day 1 differences of feature at 2.26 ppm with composite functional score. D) Regression of average donor Day 3 – Day 1 differences of feature at 8.46 ppm with composite functional score.

Input dataset	ML Regression Model - LOO-R2						
Intracellular	SR	PLSR	SVM	GBR	LASSO	RF	DT
MS Lipids	0.98	0.90	0.98	0.87	1.00	0.78	0.84
MS Small Polars	0.99	0.89	0.96	0.88	0.83	0.79	0.84
Consensus	0.99	0.89	1.00	0.88	0.92	0.83	0.60
Consensus w/o iMSC	0.99	0.94	0.89	0.86	0.88	0.80	0.72
Extracellular	SR	PLSR	SVM	GBR	LASSO	RF	DT
NMR Day 3 – Day 1	0.99	0.90	0.99	0.88	0.93	0.71	0.91
NMR Day 2 – Day 1	0.99	0.53	0.96	0.85	0.57	0.71	0.86
Consensus	0.99	0.87	0.82	0.89	0.72	0.60	0.86
Consensus w/o iMSC	0.96	0.64	0.42	0.75	0.31	0.50	0.68

Table 3.1. Summary of Machine Learning Models to Predict MSC Potency. Machine learning (ML) models using various regression types – symbolic regression (SR), partial-least-squares regression (PLSR), support vector machine (SVM), gradient-boosted regression (GBR), least absolute shrinkage and selection operator (LASSO), random forest (RF), and decision tree (DT). Models created using four different input datasets: MS lipids, MS metabolites, NMR Day 3 – Day 1, and NMR Day 2 – Day 1 feature abundances. Consensus models created from only metabolites present in more than one of the initial models for both intracellular and extracellular metabolite datasets (using all 10 MSC lines). Final panels for the consensus models were used to create additional models trained and cross-validated on only the bone marrow derived lines (Consensus w/o iMSC, 9 total MSC lines).

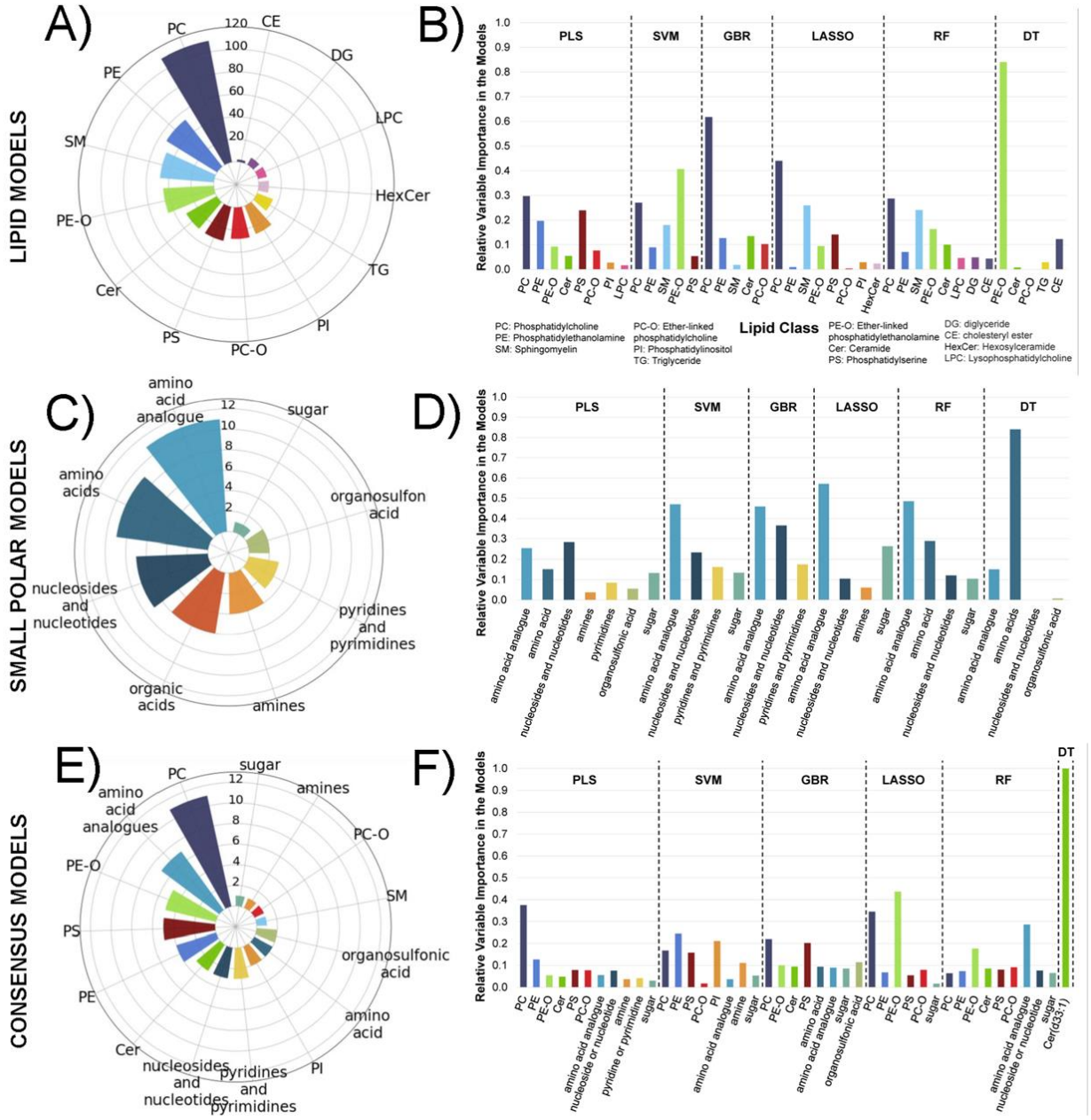

Figure 3.4. Mass Spectrometry Models to Predict MSC Potency. Radar plot (A) displaying the number of detected lipids in the annotated dataset organized according to lipid class. Bar plot (B) displaying the relative variable importance, calculated using the variable weights in the models, of each lipid class in each model type. Radar plot (C) displaying the number of detected small polar metabolites in the annotated dataset organized according to class. Bar plot (D) displaying

the relative variable importance, calculated using the variable weights in the models, of molecule class in each model type. Radar plot (E) displaying the numbers of metabolites that presented in more than one initial model organized according to class. This list of consensus metabolites was used to create the consensus models. Bar plot (F) displaying the relative variable importance, calculated using the variable weights in the models, of each metabolite in the consensus models.

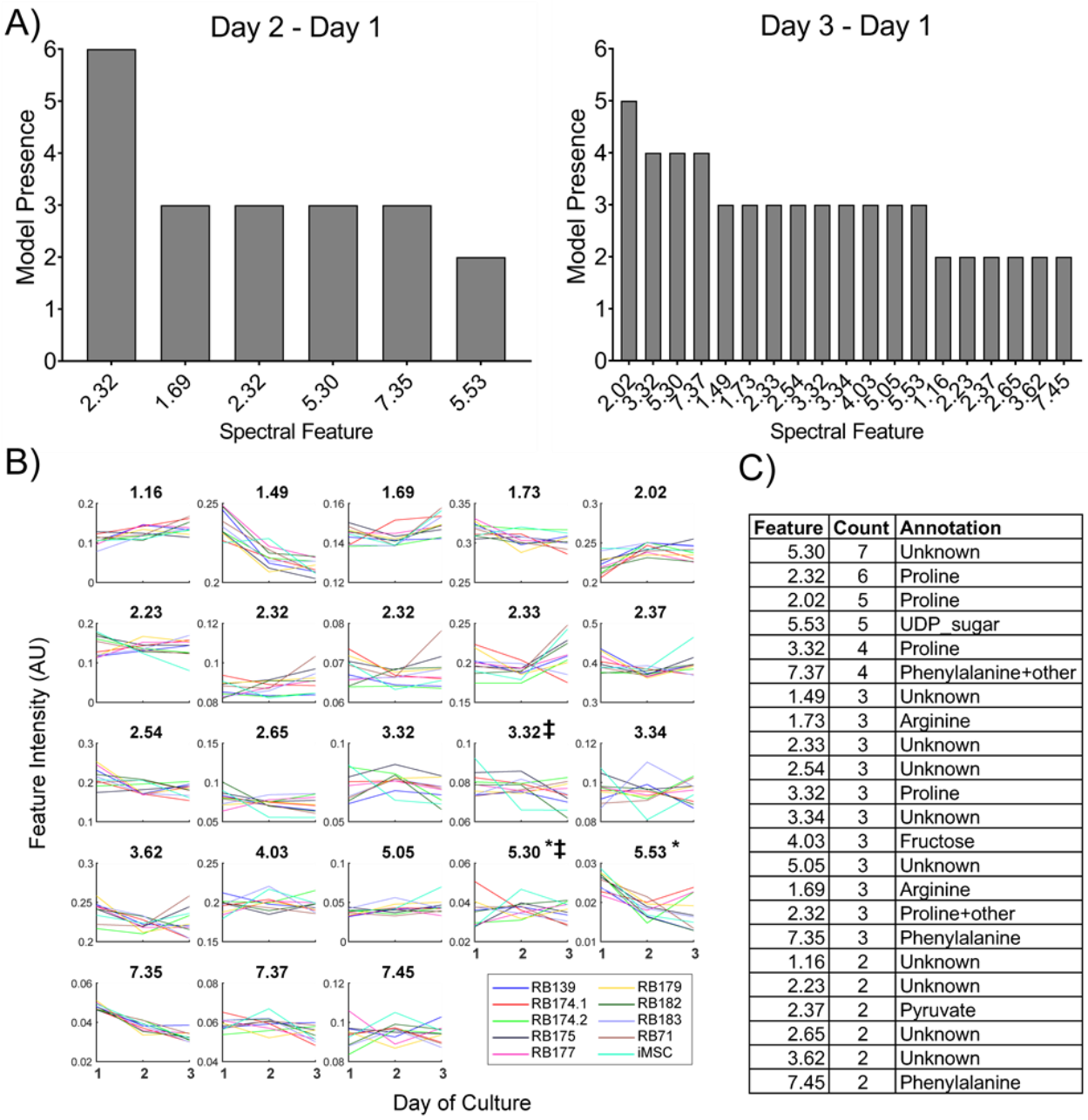

Feature	Count	Annotation
5.30	7	Unknown
2.32	6	Proline
2.02	5	Proline
5.53	5	UDP_sugar
3.32	4	Proline
7.37	4	Phenylalanine+other
1.49	3	Unknown
1.73	3	Arginine
2.33	3	Unknown
2.54	3	Unknown
3.32	3	Proline
3.34	3	Unknown
4.03	3	Fructose
5.05	3	Unknown
1.69	3	Arginine
2.32	3	Proline+other
7.35	3	Phenylalanine
1.16	2	Unknown
2.23	2	Unknown
2.37	2	Pyruvate
2.65	2	Unknown
3.62	2	Unknown
7.45	2	Phenylalanine

Figure 3.5. Consensus NMR metabolite feature trends and annotation. A) Consensus features selected as important across all modeling methods for Day 3- Day 1, and Day 2 – Day 1 datasets. Counts indicate for how many models each feature was selected within top 10% of important variables for prediction. Names of features represent approximate ppm of quantified spectral peak. B) Average spectral feature intensity trajectories over Days 1-3 (n=10 per donor per timepoint). Feature names indicate approximate chemical shift values of integrated peak.

Intensity values are in arbitrary units. * Indicates consensus features in both timepoint datasets. ‡ indicates features identified from SR consensus model. C) Putative metabolite annotations of consensus spectral features. UDP = uridine diphosphate

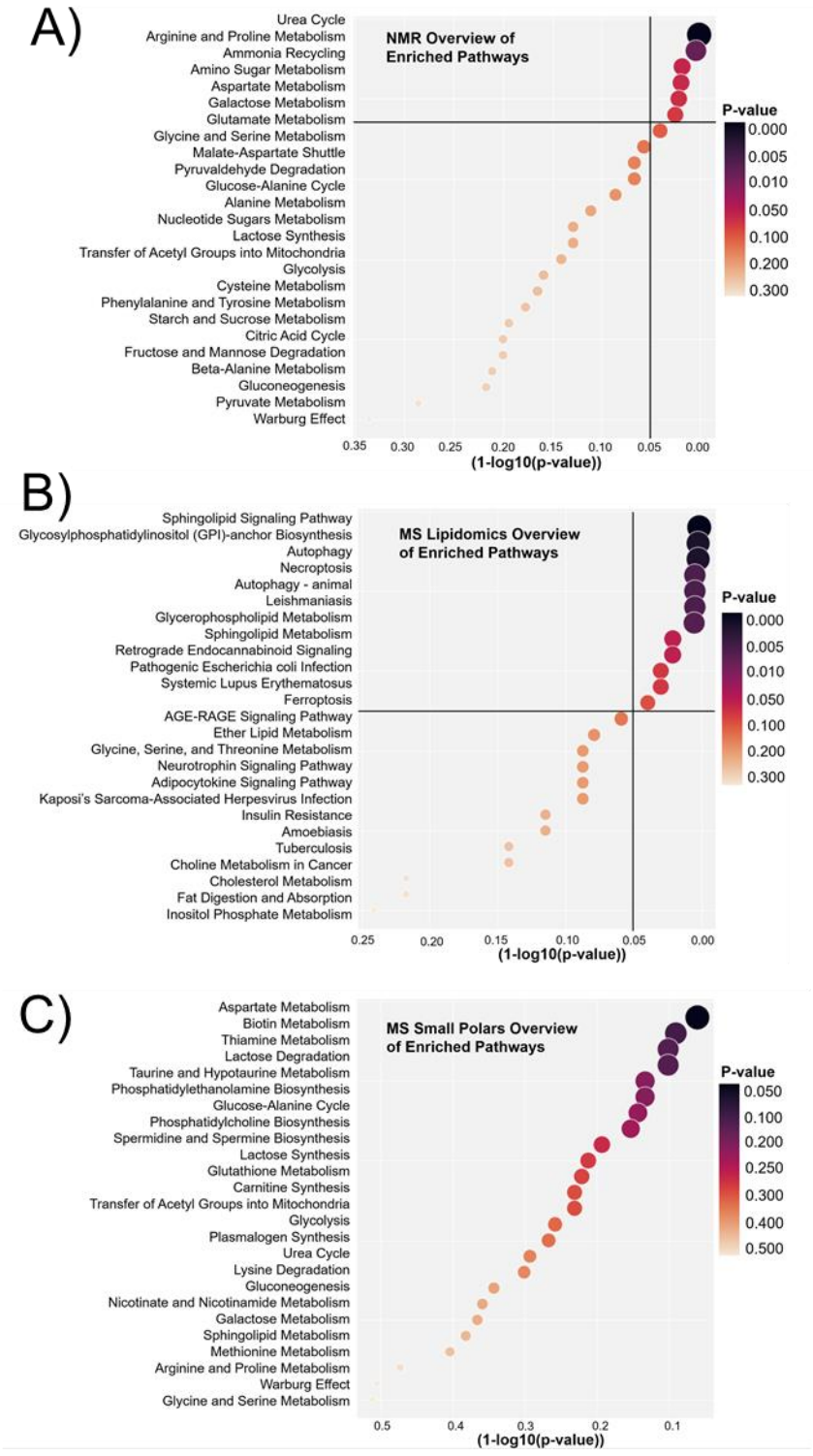

Figure 3.6. Enriched pathways identified from MS and NMR consensus metabolite datasets.

Pathway enrichments plots from NMR metabolite modeling consensus list with pathways and p-

values calculated using Metaboanalyst (A), MS lipid modeling consensus list with pathways and p-values calculated using LIPEA (B), and MS small polar consensus list with pathways and p-values calculated using Metaboanalyst (C). Size and color of markers are scaled according to p-value.

Donor	Sex	Age (years old)	Total cells seeded (C_i)	Final cell yield (C_f)	Initial population doubling level (PDL_0)	Final PDL
RB139	Male	25	3.75E+05	8.10E+06	12.2	16.6
RB174.1	Male	25	3.75E+05	9.80E+06	13.06	17.8
RB177	Male	22	3.75E+05	4.23E+06	15.1	18.6
RB179	Male	21	3.75E+05	8.20E+06	12.6	17.1
RB183	Female	26	3.75E+05	5.30E+06	12	15.8
RB71*	Female	18-30	3.75E+05	7.50E+06	12.72	17.0
RB174.2	Male	25	3.75E+05	8.43E+06	13.06	17.6
RB175	Male	25	3.75E+05	6.24E+06	12	16.1
RB182*	Female	26	3.75E+05	3.65E+06	11.48	14.8
iMSC*	Not available		3.75E+05	1.86E+07	Not available	

*MSC cell lines used in previous study[26]

Supplemental Table 3.1. MSC donor and expansion information.

Laser	EM Filter	Marker	Color / Format	Host / Target	Isotype	Clone	Company	Catalog
405	710/50	CD4	Brilliant Violet 711	Mouse anti-Human	IgG1 κ	RPA-T4	BioLegend	300558
638	660/20	CD8	APC	Mouse anti-Human	IgG1	CN9V1	BioLegend	orb248718
488	525/40	CFSE	CFSE	N/A	N/A	N/A	BioLegend	423801
405	610/20	Zombie Yellow	Zombie Yellow	N/A anti-All Species	N/A	N/A	BioLegend	423104

Supplemental Table 3.2: Antibodies used for T cell suppression assay.

HILIC Chromatography		Reverse Phase Chromatography	
0-8 min	5% Mobile Phase A	0-1 min	80% Mobile Phase A
8-10.4 min	60% Mobile Phase A	1-5 min	40% Mobile Phase A
10.5-14 min	5% Mobile Phase A	5-5.5 min	30% Mobile Phase A
		5.5-8 min	15% Mobile Phase A
		8-8.2 min	10% Mobile Phase A
		8.2-10.5 min	0% Mobile Phase A
		10.7-12 min	80% Mobile Phase A

Supplemental Table 3.3. UHPLC chromatographic gradients. Mobile Phase A used for HILIC chromatography was 80:20 water:MeCN with 10 mM ammonium formate and 0.1% formic acid. Mobile phase B for HILIC chromatography was acetonitrile with 0.1% formic acid. The flow rate was set at 0.4 mL/min. The column temperature was set to 40 °C, the injection volume was 2 µL. Mobile Phase A for Reverse Phase chromatography in positive mode was 40:60 water: acetonitrile with 10 mM ammonium formate and 0.1% formic acid and Mobile Phase B was 10:90 acetonitrile:isopropyl alcohol, with 10 mM ammonium formate and 0.1% formic acid. For negative ionization mode, the mobile phases were 40:60 water:acetonitrile with 10 mM ammonium acetate (mobile phase A) and 10:90 acetonitrile:isopropyl alcohol, with 10 mM ammonium acetate (mobile phase B). The flow rate was set at 0.40 mL min-1. The column temperature was set to 50 °C, and the injection volume was 2 µL.

A) Proposed lipid annotations for all lipids that presented in the final panel for more than one lipid model.

Metabolite ID	Elemental Formula	Proposed Annotation	Adduct Type	Monoisotopic Mass	Experimental *m/z*	Retention Time	Mass Error (ppm)	MS2 Library Database Match	Collision Energy (eV)	Confidence Level	Number of Models	Indidividual R2 with Composite Score	P-value
RP_neg_1210	$C_{37}H_{74}NO_7P$	PE(O-16:1/16:0)	[M-H]-	675.5203	674.5145	5.934	2.16	mzVault	HCD 10, 30, 50	2	4 (Lipid)	0.289	0.109
HILIC_pos_772	$C_{44}H_{86}NO_8P$	PC(36:1)	[M+H]+	787.6091	788.6162	3.764	-0.21	mzVault	HCD 15, 30, 45 & CID 35	2	4 (Lipid)	0.678	0.031
RP_pos_2480	$C_{39}H_{76}NO_8P$	PC(31:1)	[M+H]+	717.5309	718.5371	4.495	-1.43	mzVault	HCD 10, 30, 50	2	3 (Lipid)	0.361	0.066
HILIC_neg_619	$C_{42}H_{80}NO_{10}P$	PS(18:0/18:1)	[M-H]-	789.5520	788.5463	5.282	2.05	mzVault	HCD 15, 30, 45 & CID 35	2	3 (Lipid)	0.348	0.072
RP_pos_2495	$C_{39}H_{78}NO_8P$	PC(31:0)	[M+H]+	719.5465	720.5524	6.323	-1.94	mzVault	HCD 10, 30, 50	2	3 (Lipid)	0.274	0.120
RP_pos_2846	$C_{45}H_{82}NO_7P$	PE(O-18:1/22:4)	[M+H]+	779.5829	780.5892	6.555	-1.28	mzVault	HCD 10, 30, 50	2	3 (Lipid)	0.398	0.051
RP_pos_2911	$C_{45}H_{76}NO_8P$	PE(40:7)	[M+H]+	789.5309	790.5364	4.491	-2.24	mzVault	HCD 10, 30, 50	2	3 (Lipid)	0.221	0.170
RP_pos_2559	$C_{40}H_{78}NO_8P$	PC(32:1)	[M+H]+	731.5465	732.5524	4.900	-1.88	mzVault	HCD 10, 30, 50	2	3 (Lipid)	0.071	0.456
RP_neg_1419	$C_{41}H_{82}NO_7P$	PE(O-18:2/18:1)	[M-H]-	727.5516	726.5464	6.023	2.88	mzVault	HCD 10, 30, 50	2	3 (Lipid)	0.019	0.705
RP_pos_3189	$C_{48}H_{95}N_2O_6P$	SM(d43:2)	[M+H]+	826.6928	827.6988	7.392	-1.49	mzVault	HCD 10, 30, 50	2	2 (Lipid)	0.592	0.009
RP_neg_1532	$C_{43}H_{84}NO_7P$	PE(O-18:1/20:1)	[M-H]-	757.5985	756.5930	7.134	2.24	mzVault	HCD 10, 30, 50	2	2 (Lipid)	0.194	0.202
RP_neg_1789	$C_{41}H_{80}NO_8P$	PE(18:0/18:1)	[M+NaHCO2]-	745.5622	812.5443	6.422	2.41	mzVault	HCD 10, 30, 50	2	2 (Lipid)	0.238	0.153
RP_pos_2930	$C_{45}H_{78}NO_8P$	PE(40:6)	[M+H]+	791.5465	792.5529	4.731	-1.09	mzVault	HCD 10, 30, 50	2	2 (Lipid)	0.061	0.492
HILIC_pos_741	$C_{42}H_{84}NO_7P$	PC(O-34:1)	[M+H]+	745.5985	746.6065	3.784	0.91	mzVault	HCD 15, 30, 45 & CID 35	2	2 (Lipid)	0.377	0.059
RP_pos_2918	$C_{44}H_{88}NO_8P$	PC(36:0)	[M+H]+	789.6248	790.6317	7.290	-0.37	mzVault	HCD 10, 30, 50	2	2 (Lipid)	0.545	0.015
HILIC_pos_738	$C_{41}H_{78}NO_8P$	PE(36/2)	[M+H]+	743.5465	744.5544	3.704	0.82	mzVault	HCD 15, 30, 45 & CID 35	2	2 (Lipid)	0.391	0.053
RP_neg_1656	$C_{42}H_{78}NO_{10}P$	PS(18:1/18:1)	[M+H]+	787.5363	788.5450	4.475	1.78	mzVault	HCD 10, 30, 50	2	2 (Lipid)	0.642	0.005
RP_neg_901	$C_{33}H_{65}NO_3$	Cer(d33:1)	[M+OAc]-	523.4964	582.5111	4.825	1.40	mzVault	HCD 10, 30, 50	2	2 (Lipid)	0.095	0.386
RP_neg_1889	$C_{46}H_{78}NO_{10}P$	PS(18:0/22:6)	[M-H]-	835.5363	834.5308	4.252	2.05	mzVault	HCD 10, 30, 50	2	2 (Lipid)	0.485	0.025
HILIC_neg_645	$C_{46}H_{82}NO_{10}P$	PS(18:0/22:4)	[M-H]-	839.5676	838.5610	5.184	0.81	mzVault	HCD 15, 30, 45 & CID 35	2	2 (Lipid)	0.407	0.047
RP_neg_2021	$C_{45}H_{83}O_{13}P$	PI(18:1/18:1)	[M-H]-	862.5571	861.5523	4.167	2.79	mzVault	HCD 10, 30, 50	2	2 (Lipid)	0.778	0.001
RP_neg_1336	$C_{42}H_{81}NO_3$	Cer(d42:2)	[M+OAc]-	647.6216	706.6376	7.261	2.94	mzVault	HCD 10, 30, 50	2	2 (Lipid)	0.025	0.746
RP_pos_2861	$C_{44}H_{80}NO_8P$	PC(36:4)	[M+H]+	781.5622	782.5675	4.797	-2.40	mzVault	HCD 10, 30, 50	2	2 (Lipid)	0.086	0.275
RP_pos_2464	$C_{49}H_{76}O_2$	CE(22:6)	[M+NH4]+	696.5845	714.6174	9.153	1.38	mzVault	HCD 10, 30, 50	2	2 (Lipid)	0.159	0.253

B) Proposed metabolite annotations for all metabolites that presented in the final panel for more than one small polar model.

Metabolite ID	Elemental Formula	Proposed Annotation	Adduct Type	Monoisotopic Mass	Experimental *m/z*	Retention Time	Mass Error (ppm)	MS2 Library Database Match	Collision Energy (eV)	Confidence Level	Number of Models	Indidividual R2 with Composite Score	P-value
HILIC_neg_87	$C_7H_{11}NO_3$	acetylglutamic acid	[M-H]-	189.0637	188.0566	3.77	0.55	mzCloud	HCD: 15, 30, 45; CID: 35	2	5 (Small Polar)	0.004	0.859
RP_pos_129	$C_8H_{16}N_2O_3$	acetyllysine	[M+H]+	188.1161	189.1232	0.81	-1.00	MONA	HCD: 10, 30, 50	2	4 (Small Polar)	0.083	0.420
HILIC_neg_67	$C_6H_{12}O_6$	glucose isomer	[M+HCOO]-	180.0634	225.0615	8.79	-0.44	*in-silico	HCD: 15, 30, 45; CID: 35	2	4 (Small Polar)	0.285	0.117
HILIC_pos_225	$C_{11}H_{15}N_5O_3S$	5'-methylthioadenosine	[M+H]+	297.0896	298.0969	2.86	-0.28	mzCloud	HCD: 15, 30, 45; CID: 35	2	4 (Small Polar)	0.291	0.107
RP_pos_430	$C_{12}H_{16}N_4OS$	thiamine	[M+H]+	264.1045	265.1116	0.81	0.48	mzCloud	HCD: 10, 30, 50	2	4 (Small Polar)	0.233	0.158
HILIC_neg_444	$C_{11}H_{26}N_4O_{11}P_2$	cytidine disphosphate ethanolamine	[M-H]-	446.0604	445.0532	9.62	0.26	MONA	HCD: 15, 30, 45; CID: 35	2	3 (Small Polar)	0.007	0.813
HILIC_neg_13	$C_5H_7NO_3$	pyroglutamic acid	[M-H]-	129.0426	128.0353	3.59	-0.21	mzCloud	HCD: 15, 30, 45; CID: 35	2	3 (Small Polar)	0.034	0.607
HILIC_neg_62	$C_6H_9NO_5$	acetylaspartic acid	[M-H]-	175.0481	174.0408	3.97	0.15	mzCloud	HCD: 15, 30, 45; CID: 35	2	3 (Small Polar)	0.002	0.899
HILIC_neg_40	$C_5H_9NO_4$	methylaspartic acid	[M-H]-	147.0532	146.0459	3.86	-0.01	*in silico	HCD: 15, 30, 45; CID: 35	2	3 (Small Polar)	0.569	0.012
HILIC_neg_61	$C_6H_{14}N_4O_2$	arginine	[M-H]-	174.1117	173.1044	9.32	-0.08	mzCloud	HCD: 15, 30, 45; CID: 35	2	2 (Small Polar)	0.056	0.510
HILIC_neg_6	$C_2H_7NO_3S$	taurine	[M-H]-	125.0146	124.0073	7.35	-0.03	mzCloud	HCD: 15, 30, 45; CID: 35	2	2 (Small Polar)	0.023	0.676
HILIC_pos_15	$C_6H_{14}N_2O_2$	lysine	[M+H]+	146.1055	147.1128	5.18	-0.11	mzCloud	HCD: 15, 30, 45; CID: 35	2	2 (Small Polar)	0.018	0.709
HILIC_pos_58	$C_9H_{12}N_2O_2$	hydroxykynurenamine	[M+NH4]+	180.0899	198.1238	1.47	-0.30	MONA	HCD: 15, 30, 45; CID: 35	2	2 (Small Polar)	0.458	0.032
RP_pos_153	$C_{10}H_{13}NO_3$	tyrosine methyl ester	[M+H]+	195.0895	196.0967	0.81	-0.81	mzCloud	HCD: 10, 30, 50	2	2 (Small Polar)	0.138	0.291
HILIC_neg_177	$C_9H_{12}N_2O_6$	uridine	[M-H]-	244.0694	243.0624	4.26	0.81	mzCloud	HCD: 15, 30, 45; CID: 35	2	2 (Small Polar)	0.125	0.316
HILIC_pos_10	$C_7H_8N_2O$	1-methylnicotinimide	[M+H]+	136.0637	137.0709	5.52	-0.12	mzCloud	HCD: 15, 30, 45; CID: 35	2	2 (Small Polar)	0.170	0.237

*in-silico fragmentation in Compound Discoverer

C) All metabolites, regardless of class, that had individual correlations with potency score with an R2 of 0.5 or greater.

Metabolite ID	Elemental Formula	Proposed Annotation	Adduct Type	Monoisotopic Mass	Experimental *m/z*	Retention Time	Mass Error (ppm)	MS2 Library Database Match	Collision Energy (eV)	Confidence Level	Number of Models	Indidividual R2 with Composite Score	P-value
RP_neg_2021	$C_{45}H_{83}O_{13}P$	PI(18:1/18:1)	[M-H]-	862.5571	861.5523	4.17	2.79	mzVault	HCD 10, 30, 50	2	2 (Lipid)	0.778	0.001
HILIC_neg_97	$C_{10}H_{11}NO_3$	phenylacetylglycine	[M-H]-	193.0739	192.0667	1.81	0.19	mzCloud	HCD: 15, 30, 45; CID: 35	2	1 (Small Polar)	0.734	0.002
RP_pos_3377	$C_{50}H_{88}NO_8P$	PC(42:6)	[M+H]+	861.6248	862.6299	5.58	-2.42	mzVault	HCD 10, 30, 50	2	1 (Lipid)	0.694	0.003
RP_neg_1656	$C_{42}H_{78}NO_{10}P$	PS(18:1/18:1)	[M-H]-	787.5363	786.5306	4.48	2.02	mzVault	HCD 10, 30, 50	2	2 (Lipid)	0.642	0.005
RP_pos_2542	$C_{40}H_{74}NO_8P$	PC(32:3)	[M+H]+	727.5152	728.5217	3.89	-1.02	mzVault	HCD 10, 30, 50	2	1 (Lipid)	0.632	0.006
RP_neg_1983	$C_{47}H_{91}N_2O_6P$	SM(d42:3)	[M+HCOO]-	810.6615	855.6616	6.45	2.24	mzVault	HCD 10, 30, 50	2	1 (Lipid)	0.603	0.008
HILIC_neg_143	$C_9H_{17}NO_5$	pantothenic acid	[M-H]-	219.1107	218.1034	2.62	0.12	mzCloud	HCD: 15, 30, 45; CID: 35	2	0 Models	0.602	0.008
RP_neg_1811	$C_{43}H_{87}N_2O_6P$	SM(d38:1)	[M+OAc]-	758.6302	817.6459	6.39	2.34	mzVault	HCD 10, 30, 50	2	0 Models	0.594	0.009
RP_pos_3189	$C_{48}H_{95}N_2O_6P$	SM(d43:2)	[M+H]+	826.6928	827.6990	7.39	-1.22	mzVault	HCD 10, 30, 50	2	0 Models	0.592	0.009
RP_neg_1997	$C_{47}H_{93}N_2O_6P$	SM(d42:2)	[M+HCOO]-	812.6771	857.6780	6.99	3.07	mzVault	HCD 10, 30, 50	2	1 (Lipid)	0.574	0.011
HILIC_neg_40	$C_5H_9NO_4$	methylaspartic acid	[M-H]-	147.0532	146.0459	3.86	-0.01	*in silico	HCD: 15, 30, 45; CID: 35	2	3 (Small Polar)	0.569	0.012
RP_pos_2469	$C_{39}H_{74}NO_8P$	PE(34:2)	[M+H]+	715.5152	716.5208	4.65	-2.41	mzVault	HCD 10, 30, 50	2	1 (Lipid)	0.561	0.013
RP_neg_1617	$C_{45}H_{80}NO_7P$	PE(O-18:1/22:5)	[M-H]-	777.5672	776.5627	6.10	3.50	mzVault	HCD 10, 30, 50	2	1 (Lipid)	0.549	0.014
RP_pos_2314	$C_{36}H_{72}NO_8P$	PC(28:0)	[M+H]+	677.4996	678.5059	3.96	-1.34	mzVault	HCD 10, 30, 50	2	1 (Lipid)	0.547	0.014
RP_pos_2918	$C_{44}H_{88}NO_8P$	PC(36:0)	[M+H]+	789.6248	790.6317	7.29	-0.37	mzVault	HCD 10, 30, 50	2	2 (Lipid)	0.545	0.015
RP_pos_2820	$C_{45}H_{78}NO_7P$	PE(O-18:1/22:6)	[M+H]+	775.5516	776.5581	5.76	-0.97	mzVault	HCD 10, 30, 50	2	1 (Lipid)	0.544	0.015
RP_pos_3079	$C_{47}H_{91}N_2O_6P$	SM(d42:3)	[M+H]+	810.6615	811.6680	6.57	-0.88	mzVault	HCD 10, 30, 50	2	0 Models	0.515	0.020
RP_neg_2064	$C_{47}H_{93}N_2O_6P$	SM(d42:1)	[M+OAc]-	814.6928	873.7094	7.59	3.12	mzVault	HCD 10, 30, 50	2	0 Models	0.511	0.020

Supplemental Table 3.4. Proposed annotations for metabolites in models. The table shows high resolution experimental m/z value for the species of interest, proposed annotation, main adduct type detected, retention time and metabolite ID which includes which chromatography type and ionization mode, elemental formula, mass error (ppm) calculated from exact monoisotopic mass, annotation confidence level, MS/MS collision energies, and the online database used for the MS2 spectra library match. The confidence level for lipid annotation was assigned as (1) exact mass, isotopic pattern, and MS/MS spectrum of a chemical standard matched to the feature. (2) exact mass, isotopic pattern, retention time, and MS/MS spectrum matched to an in-house spectral database or literature spectra (3) putative ID assignment based only on elemental formula match. (4) unknown compound. Asterisks (*) designate compounds for which MS2 spectral match was done using in-silico fragmentation in Compound Discoverer.

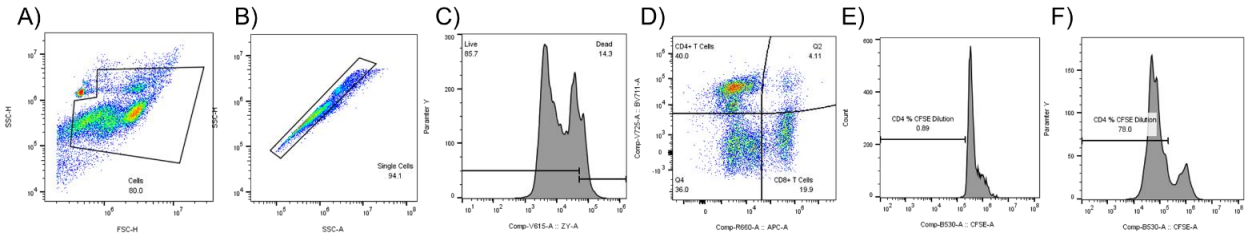

Supplemental Figure 3.1. Gating strategy to assess T cell proliferation. Cellular debris and Dynabeads were first removed (A) followed by cell doublets (B). Using FMO controls, live cells were then gated based on Zombie Yellow staining (C) and used to determine CD4+ and CD8+ T cell populations (D). Negative control PBMCs (No stimulation, no MSCs) were then used for the CFSE dilution gate (E) and positive control PBMCs (stimulation, no MSCs) were used for baseline comparison (F).

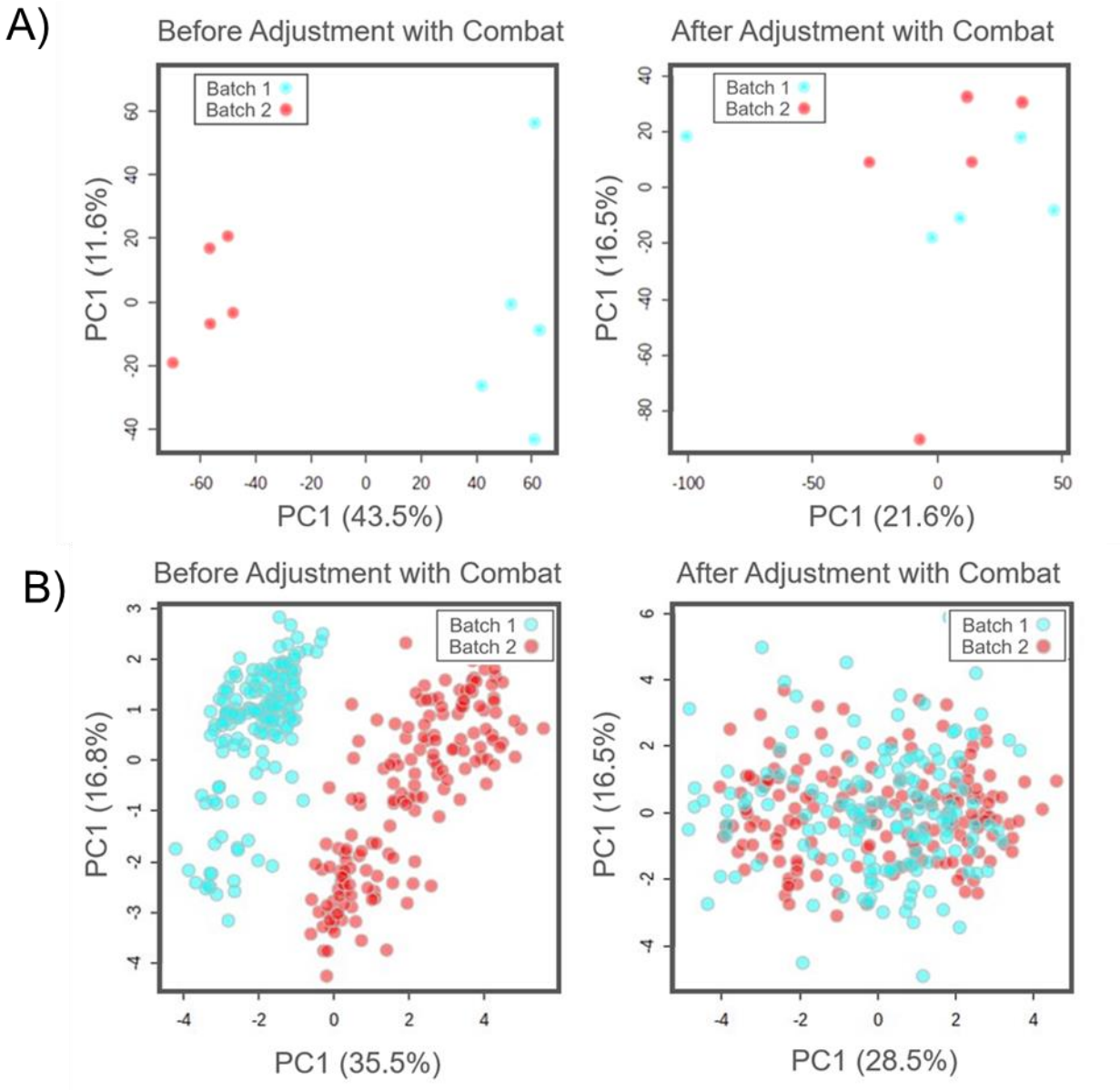

Supplemental Figure 3.2. Batch Correction of MS and NMR datasets. MS (A) and NMR (B) results of PCA scores plot before and after batch adjustment using Combat in Metaboanalyst. For MS, each point is one of the cell lines at end-of-process. For NMR, each point is a sample from each culture replicate at each timepoint.

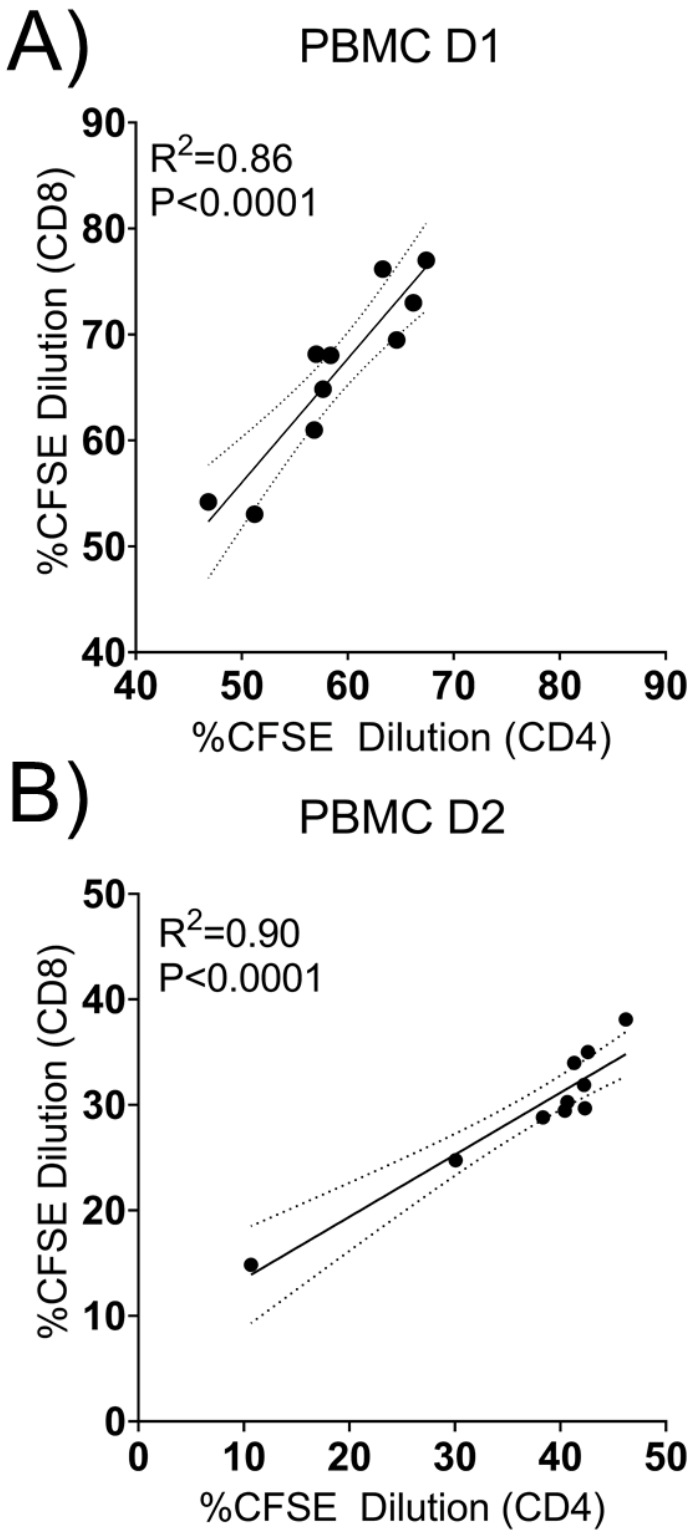

Supplemental Figure 3.3. Linear Regression of CD4/CD8 Proliferation for PBMC donor 1 (A) and PBMC donor 2 (B)

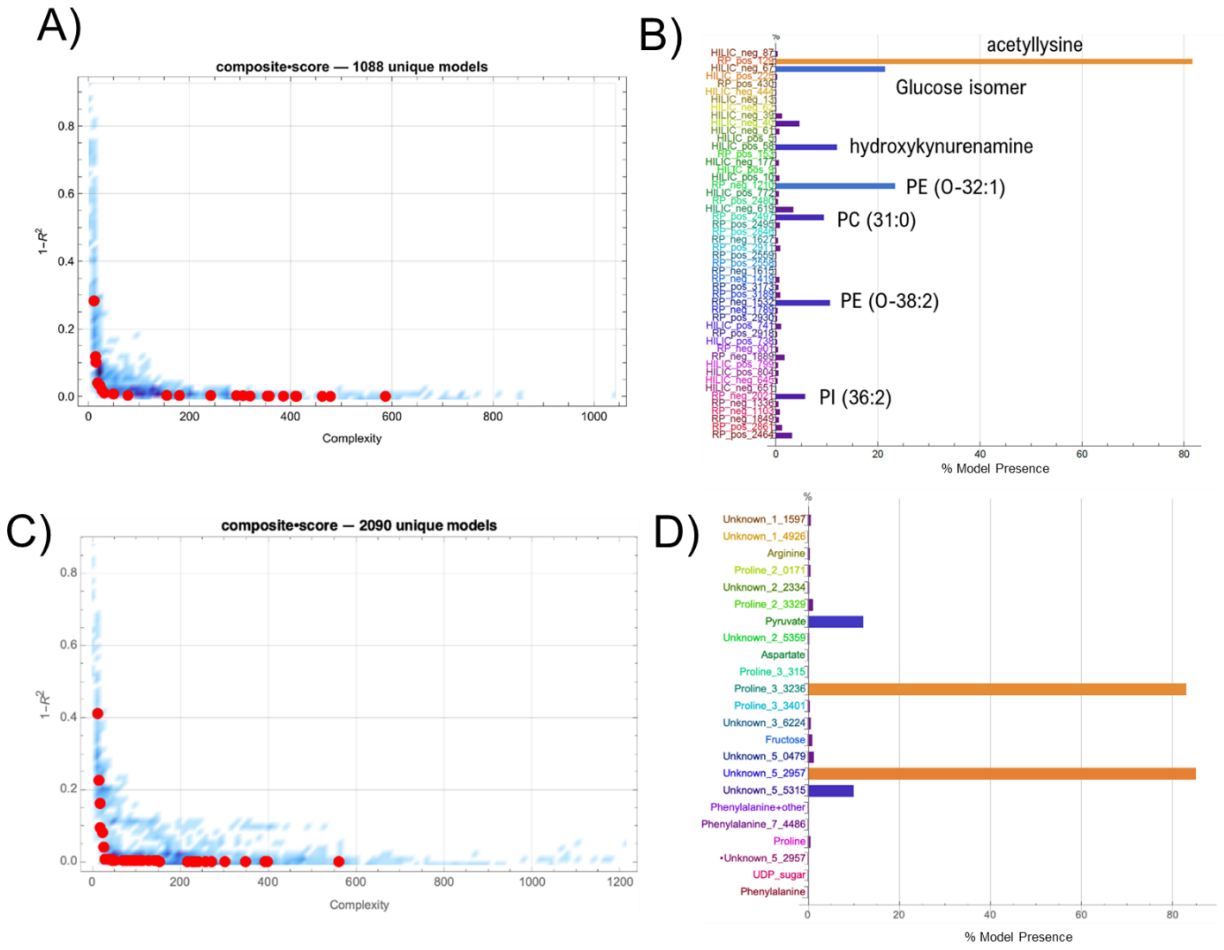

Supplemental Figure 3.4: Evolved Analytics Data Modeler ML consensus feature results. Pareto front plot of final suite of models using consensus features for MS (A) and NMR (C). Bar plots of metabolites from consensus feature list present in the final suite of models for MS (B), and NMR (D).

CHAPTER 4

LITERATURE REVIEW

4.1 ABSTRACT

The use of mesenchymal stem/stromal cells (MSCs) as a cell therapeutic has been widely researched and clinical trials are ongoing. It has been shown in the literature that much of the therapeutic effect of MSC is due to paracrine signals which includes extracellular vesicles (EVs). EVs have a lipid bilayer and contain proteins, lipids, metabolites, and nucleic acids that can have a therapeutic effect on diseased cells. MSC EVs have been shown to have a therapeutic effect on multiple diseases. Consistent and quality manufacturing of MSC EVs loaded with specific cargos for target diseases is difficult and will slow down clinical translation. This is because MSC EV cargo can change depending on various manufacturing conditions. This review will go over the challenges in manufacturing that effects MSC EV cargo, and how characterization techniques can be used to optimize the manufacturing process and ensure MSC EV quality.

4.2 MSC THERAPIES

Mesenchymal stem/stromal cells (MSCs) have been widely studied due to their differentiation and immunomodulatory potential. Despite their potential, it has been a challenge translating these therapies to the clinic. This, in part, can be attributed to MSC heterogeneity making it hard to produce a consistent product, and cell death upon administration straight out of cryopreservation.[1–3] Therefore, cell free therapeutics may be a better option. Studies have found that one mechanism by which MSCs exert their therapeutic effect is through the release of extracellular vesicles (EVs).[4,5]

4.3 EXTRACELLULAR VESICLES AND THEIR BIOGENESIS

EVs are nano-sized lipid-bilayer vesicles secreted by all cells in the body. They contain proteins, lipids, metabolites, and nucleic acids, and the cargo of EVs is dependent upon the originating cell.[6–8] EVs encompass a broad size range (~30-1000 nm) of vesicles and can be categorized into three groups based on size and release mechanism which include exosomes, microvesicles (MVs), and apoptotic bodies. Apoptotic bodies are large vesicles (~1000 nm) that are released by cells undergoing apoptosis, and although important in biological functions, this review focuses specifically on exosomes and MVs as EVs.[9] Exosomes are the smallest group of EVs ranging from 30-150nm.[9,10] Exosomes are formed by the invagination of the cellular membrane creating an endosome. Intraluminal vesicles are then formed by another invagination of the endosomal membrane creating a multivesicular body (MVB). Here, the intraluminal vesicles are packaged with specific molecules by the endosomal sorting complex required for transport (ESCRT).[11–14] Following the loading of intraluminal vesicles, the MVB fuses with the cellular membrane to release the exosomes via exocytosis. Exosomes are rich with ALIX and tumor susceptibility gene 101 (TSG101), which are components of the ESRCT.[15] They also express tetraspanins such as CD9, CD63, and CD81, which are involved in endosomal vesicle trafficking.[16,17] Because they are highly abundant in exosomes, these molecules are used for the identification of exosomes although they can also be expressed on MVs.18 MVs are formed by the budding or shedding of the cellular membrane and can range anywhere between 100-1000 nm. Similar to exosomes, MVs contain surface markers that mirror the cell origin, nucleic acids, and various metabolites making them difficult to distinguish from exosomes at similar sizes.[19,20]

4.4 THERAPEUTIC POTENTIAL OF MSC EVS

MSC EVs are currently being investigated as a therapeutic treatment for various diseases due to the inherent properties and cargo derived from MSCs. In vitro, MSC EVs have displayed an immunomodulatory effect on T cell subtypes, B cells, NK cells, and macrophages.[21–24] MSC EVs have also shown efficacy in animal models for diseases such as traumatic brain injury, stroke, myocardial infarction, colitis, osteoarthritis, and graft versus host disease.[25–30] With their potential well established, clinical trials have now begun to evaluate their efficacy in humans.[31] Manufacturing consistent and quality MSC EVs will be crucial for translation of these therapies. This review will discuss the challenges faced in MSC EV manufacturing and how current and emerging characterization techniques can help overcome manufacturing hurdles to ensure a quality MSC EV therapy.

4.5 CHALLENGES IN MSC EV MANUFACTURING

During the manufacturing of EVs, many challenges can arise that have an effect on the consistency, quality, and safety of the therapeutic product. Some of these challenges include identity, purity, sterility, storage, and potency.[32] Although all processes of EV manufacturing are important to take into consideration, this review focuses on the manufacturing challenges that should be considered that can affect the production of a consistent and quality MSC EV product (Figure 4.1).

EV source

One of the biggest considerations for MSC EV manufacturing is the MSC line used for producing the EVs. MSCs can be derived from a wide range of tissue sources such as bone marrow (BM-MSC), adipose (AD-MSC), umbilical cord (U-MSC), and induced pluripotent cells (iPS-MSC).[33–35] Tissue donor source can affect MSC functional capacity including proliferation,

differentiation potential, and immunomodulation.[35–37] Donor-donor variability also arises within the same tissue source based on the donors age, gender, and health.[33,35,36] As mentioned previously, EV cargo is dependent on the cell of origin and the state in which the cell is in. Because of this, MSC EV cargo can differ based on the tissue source and donor. Therefore, choosing the right MSC source and line for a given clinical application is important for clinical translation. Comparison of MSC EVs derived from U-MSCs, AD-MSCs, and BM-MSCs revealed that U-MSCs had a larger average particle diameter than AD-MSCs and BM-MSCs, and U-MSCs also secreted more particles per cell than the other two MSC sources.[38] Similarly, another study compared EVs from BM-MSCs and amniotic fluid MSCs found that although the EVs have similar size distribution and tetraspanin expression (CD9, CD63, and CD81) EVs derived from amniotic fluid MSCs generated a higher yield of particles per mL.[39] MSC age also has an effect on the cargo and potency of MSC EVs. Young MSC EVs displayed greater macrophage M2 polarization, lower macrophage recruitment, greater macrophage uptake, and greater therapeutic efficacy in an acute lung injury model. Furthermore, micro-RNA (miRNA) levels were differentially expressed between young and aged MSC donors.[40] Despite this known source variability in MSC EV therapeutic potential, only a few studies have compared MSC EVs from different sources and few look at quantifiable biochemical differences. More comparison studies are needed in order to determine quality EV sources based on cargo and therapeutic application.

Culture system

Another manufacturing consideration that has an impact on EV yield and cargo is the cell culture system used to produce the EVs. The two major cell culture system parameters that have an effect on the production and cargo of EVs are culture vessel (i.e. 2D vs 3D) and growth

medium. Scalability is an important consideration when manufacturing EVs for clinical use, and EV dosage and therapeutic need only support the need for higher EV yield.[41] There is growing evidence that 3D bioreactors increase the production of EVs when compared to standard 2D tissue culture flasks.[38,42] Watson et al. even saw a 40x increase in EVs per mL over standard 2D flasks.[42] Both studies also saw varying levels of protein expression from 2D vs. 3D cultures, and Haraszti et al improved small interfering RNA (siRNA) delivery from MSC EVs grown in 3D cultures.[38,42] Another advantage of the use of bioreactors is cost reduction. Bioreactors decrease the overall cost per EV since there is a greater density of cells in the same media volume and higher EV yields.[41] Bioreactors may also allow for extended production of MSC EVs with little change to their cargo. Gobin et al. found that EVs harvested from four BM-MSC donors had little change in glycans, surface proteins, and cytokines/growth factors when compared at days 1, 13, and 25. This study is somewhat limited though due to the fact that the MSC EVs from the four donors were averaged together at each time point. Therefore, there is limited interpretation of the stability of each cell line individually.[43] In order to determine optimal culture vessels, more studies are needed to determine the effects it has on EV production and cargo. More specifically, comparisons of various 3D bioreactors will be necessary as there is little to no evidence currently published.

Cell culture media composition also plays an important role in the manufacturing of EVs. Fetal bovine serum (FBS) has often been used in cell culture media but there are xenogenic concerns with FBS. Human platelet lysate (hPL) is often used as a xeno-free alternative for cell culture media.[32] hPL and FBS contain EVs and miRNAs which can make it difficult to distinguish EVs produced from MSCs and EVs already found in the serum, and although some EVs can be depleted from serum via ultracentrifugation (UC), not all EVs are removed. EVs left

over from the serum used decreases purity and could potentially have off target effects.[44,45] As with FBS, hPL can also have lot to lot variability which can affect MSC DNA content and function.[46,47] Therefore, a chemically defined media may be a better option for clinical translation. Bobis-Wozowicz et al tested seven media formulations and found that it has a major effect on MSC EV miRNA profiles and functional capacity demonstrating the importance of screening media for MSC EV production.[48]

Preconditioning or priming MSCs with relevant physical or chemical cues such as hypoxia, interferon gamma (IFN-γ), tumor necrosis factor alpha (TNFα), or low pH is another cell culture parameter to consider that has an impact on EV yield, cargo, and potency.[21,49–51] For example, comparison of U-MSC EVs from normal culture conditions, hypoxia, low pH, and IFN- γ/TNFα demonstrated that hypoxic conditions increased EV yields, IFN- γ/TNFα increased average EV size, and low pH EVs induced regulator T cell (Treg) production.[21] Similarly, BM-MSCs grown in hypoxic condition had an enrichment of miR-125b compared to normal cell culture conditions and an increase in cardio protection in a myocardial infarction mouse model.[51] Thus, Priming MSCs prior to EV harvest could potentially be used to help control EV cargo and improve therapeutic efficacy, but further studies need to be conducted to determine optimal priming conditions for specific therapeutic targets.

EV Isolation Techniques

Currently, there are multiple methods that can be used to isolate EVs from cell culture media, but scalability should be taken into consideration when manufacturing MSC EVs. Common techniques used include UC, tangential flow filtration (TFF), size exclusion chromatography (SEC), and immunoaffinity. Each of these techniques has its advantages and disadvantages and can affect the yield and cargo of EVs.[52] Comparison of UC and TFF showed a

40-fold decrease in albumin contamination in EVs isolated with TFF making a more pure EV population.[53] When combining TFF with SEC, excess proteins in isolated EVs were significantly decreased compared to UC and SEC alone.[42] Studies comparing MSC EVs isolated using TFF also saw increases in yield when compared to UC.[38,53] Haraszti et al also showed an increase in siRNA delivery to neurons from TFF isolated MSC EVs compared to UC in both 2D and 3D cell cultures.[38] TFF and SEC also are more scalable and can reduce the cost of EV production over UC due to their scale up potential which is important to consider for clinical translation.[41]

4.6 CHARACTERIZATION OF EVS

The minimal information for the studies of extracellular vesicles (MISEV) 2018 states that characterization of EVs should have at least one transmembrane protein (i.e CD9, CD63, CD81), one cytosolic protein (i.e. ALIX, TSG101), and one negative marker (i.e. apolipoproteinsA1/2, apolipoproteinB, albumin). These guidelines also require image-based techniques for assessing EV structure and non-image-based analysis of particle number.[54] Although these guidelines serve as a good base for confirming the presence and abundance of EVs, more characterization is necessary to determine release criteria for MSC EV therapies. Different characterization methods should be considered for EV cargo analysis (Figure 4.2).

Physical Characterization

Characterization of an EVs physical qualities are important for determining size, concentration, and morphology. Knowing the size and concentration of EVs produced is important for ensuring quality of EVs within a certain size range (i.e. no apoptotic bodies) and for calculating EV dosage, respectively. Several technologies are readily available that can be used to determine the size and concentration of EVs. Dynamic light scattering (DLS) and nanoparticle tracking analysis (NTA) both use Brownian motion in order to determine size and

concentration of EVs. DLS relies on bulk light scattering for this measurement while NTA tracks individual particles and measures the light scattered.[55,56] Tunable resistive pulse sensing (TRPS) is another common method used to determine the size and concentration of EVs. Unlike DLS and NTA, TRPS is also able to measure the charge of EVs as well.[57] Each of these methods have distinct advantages and disadvantages for determining size and concentration of EVs. For example, a study comparing EVs collected from cerebral spinal fluid showed that NTA detected more particles that were less than 150 nm in size, while TRPS detected more particles that were greater than 150 nm.[58]

Due to their small nature, EVs are difficult to image by traditional imaging methods. Specialized high-resolution images can be taken with scanning electron microscopy (SEM), transmission electron microscopy (TEM), cryo-TEM, and atomic force microscopy (AFM).[59] These imaging techniques can allow for size quantification of EVs and visualization, but cannot be used to determine concentration. With their limited throughput, high costs, and operator variability, use in a clinical manufacturing setting may prove more difficult than helpful.[33,59]

Biochemical Characterization

Proteomics

Although, detection of EV surface and cytosolic markers is necessary for EV identification, deeper protein analysis is needed in order to discover important proteins of interest for MSC EV therapies. Bulk protein measures such as bicinchoninic acid (BCA) are often used because they are reliable and high-throughput. Protein contamination in samples can reduce the accuracy of these assays, but they may be useful for determining purity of an EV sample.[54] For specific proteins, EV protein analysis has traditionally been done using western blotting and enzyme-linked immunosorbent assay (ELISA). Western blotting and ELISA are well established

techniques but low limits of detection, high processing time, and low throughput limit the use of these techniques in clinical manufacturing.[60] Mass spectrometry (MS) is another valuable tool that has been widely used for characterizing EV proteins. MS can be used for targeted or untargeted protein analysis making it an ideal discovery tool for proteins that may be of interest to the therapeutic potential of EVs.[61,62] Although MS is great for discovery, integration into a therapeutic manufacturing setting may be difficult due to high preparation and processing times.[59] Therefore, newer techniques are also needed for assessing EV proteins for clinical evaluation.

Flow cytometry is one technique that can be used for evaluating MSC EVs. Conjugating EVs to beads overcomes some of the difficulty that arises when with the small size of EVs and is an effective way at profiling and quantifying proteins. Bead based flow cytometry can be used to quantify surface proteins and proteins inside of the EVs. It is also fast and high-throughput making it a useful option for both protein discovery and as a therapeutic release criterion.[63] Profiling of EVs using flow cytometry are also being looked at without the use of beads. More sensitive cytometers are being developed, and specialized sheath fluid is needed in order to prevent artifacts from triggering scatter principles. Currently, these cytometers can't measure particles that are less than 100 nm. Thus, more testing needs to be conducted in order to optimize this technique.[64,65] Another technique currently being developed for protein identification is micro-nuclear magnetic resonance (μNMR) which attaches a magnetic nanoparticle to proteins of interest. The magnetic nanoparticles allow for better sensitivity and amplified signal.[66] EVs bound to these nanoparticles are then filtered using a microfluidic device and analyzed using μNMR. Shao et al. demonstrated that this device yields a 1000-fold increase in sensitivity when compared to western blotting and ELISAs. [67]

In-process EV monitoring would be ideal for manufacturing EVs because it could better inform manufacturers of downstream EV quality. There are several technologies currently being developed for EV biomarker discovery related to specific diseases.[68] These technologies could potentially be translated into a manufacturing setting that would allow for in-process monitoring of EV proteins that are important for a given therapeutic. One potential technology is the ExoScreen which uses principles somewhat similar to an ELISA, but only measures particles that are less than 200 nm. The ExoScreen only requires 5 μL of serum sample and can be used in a multi-well plates allowing for the analysis of multiple markers.[69] Other technologies that are being developed for sensitive EV protein identification are the nano-plasmonic exosome (nPLEX) system and the integrated magnetic electrochemical exosome (iMEX) sensor. Both of these technologies require no centrifugation of EVs and can detect EVs at concentration as low as ~3000 and ~10000 EVs, respectively.[70,71] These types of technology hold great promise for their potential to be translated into in-process or in-line monitoring for EV production, but further optimization and commercialization is needed before this can happen.

MSC identifying markers such as CD105, CD90, and CD73 have been also been identified on the surface of MSC EVs which is not surprising knowing the biogenesis of EVs.[34,72] Although another means to characterize MSC EVs, these markers do not give a clear picture of the cargo and functional characteristics contained within MSC EVs.[43,73] MS comparison of UC-MSC EVs and BM-MSC EVs identified 623 total proteins and 797 total proteins, respectively. Of these proteins, 564 proteins were found in both UC-MSC EVs and BM-MSC EVs. The authors then looked at the abundance of proteins and saw that UC-MSC EVs had more proteins related to angiogenesis and cell motility while the BM-MSC EVs contained more proteins with an immunomodulatory effect.[73] Angulski et al shows the utility of MS for discovering proteins of

interest. After discovery, proteins can be further interrogated to further determine proteins to measure during manufacturing and pass/fail criteria for batch release using other technologies such as flow cytometry.

Nucleic Acids

Many studies have shown that the transfer of various nucleic acids (mostly RNAs) is one of the ways that EVs exert their therapeutic effect on diseased cells. Therefore, identification and quantification of these nucleic acids is very important for manufacturing MSC EVs for clinical translation. As with bulk protein assays, assays that measure bulk RNA and DNA could be used to help determine the purity of a manufactured EV therapeutic. Electrophoresis based techniques can give bulk RNA and DNA while RiboGreen only gives bulk RNA, and both of these techniques have commercially available products.[74] For manufacturing quality EVs, specific RNAs will be important for ensuring quality. Polymerase chain reaction (PCR) based techniques such as quantitative reverse transcription (qRT)-PCR have high sensitivity, need minimal sample volume to run, and can give quantitative results of multiple RNAs at the same time. They do require known sequences which limits their ability to be used for discovering RNAs of importance.[75,76] For comprehensive profiling of nucleic acids, next generation sequencing techniques such as RNA-seq is a powerful tool for RNA discovery that could be used to help inform therapeutic release criteria.[77,78] Other techniques being developed for nucleic acid quantification include droplet PCR, BEAMing (beads, emulsion, amplification, magnetics) PCR, ion exchange nanodetectors, and localized surface plasmon resonance (LSPR) assays. These techniques are highly sensitive and can detect very low amounts of RNAs. Currently, these techniques are mainly being developed for liquid biopsies, and their use in manufacturing EV therapeutics has yet to be see.[79–81] Microfluidic devices that capture EVs, isolate RNAs, and run

PCR are currently being developed for liquid biopsies and may be better suited for use in manufacturing. Translation of these technologies into a manufacturing setting can help overcome the hurdles previously discusses, but further optimization needs to be done.

Delivery of miRNAs from MSC EVs has been attributed to their efficacy for various diseases. For example, Zhu et al showed that MSC EVs enriched with miR-125b reduced infarct size and enhanced cardiac function, and knockdown of miR-125b significantly increased infarct size and suppressed cardiac cell survival in a myocardial infarction mouse model.[51] Similarly, Zhou et al assessed the effects of BM-MSC EVs on spinal cord injuries in a rat model and found that treatment with BM-MSC EVs significantly improved functional recovery, reduced lesion size, and reduced apoptosis. BM-MSC EVs had high abundance of miR-21-5p inhibition of saw a reverse of these positive effects.[82] These studies serve as examples that different nucleic acids are involved in EV therapeutic applications, and thus, using nucleic acids as a release criterion for MSC EV therapeutics will largely depend on the target disease. Screening for specific nucleic acids using multiple donors and culture systems and setting a quantitative pass/fail threshold will be important for clinical translation.

Lipidomics and Metabolomics

MS is currently used for detecting and profiling lipids present in EVs. Although not as widely studied as EV proteins and RNAs, many lipids have been identified in EVs derived from various cell sources. Cholesterol, sphingomyelin, phosphatidylserine, and phosphatidylcholine are all common lipids found in EVs.[83,84] Lipid analysis of MSC EVs revealed three distinct EV population with different lipid compositions. These EVs were segregated based on binding to cholera toxin B chain (CTB), Annexin V, and Shiga toxin B subunit (ST). EVs that were bound to CTB showed greater expression of the classical exosomal markers CD9, CD81, and ALIX.[84]

Thus, lipids could serve as another useful measure as release criteria for EV quality and for assessing the purity of subpopulations of interest though more studies need to be conducted to confirm these results and determine the effects of MSC donor and culture conditions.

EV metabolomics is another rapidly growing field due to the biological activity of the metabolites contained in EVs, but studies have mostly looked at metabolites from cancer cells.[85,86] Metabolite analysis using MS can allow for targeted or untargeted detection, but sample preparation can affect detected metabolites.[86] Characterization of MSC EV metabolites is extremely limited thus far, but Showalter et al. found that MSCs grown in hypoxic conditions release EVs that contained 21 metabolites associated with immunomodulatory function including M2 macrophage polarization and Treg induction.[87] More studies are needed to obtain definitive metabolites for manufacturing purposes, but this study demonstrates the promise of metabolic characterization.

4.7 CONCLUSIONS

MSC EVs hold great promise as a therapeutic for a multitude of disease due to their diverse cargos. The therapeutic efficacy of MSC EVs has already been established in vitro and in animal models with clinical trials underway. Manufacturing quality EVs is a major hurdle that needs to be addressed to help ensure clinical translation. MSC donor, cell culture vessel and media, and EV isolation technique all play a factor in the cargo of MSC EVs. Screening techniques for these different manufacturing parameters need to be developed in order to overcome these hurdles. MISEV recommendations alone are insufficient for characterizing a consistent and quality MSC EV for therapeutic use. Thus, current and emerging characterization techniques need to be integrating into optimizing the manufacturing process and ensuring therapeutic quality (Figure 4.3). Although mainly being developed for biomarker discovery, emerging techniques could

easily be integrated into a manufacturing setting. It is recommended that the readers look at Shao et al. 2018 [59] and Gandham et al 2020 [88] for more information on how these technologies work as the focus of this paper is on how various characterization techniques can help overcome manufacturing hurdles. Understanding the manufacturing challenges before attempting to translate MSC EV therapies will aid in clinical translation.

4.8 REFERENCES

1. Galipeau, J. The mesenchymal stromal cells dilemma-does a negative phase III trial of random donor mesenchymal stromal cells in steroid-resistant graft-versus-host disease represent a death knell or a bump in the road? Cytotherapy vol. 15 2–8 (2013).
2. Castro-Manrreza, M. E. & Montesinos, J. J. Immunoregulation by mesenchymal stem cells: Biological aspects and clinical applications. J. Immunol. Res. 2015, (2015).
3. ROBB, K. P., FITZGERALD, J. C., BARRY, F. & VISWANATHAN, S. Mesenchymal stromal cell therapy: progress in manufacturing and assessments of potency. Cytotherapy 21, 289–306 (2019).
4. Iso, Y. et al. Multipotent human stromal cells improve cardiac function after myocardial infarction in mice without long-term engraftment. Biochem. Biophys. Res. Commun. 354, 700–706 (2007).
5. Nagaishi, K. et al. Mesenchymal stem cell therapy ameliorates diabetic nephropathy via the paracrine effect of renal trophic factors including exosomes. Sci. Rep. 6, 1–16 (2016).
6. Raposo, G. & Stoorvogel, W. Extracellular vesicles: Exosomes, microvesicles, and friends. Journal of Cell Biology vol. 200 373–383 (2013).
7. Davison, J., O'Gorman, A., Brennan, L. & Cotter, D. R. A systematic review of metabolite biomarkers of schizophrenia. Schizophrenia Research vol. 195 32–50 (2018).

8. Voge, N. V. et al. Metabolomics-Based Discovery of Small Molecule Biomarkers in Serum Associated with Dengue Virus Infections and Disease Outcomes. PLoS Negl. Trop. Dis. 10, (2016).
9. Kalra, H., Drummen, G. P. C. & Mathivanan, S. Focus on extracellular vesicles: Introducing the next small big thing. International Journal of Molecular Sciences vol. 17 (2016).
10. Gurunathan, S., Kang, M.-H., Jeyaraj, M., Qasim, M. & Kim, J.-H. Review of the Isolation, Characterization, Biological Function, and Multifarious Therapeutic Approaches of Exosomes. Cells 8, 307 (2019).
11. Piper, R. C. & Katzmann, D. J. Biogenesis and function of multivesicular bodies. Annual Review of Cell and Developmental Biology vol. 23 519–547 (2007).
12. Hurley, J. H. & Hanson, P. I. Membrane budding and scission by the ESCRT machinery: It's all in the neck. Nature Reviews Molecular Cell Biology vol. 11 556–566 (2010).
13. Théry, C. Exosomes: Secreted vesicles and intercellular communications. F1000 Biology Reports vol. 3 15 (2011).
14. Colombo, M., Raposo, G. & Théry, C. Biogenesis, secretion, and intercellular interactions of exosomes and other extracellular vesicles. Annual review of cell and developmental biology vol. 30 255–289 (2014).
15. Kowal, J., Tkach, M. & Théry, C. Biogenesis and secretion of exosomes. Current Opinion in Cell Biology vol. 29 116–125 (2014).
16. van Niel, G. et al. The Tetraspanin CD63 Regulates ESCRT-Independent and -Dependent Endosomal Sorting during Melanogenesis. Dev. Cell 21, 708–721 (2011).

17. Verweij, F. J. et al. LMP1 association with CD63 in endosomes and secretion via exosomes limits constitutive NF-κB activation. EMBO J. 30, 2115–2129 (2011).

18. Lötvall, J. et al. Minimal experimental requirements for definition of extracellular vesicles and their functions: A position statement from the International Society for Extracellular Vesicles. Journal of Extracellular Vesicles vol. 3 (2014).

19. Bonifacino, J. S. & Glick, B. S. The Mechanisms of Vesicle Budding and Fusion. Cell vol. 116 153–166 (2004).

20. Mathieu, M., Martin-Jaular, L., Lavieu, G. & Théry, C. Specificities of secretion and uptake of exosomes and other extracellular vesicles for cell-to-cell communication. Nature Cell Biology vol. 21 9–17 (2019).

21. Andrews, S., Maughon, T., Marklein, R. & Stice, S. Priming of MSCs with inflammation-relevant signals affects extracellular vesicle biogenesis, surface markers, and modulation of T cell subsets. J. Immunol. Regen. Med. 100036 (2021) doi:10.1016/j.regen.2020.100036.

22. Muraca, M. et al. Immunoregulatory Effects of Mesenchymal Stem Cell-Derived Extracellular Vesicles on T Lymphocytes. Cell Transplant. 24, 2615–2627 (2015).

23. Di Trapani, M. et al. Differential and transferable modulatory effects of mesenchymal stromal cell-derived extracellular vesicles on T, B and NK cell functions. Sci. Rep. 6, 1–13 (2016).

24. Heo, J. S., Choi, Y., Kim, H. O. & Matta, C. Adipose-Derived Mesenchymal Stem Cells Promote M2 Macrophage Phenotype through Exosomes. Stem Cells Int. 2019, (2019).

25. Zhang, Y. et al. Effect of exosomes derived from multipluripotent mesenchymal stromal cells on functional recovery and neurovascular plasticity in rats after traumatic brain injury. J. Neurosurg. 122, 856–867 (2015).

26. Doeppner, T. R. et al. Extracellular Vesicles Improve Post-Stroke Neuroregeneration and Prevent Postischemic Immunosuppression. Stem Cells Transl. Med. 4, 1131–1143 (2015).

27. Bian, S. et al. Extracellular vesicles derived from human bone marrow mesenchymal stem cells promote angiogenesis in a rat myocardial infarction model. J. Mol. Med. 92, 387–397 (2014).

28. Yang, J. et al. Extracellular vesicles derived from bone marrow mesenchymal stem cells protect against experimental colitis via attenuating colon inflammation, oxidative stress and apoptosis. PLoS One 10, (2015).

29. Cosenza, S., Ruiz, M., Toupet, K., Jorgensen, C. & Noël, D. Mesenchymal stem cells derived exosomes and microparticles protect cartilage and bone from degradation in osteoarthritis. Sci. Rep. 7, (2017).

30. Kordelas, L. et al. MSC-derived exosomes: A novel tool to treat therapy-refractory graft-versus-host disease. Leukemia vol. 28 970–973 (2014).

31. Maumus, M., Rozier, P., Boulestreau, J., Jorgensen, C. & Noël, D. Mesenchymal Stem Cell-Derived Extracellular Vesicles: Opportunities and Challenges for Clinical Translation. Frontiers in Bioengineering and Biotechnology vol. 8 (2020).

32. Wiest, E. F. & Zubair, A. C. Challenges of manufacturing mesenchymal stromal cell–derived extracellular vesicles in regenerative medicine. Cytotherapy vol. 22 606–612 (2020).

33. Adlerz, K., Patel, D., Rowley, J., Ng, K. & Ahsan, T. Strategies for scalable manufacturing and translation of MSC-derived extracellular vesicles. Stem Cell Res. 48, 101978 (2020).

34. Dominici, M. et al. Minimal criteria for defining multipotent mesenchymal stromal cells. The International Society for Cellular Therapy position statement. Cytotherapy 8, 315–317 (2006).

35. Kern, S., Eichler, H., Stoeve, J., Klüter, H. & Bieback, K. Comparative Analysis of Mesenchymal Stem Cells from Bone Marrow, Umbilical Cord Blood, or Adipose Tissue. Stem Cells 24, 1294–1301 (2006).

36. Klinker, M. W., Marklein, R. A., Lo Surdo, J. L., Wei, C. H. & Bauer, S. R. Morphological features of IFN-γ-stimulated mesenchymal stromal cells predict overall immunosuppressive capacity. Proc. Natl. Acad. Sci. U. S. A. 114, E2598–E2607 (2017).

37. Marklein, R. A. et al. High Content Imaging of Early Morphological Signatures Predicts Long Term Mineralization Capacity of Human Mesenchymal Stem Cells upon Osteogenic Induction. Stem Cells 34, 935–947 (2016).

38. Haraszti, R. A. et al. Exosomes Produced from 3D Cultures of MSCs by Tangential Flow Filtration Show Higher Yield and Improved Activity. Mol. Ther. 26, 2838–2847 (2018).

39. Tracy, S. A. et al. A comparison of clinically relevant sources of mesenchymal stem cell-derived exosomes: Bone marrow and amniotic fluid. J. Pediatr. Surg. 54, 86–90 (2019).

40. Huang, R. et al. Differential effects of extracellular vesicles from aging and young mesenchymal stem cells in acute lung injury. Aging (Albany. NY). 11, 7996–8014 (2019).

41. Ng, K. S. et al. Bioprocess decision support tool for scalable manufacture of extracellular vesicles. Biotechnol. Bioeng. 116, 307–319 (2019).

42. Watson, D. C. et al. Efficient production and enhanced tumor delivery of engineered extracellular vesicles. Biomaterials 105, 195–205 (2016).

43. Gobin, J. et al. Hollow-fiber bioreactor production of extracellular vesicles from human bone marrow mesenchymal stromal cells yields nanovesicles that mirrors the immuno-modulatory antigenic signature of the producer cell. Stem Cell Res. Ther. 12, 1–20 (2021).

44. Shelke, G. V., Lässer, C., Gho, Y. S. & Lötvall, J. Importance of exosome depletion protocols to eliminate functional and RNA-containing extracellular vesicles from fetal bovine serum. J. Extracell. Vesicles 3, (2014).

45. Wei, Z., Batagov, A. O., Carter, D. R. F. & Krichevsky, A. M. Fetal Bovine Serum RNA Interferes with the Cell Culture derived Extracellular RNA. Sci. Rep. 6, 1–6 (2016).

46. Cho, H. S. et al. Individual variation in growth factor concentrations in platelet-rich plasma and its influence on human mesenchymal stem cells. Korean J. Lab. Med. 31, 212–218 (2011).

47. Vennila, R. et al. Effect of Human Platelet Lysate in Differentiation of Wharton's Jelly Derived Mesenchymal Stem Cells. Endocrine, Metab. Immune Disord. - Drug Targets 19, 1177–1191 (2019).

48. Bobis-Wozowicz, S. et al. Diverse impact of xeno-free conditions on biological and regenerative properties of hUC-MSCs and their extracellular vesicles. J. Mol. Med. 95, 205–220 (2017).

49. Cui, G. H. et al. Exosomes derived from hypoxia-preconditioned mesenchymal stromal cells ameliorate cognitive decline by rescuing synaptic dysfunction and regulating inflammatory responses in APP/PS1 mice. FASEB J. 32, 654–668 (2018).

50. Xue, C. et al. Exosomes Derived from Hypoxia-Treated Human Adipose Mesenchymal Stem Cells Enhance Angiogenesis Through the PKA Signaling Pathway. Stem Cells Dev. 27, 456–465 (2018).

51. Zhu, L. P. et al. Hypoxia-elicited mesenchymal stem cell-derived exosomes facilitates cardiac repair through miR-125b-mediated prevention of cell death in myocardial infarction. Theranostics 8, 6163–6177 (2018).

52. Mcnamara, R. P. & Dittmer, D. P. Modern Techniques for the Isolation of Extracellular Vesicles and Viruses. doi:10.1007/s11481-019-09874-x.

53. Busatto, S. et al. Tangential Flow Filtration for Highly Efficient Concentration of Extracellular Vesicles from Large Volumes of Fluid. Cells 7, 273 (2018).

54. Théry, C. et al. Minimal information for studies of extracellular vesicles 2018 (MISEV2018): a position statement of the International Society for Extracellular Vesicles and update of the MISEV2014 guidelines. J. Extracell. Vesicles 7, (2018).

55. Sitar, S. et al. Size Characterization and Quantification of Exosomes by Asymmetrical-Flow Field-Flow Fractionation. Anal. Chem. 87, 9225–9233 (2015).

56. Gardiner, C., Ferreira, Y. J., Dragovic, R. A., Redman, C. W. G. & Sargent, I. L. Extracellular vesicle sizing and enumeration by nanoparticle tracking analysis. J. Extracell. Vesicles 2, (2013).

57. Buzás, E. I., Gardiner, C., Lee, C. & Smith, Z. J. Single particle analysis: Methods for detection of platelet extracellular vesicles in suspension (excluding flow cytometry). Platelets vol. 28 249–255 (2017).

58. Akers, J. C. et al. Comparative analysis of technologies for quantifying extracellular vesicles (EVs) in clinical cerebrospinal fluids (CSF). PLoS One 11, (2016).

59. Shao, H. et al. New Technologies for Analysis of Extracellular Vesicles. Chemical Reviews vol. 118 1917–1950 (2018).

60. Ueda, K. et al. Antibody-coupled monolithic silica microtips for highthroughput molecular profiling of circulating exosomes. Sci. Rep. 4, (2014).

61. Kreimer, S. et al. Mass-spectrometry-based molecular characterization of extracellular vesicles: Lipidomics and proteomics. J. Proteome Res. 14, 2367–2384 (2015).

62. Pocsfalvi, G. et al. Mass spectrometry of extracellular vesicles. Mass Spectrometry Reviews vol. 35 3–21 (2016).

63. Theodoraki, M., Hong, C., Donnenberg, V. S., Donnenberg, A. D. & Whiteside, T. L. Evaluation of Exosome Proteins by on-Bead Flow Cytometry. Cytom. Part A cyto.a.24193 (2020) doi:10.1002/cyto.a.24193.

64. Pospichalova, V. et al. Simplified protocol for flow cytometry analysis of fluorescently labeled exosomes and microvesicles using dedicated flow cytometer. J. Extracell. Vesicles 4, 1–15 (2015).

65. Hoen, E. N. M. N. t. et al. Quantitative and qualitative flow cytometric analysis of nanosized cell-derived membrane vesicles. Nanomedicine Nanotechnology, Biol. Med. 8, 712–720 (2012).

66. Lee, H., Sun, E., Ham, D. & Weissleder, R. Chip-NMR biosensor for detection and molecular analysis of cells. Nat. Med. 14, 869–874 (2008).

67. Shao, H. et al. Protein typing of circulating microvesicles allows real-time monitoring of glioblastoma therapy. Nat. Med. 18, 1835–1840 (2012).

68. Raimondo, F., Morosi, L., Chinello, C., Magni, F. & Pitto, M. Advances in membranous vesicle and exosome proteomics improving biological understanding and biomarker discovery. Proteomics vol. 11 709–720 (2011).

69. Yoshioka, Y. et al. Ultra-sensitive liquid biopsy of circulating extracellular vesicles using ExoScreen. Nat. Commun. 5, 3591 (2014).

70. Im, H. et al. Label-free detection and molecular profiling of exosomes with a nano-plasmonic sensor. Nat. Biotechnol. 32, 490–495 (2014).

71. Jeong, S. et al. Integrated Magneto-Electrochemical Sensor for Exosome Analysis. ACS Nano 10, 1802–1809 (2016).

72. Kim, H. S. et al. Proteomic analysis of microvesicles derived from human mesenchymal stem cells. J. Proteome Res. 11, 839–849 (2012).

73. Angulski, A. B. B. et al. The Protein Content of Extracellular Vesicles Derived from Expanded Human Umbilical Cord Blood-Derived CD133 + and Human Bone Marrow-Derived Mesenchymal Stem Cells Partially Explains Why both Sources are Advantageous for Regenerative Medicine. (2015) doi:10.1007/s12015-016-9715-z.

74. Mateescu, B. et al. Obstacles and opportunities in the functional analysis of extracellular vesicle RNA - An ISEV position paper. J. Extracell. Vesicles 6, (2017).

75. Rekker, K. et al. Comparison of serum exosome isolation methods for microRNA profiling. Clin. Biochem. 47, 135–138 (2014).

76. Andreu, Z. et al. Comparative analysis of EV isolation procedures for miRNAs detection in serum samples. J. Extracell. Vesicles 5, (2016).

77. Huang, X. et al. Characterization of human plasma-derived exosomal RNAs by deep sequencing. BMC Genomics 14, 1–14 (2013).

78. Amorim, M. G. et al. A total transcriptome profiling method for plasma-derived extracellular vesicles: Applications for liquid biopsies. Sci. Rep. 7, 1–11 (2017).

79. Chen, W. W. et al. Beaming and droplet digital pcr analysis of mutant idh1 mrna in glioma patient serum and cerebrospinal fluid extracellular vesicles. Mol. Ther. - Nucleic Acids 2, e109 (2013).

80. Taller, D. et al. On-chip surface acoustic wave lysis and ion-exchange nanomembrane detection of exosomal RNA for pancreatic cancer study and diagnosis. Lab Chip 15, 1656–1666 (2015).

81. Joshi, G. K. et al. Label-Free Nanoplasmonic-Based Short Noncoding RNA Sensing at Attomolar Concentrations Allows for Quantitative and Highly Specific Assay of MicroRNA-10b in Biological Fluids and Circulating Exosomes. ACS Nano 9, 11075–11089 (2015).

82. Zhou, X. et al. Mesenchymal stem cell derived EVs mediate neuroprotection after spinal cord injury in rats via the microRNA-21-5p/FasL gene axis. Biomed. Pharmacother. 115, 108818 (2019).

83. Skotland, T., Hessvik, N. P., Sandvig, K. & Llorente, A. Exosomal lipid composition and the role of ether lipids and phosphoinositides in exosome biology. Journal of Lipid Research vol. 60 9–18 (2019).

84. Lai, R. C. et al. MSC secretes at least 3 EV types each with a unique permutation of membrane lipid, protein and RNA. J. Extracell. Vesicles 5, (2016).

85. Veziroglu, E. M. & Mias, G. I. Characterizing Extracellular Vesicles and Their Diverse RNA Contents. Frontiers in Genetics vol. 11 700 (2020).

86. Williams, C., Palviainen, M., Reichardt, N. C., Siljander, P. R. M. & Falcón-Pérez, J. M. Metabolomics applied to the study of extracellular vesicles. Metabolites vol. 9 (2019).

87. Showalter, M. R. et al. Primed mesenchymal stem cells package exosomes with metabolites associated with immunomodulation. Biochem. Biophys. Res. Commun. 512, 729–735 (2019).

88. Gandham, S. et al. Technologies and Standardization in Research on Extracellular Vesicles. Trends in Biotechnology vol. 38 1066–1098 (2020).

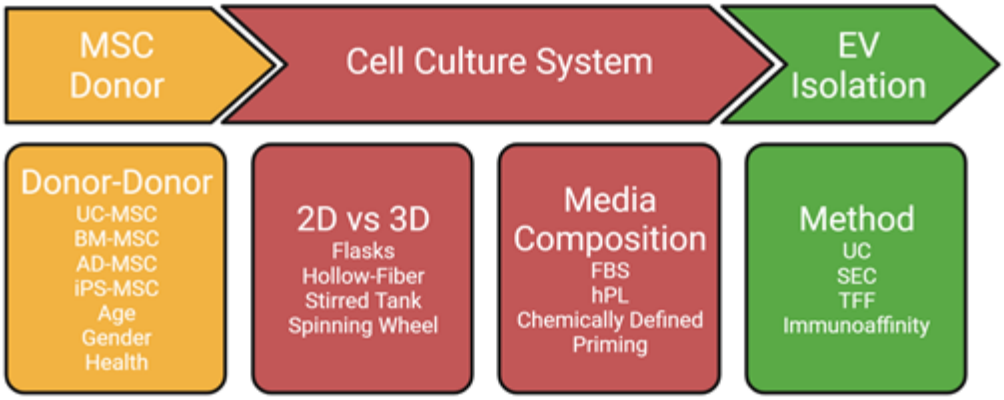

Figure 4.1. Manufacturing considerations that affect MSC EV cargo.

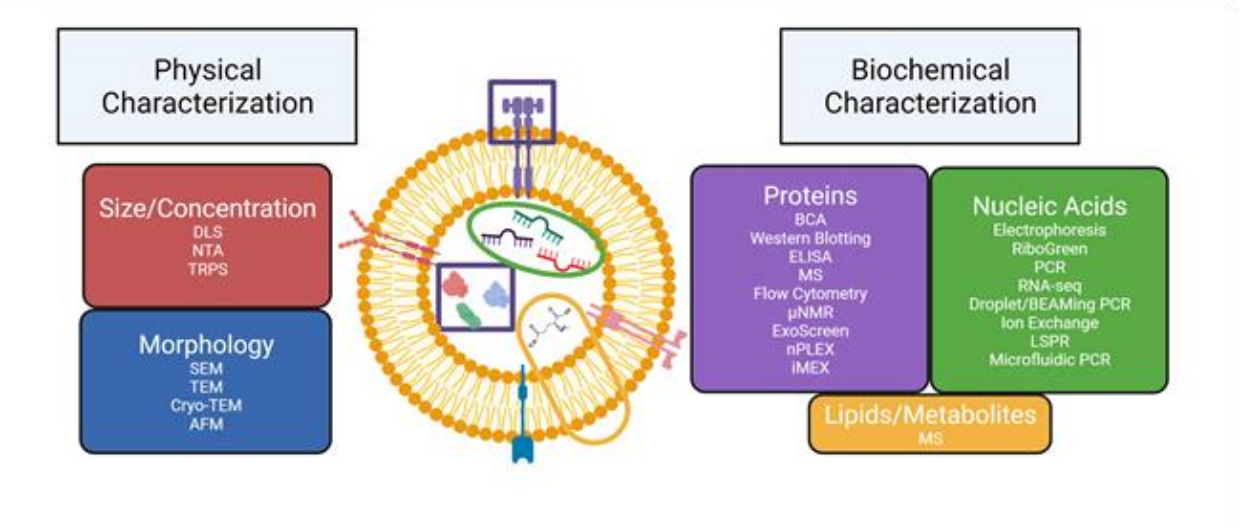

Figure 4.2. Examples of current and emerging techniques for EV characterization.

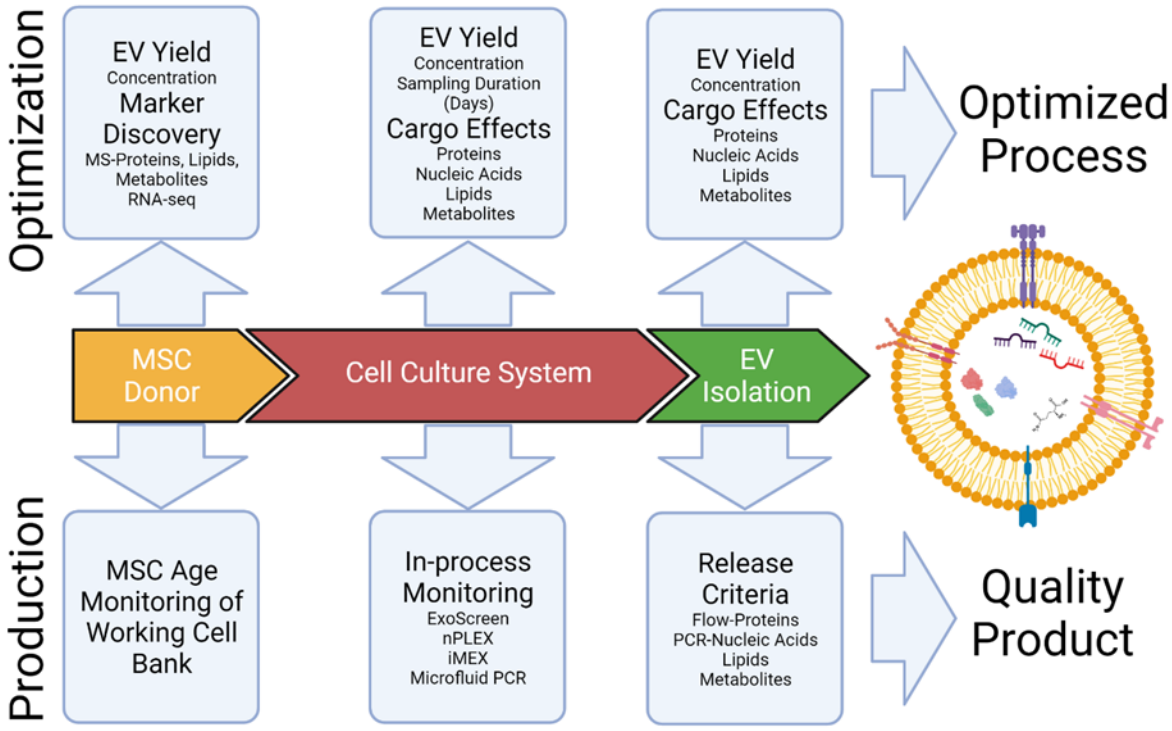

Figure 4.3. Integration of characterization techniques for manufacturing process optimization (top) and therapeutic quality control (bottom).

CHAPTER 5

METABOLITES AS ROBUST CRITICAL QUALITY ATTRIBUTES FOR MSC AND CAR-T POTENCY

[3]Ty Maughon, Ross Marklein, Steven Stice. To be submitted to Current Opinions in Biomedical Engineering.

5.1 INTRODUCTION

Cell therapies have demonstrated ability to respond to biological cues to repair damaged tissue, regulate the immune system, and aid in preventing disease progression.[1,2] The majority of licensed products are cord blood therapies that transplant hematopoietic stem cells, but recently chimeric antigen receptor T-cell (CAR-T) therapies were approved.[2] Besides CAR-T therapies, mesenchymal stromal cells (MSCs) have been widely studied in academic settings, and there are an abundance of MSC clinical trials being conducted.[2] However, there are currently no commercially approved MSC therapies in the United States.[3] Although promising, both immune and stem cell therapies have had limited success receiving approval through the Food and Drug Administration (FDA) with only six CAR-T therapies being approved from 2017-2022 (fda.gov) and fifteen small molecule drugs being approved in 2022 alone.[4] The FDA approval process is complex for any drug; but because cells are living and dynamically changing during manufacture processes, generating a consistent high quality FDA approved cell product is difficult.[5] This complexity has made it difficult for manufacturers to establish critical quality attributes (CQAs) to ensure cell product safety and efficacy. In the International Conference on Harmonization (ICH) guideline ICH Q8 (R2), the FDA defines a CQA as "a physical, chemical, biological, or microbiological property or characteristic that should be within an appropriate limit, range, or distribution to ensure the desired product quality. CQAs are generally associated with the drug substance, excipients, intermediates (in-process materials), and drug product." This guideline also discusses the importance of both in-process and end of manufacturing monitoring and evaluation of the drug product in order to have greater control over quality to help ensure approval.[6,7] Currently, there is no guideline on what physical, chemical, or biological characteristic of the cells should be used as CQAs for potency.

An emerging and promising field for developing CQAs is through the monitoring and measuring of metabolites during manufacturing.8 Metabolites are small molecules that are produced by cells as a result of metabolism, and give key insights into cellular phenotypes.[9,10] Currently in cell therapy manufacturing, metabolites such as glucose and lactate are monitored along with other culture parameters (i.e. pH, O2, CO2) which are referred to as Process Analytical Tools (PATs).[11,12] PATs can be any device that measures a physical, chemical, or biological variable in cell cultures. Although PATs are used for assessing cell growth rates and overall cellular health, these measurements are not typically used to predict cellular potency.[12] More comprehensive monitoring of metabolites will advance the field's understanding of the complex relationship between metabolism and potency. Therefore, new PATs measuring a broader range of high and low abundant metabolites both in-process and at the end of manufacturing may lead to potency CQAs.[11] Although specific cell therapies have their own unique manufacturing challenges, monitoring a range of metabolites could ensure the potency of cell therapy manufacturing, allowing for the production of safe and effective cell therapies.

5.2 EMERGING TECHNOLOGIES AND DATA MODELING FOR METABOLITE MONITORING

Currently, the two most common approaches for measuring metabolites are nuclear magnetic resonance (NMR) and mass spectrometry (MS).[13,14] While these tools are extremely powerful, the cost of these machines, consumables, maintenance and expertise needed to run and analyze the data make it difficult to implement in a small or medium company manufacturing cell therapies.[15] Therefore, new PATs for measuring metabolites must be developed to implement metabolite monitoring in commercial manufacturing. Several technologies are currently being developed to help overcome the manual, time-consuming, and labor that is

currently associated with metabolite monitoring and measuring.[16] First, benchtop NMR machines as well as automated benchtop MS machines can be attached to bioreactors for real time, in-line monitoring.[15,17] These machines hold promise for integration into manufacturing because they are currently available, but aren't as sensitive to lower abundance metabolites. Other PATs are also being developed to better monitor and measure metabolites. Microfluidic sampling devices are being implemented directly in the manufacturing process to collect, filter, and process media and cells to be measured using MS.[18,19] These direct sample technologies require minimal sample volume for non-destructive analysis which is important when continuously monitoring a cell expansion over several days.[19] Low numbers of non-adherent cells (CAR-T) can also be sampled for intracellular metabolite analysis making these microfluidic devices a potentially powerful tool for potency prediction when combining intracellular and extracellular metabolites.[20] With minimal sample volume needed, these microfluidic MS tools can be used to sample multiple time points without significant loss of potentially precious cells. Lastly, metabolite monitoring via fluorescence using an NAD(P)H-sensitive polymer dot may have utility. These polymer dot biosensors are combined with specific enzymes that catalyze a reaction for a given metabolite to produce NAD(P)H. Once exposed to UV light, the NAD(P)H transfer electrons to the polymer dot causing it to fluoresce at 458nm while quenching the polymer dot's fluorescent emission at 627nm. This ratio of fluorescence is used to measure the abundance of a metabolite. Although a more affordable option than NMR and MS tools, only metabolites oxidized by NAD+ or NADP+ or reduced by NADH or NADPH can be measured due to the interaction with the polymer dot. Thus, the number of metabolites measured is limited.[21] Moving to targeted metabolomics studies based on potential CQAs from untargeted studies could help advance the development of new

technologies even further by establishing cell specific/application specific CQAs that can be measured by new, cost effective devices.

Additionally, data modeling is an important tool for taking large data sets and determining which CQAs are important predictors of potency during various phases of manufacturing. These CQAs could be different depending on the cell therapy or the manufacturing stage such as those for T-cell expansion vs CAR-T expansion. Thus, using a machine learning (ML) modeling approach may be beneficial for these therapies to determine what to monitor at certain stages of manufacturing.[22] Using multiple ML models during the CQA discovery process can help limit the bias of only using one model. This, paired with cross-validation and leave-one-out model performance calculations, can increase confidence in the discovered CQAs.[22,23]

5.3 ENERGY METABOLISM AND OTHER PREDICTORS OF MSC IMMUNOMODULATION

MSCs are widely studied for therapeutic use due to their ability to differentiate into osteoblasts, chondrocytes, and adipocytes and for their immunomodulatory properties.[24–26] As mentioned previously, there are currently no MSC therapies on the market in the US largely due to the inability to ensure potency. Recently, a MSC therapy for graft versus host disease, remestemcel-L, submitted a biological license application to market their therapy but was rejected over concerns that the proposed CQAs did not correlate with in vivo outcomes.[27] MSC heterogeneity is attributed to a variety of factors including tissue source, donor, and expansion materials (i.e. medium or culture vessel).[28] Heterogeneity has made it difficult to standardize the manufacturing process and develop CQAs for ensuring a potent final product.[24,27] To help overcome these problems, the International Society for Cell and Gene Therapy (ISCT)

recommends a multitude of markers that, when used in combination, can overcome heterogeneity and better predict MSC potency.[29,30]

By analyzing the metabolic profile of MSCs, it is possible to identify biomarkers that can be used to monitor and optimize the manufacturing process, as well as to understand the underlying mechanisms that regulate the potency of these cells.[31,32] One way in which metabolomics can be used to improve MSC manufacturing is through the identification of metabolic pathways, such as glycolysis, that can be manipulated to improve the immunomodulatory function of the cells.[14,33] Preconditioning MSCs with interferon gamma (IFN-γ) was shown to shift MSC energy metabolism towards glycolysis rather than oxidative phosphorylation (OXPHOS) which was preferred by MSCs grown in normal growth conditions (Figure 5.1A).[34] MSCs treated with IFN-γ also showed greater T-cell suppression from the control MSCs.[34] Additionally, understanding the metabolic changes that occur during the expansion and cryopreservation of MSCs can help to identify potential strategies to improve the survival and functionality of these cells post-thawing. MSCs are often transplanted into an inflammatory microenvironment compared to the nutrient rich environment that they are expanded in. Identifying metabolic factors that lead to enhanced survival may increase the potency of these cells upon implantation. For example, implanted MSCs must switch their energy metabolism to glycolysis and quickly run out of glucose reserves. This sudden stress and lack of glucose ultimately causes cell death. Therefore, priming these cells with various factors such as IFN-γ, hypoxia, or low pH to condition the cells metabolically before implantation may help survival and potency of these cells depending on the target disease.[35] By analyzing the levels of specific metabolites it is possible to gain insights into the signaling pathways that regulate MSC immunomodulation or differentiation.[23,31] This knowledge can then be used to

develop new strategies for manipulating these pathways to improve the performance of the cells by enhancing or inhibiting certain pathways such as OXPHOS by growing MSCs in a hypoxic environment. MSCs grown in a hypoxic environment had higher activation of hypoxia inducible factor 1a (HIF-1a) which inhibits OXPHOS.[31,33]

This can be achieved by analyzing and monitoring that are involved in energy metabolism, amino acid metabolism, and nucleotide metabolism.[31] For example, changes in the levels of specific amino acids over time, such as proline, arginine, and phenylalanine, can indicate changes in the immunomodulatory potential of the cells. Changes over time in other molecules including aspartate, pyruvate, and fructose were also predictive of MSC immunomodulation early in the expansion process (Figure 5.1B).[23] Another non-destructive, in-line monitoring tool is through two-dimensional gas chromatography mass spectrometry (GCxGC-MS). Here, gases given off from MSC cultures can be continuously monitored and used to predict immunomodulatory potency (Figure 5.1C).[36] Thus, monitoring metabolites can provide valuable insights into the phenotype of MSCs, and can be used as CQAs for ensuring MSC potency and helping navigate the regulatory process.

5.4 CAR-T METABOLISM FOR INFORMED MANUFACTURING AND SAFETY PREDICTION

CAR-T therapy is a promising treatment option for cancer patients, in which the patient's own T-cells are genetically modified to target and eliminate cancer cells. Currently, there several approved CAR-T therapies on the market for treating bloodborne cancers.[37] Although there are approved therapies, a number of manufacturing challenges must be overcome to get more therapies approved for other cancers.[38] CAR-T therapies have a high recurrence rate for these cancers and have trouble with efficacy against solid tumors.[39–41] Currently, CAR-T cells are

expanded in six steps; (1) peripheral blood mononuclear cell isolation from patient (2) T-cell isolation (3) T-cell expansion (4) T-cell transduction to express CAR antigen (5) CAR-T expansion (6) Patient administration.[42] By targeting the metabolism of T-cells at different phases of the manufacturing, more potent and longer lasting potency of CAR-T cells may be achieved.

By understanding the metabolic energy pathways that are involved during certain manufacturing steps, researchers can identify key metabolites to use as CQAs to better inform manufacturing decisions. There are four main subgroups of T-cells; naïve T-cells (Tn), effector T-cells (Teff), memory T-cells (Tm), and memory effector T-cells (Tmeff). All of these subgroups of T-cells have different metabolic requirements.[43] For example, Tn cells utilize OXPHOS and fatty acid oxidation (FAO) for energy metabolism while CAR-T cells that utilize glycolysis at the time of administration have an increased chance of complete cancer remission.[44–46] By supplementing the culture media with molecules that are known to promote T-cell growth or maturation, researchers can increase the yield of functional T-cells. For example, inhibiting glycolysis with 2-Deoxy-D-glucose (2DG) during the expansion of CAR-T cells enhances Tmeff formation which is directly associated with persistence and efficacy of the CAR-T therapy in vivo.[47–49] Metabolomics can also be used to identify metabolic markers that are associated with T-cell function and potency. By monitoring these metabolic markers, such as those of glycolysis or OXPHOS, during the manufacturing process, researchers can ensure that the final product has optimal yields and maintains a consistent potency by adjusting the manufacturing accordingly (Figure 5.2). For example, changes in glucose, pyruvate, lactate, citrate, glutamate, and succinate could be monitored in-process to determine the energy metabolism of the cells. This could help inform the manufacturer to add inhibitors of glycolysis or OXPHOS into the medium to correct the energy demand as needed.[42]

Safety remains another challenge during CAR-T manufacturing. Besides the risks associated with batch contamination, toxicities to the patient, such as cytokine release syndrome (CRS), remains a challenge for these therapies. Recently, the patient metabolome was used to predict CRS. Patients that had higher pre-treatment levels of plasma glucose and lower levels of cholesterol and glutamate were associated with faster CRS onset while low levels of proline and glycine were associated with significant CRS. Since the CAR-T cells are derived from the patient, metabolites could potentially be discovered during the manufacturing process for prediction of CRS in conjunction with the patient's metabolism.[50]

5.5 CONCLUSION

Cell therapies have shown great potential in the lab and even in the clinic with several approved therapies in the US. Despite this promise, several manufacturing challenges remain for cell therapies with ensuring a consistent and potent product being one of the biggest challenges. Since these cells are growing and dynamically changing both in vitro and in vivo, it is more difficult to ensure the potency of these cell therapies when compared to small molecule drugs. Unique manufacturing challenges also exist for specific cell therapies such as identifying and controlling heterogeneity of MSCs or expansion stages and safety of CAR-T. Metabolomics can help overcome these manufacturing hurdles whether it is specific to all cell therapies or unique to certain types. Monitoring metabolites and metabolic pathways both during and at the end of manufacturing can help ensure potency of cell therapies. New and emerging PATs will be crucial for better monitoring and control of the manufacturing process. PATs for both in-process and end of manufacturing will allow for greater and more accurate potency prediction. Ultimately, this technology will allow for more robust CQAs for these cell therapies to help unlock their clinical potential.

5.6 REFERENCES

1. Hunsberger, J. & Somara, S. Manufacturing challenges and solutions for regenerative medicine technologies. Regenerative Nephrology 487–500 (2022) doi:10.1016/B978-0-12-823318-4.00014-7.
2. Wang, L. L. W. et al. Cell therapies in the clinic. Bioeng Transl Med 6, e10214 (2021).
3. Kebriaei, P. et al. A Phase 3 Randomized Study of Remestemcel-L versus Placebo Added to Second-Line Therapy in Patients with Steroid-Refractory Acute Graft-versus-Host Disease. Biol Blood Marrow Transplant 26, 835 (2020).
4. Tiz, D. B. et al. FDA-Approved Small Molecules in 2022: Clinical Uses and Their Synthesis. Pharmaceutics 14, (2022).
5. Hunsberger, J. et al. Manufacturing Road Map for Tissue Engineering and Regenerative Medicine Technologies. Stem Cells Transl Med 4, 130–135 (2015).
6. Guidance for Industry Q8(R2) Pharmaceutical Development. (2009).
7. Lipsitz, Y. Y., Timmins, N. E. & Zandstra, P. W. Quality cell therapy manufacturing by design. Nature Biotechnology 2016 34:4 34, 393–400 (2016).
8. CELL & GENE THERAPY INSIGHTS. doi:10.18609/cgti.2022.232.
9. Goodarzi, P. et al. Metabolomics Analysis of Mesenchymal Stem Cells. Int J Mol Cell Med 8, 30 (2019).
10. Rinschen, M. M., Ivanisevic, J., Giera, M. & Siuzdak, G. Identification of bioactive metabolites using activity metabolomics. Nature Reviews Molecular Cell Biology vol. 20 353–367 Preprint at https://doi.org/10.1038/s41580-019-0108-4 (2019).

11. Reyes, S. J., Durocher, Y., Pham, P. L. & Henry, O. Modern Sensor Tools and Techniques for Monitoring, Controlling, and Improving Cell Culture Processes. Processes 2022, Vol. 10, Page 189 10, 189 (2022).

12. Challener, C. PROCESS ANALYTICAL TECHNOLOGIES FOR MANUFACTURING CELL AND GENE THERAPIES. Biopharm Int 34, 10–14 (2021).

13. Dunn, W. B., Bailey, N. J. C. & Johnson, H. E. Measuring the metabolome: Current analytical technologies. Analyst vol. 130 606–625 Preprint at https://doi.org/10.1039/b418288j (2005).

14. Yuan, X., Logan, T. M. & Ma, T. Metabolism in human mesenchymal stromal cells: A missing link between HMSC biomanufacturing and therapy? Frontiers in Immunology vol. 10 977 Preprint at https://doi.org/10.3389/fimmu.2019.00977 (2019).

15. van Beek, T. A. Low-field benchtop NMR spectroscopy: status and prospects in natural product analysis†. Phytochemical Analysis 32, 24–37 (2021).

16. Courant, F., Antignac, J. P., Dervilly-Pinel, G. & Le Bizec, B. Basics of mass spectrometry based metabolomics. Proteomics 14, 2369–2388 (2014).

17. Grootveld, M. et al. Progress in low-field benchtop NMR spectroscopy in chemical and biochemical analysis. Anal Chim Acta 1067, 11–30 (2019).

18. Chilmonczyk, M. A., Kottke, P. A., Stevens, H. Y., Guldberg, R. E. & Fedorov, A. G. Dynamic mass spectrometry probe for electrospray ionization mass spectrometry monitoring of bioreactors for therapeutic cell manufacturing. Biotechnol Bioeng 116, 121–131 (2019).

19. Chilmonczyk, M. A. et al. Localized Sampling Enables Monitoring of Cell State via Inline Electrospray Ionization Mass Spectrometry. Biotechnol J 16, 2000277 (2021).

20. Culberson, A. L. et al. Sample-to-analysis platform for rapid intracellular mass spectrometry from small numbers of cells. Lab Chip 21, 4696–4706 (2021).

21. Chen, H. et al. Monitoring Metabolites Using an NAD(P)H-sensitive Polymer Dot and a Metabolite-Specific Enzyme. Angewandte Chemie International Edition 60, 19331–19336 (2021).

22. Odeh-Couvertier, V. Y. et al. Predicting T-cell quality during manufacturing through an artificial intelligence-based integrative multiomics analytical platform. Bioeng Transl Med e10282 (2022) doi:10.1002/btm2.10282.

23. Grouw, A. Van et al. Development of a Robust Consensus Modeling Approach for Identifying Cellular and Media Metabolites Predictive of Mesenchymal Stromal Cell Potency. bioRxiv 2023.02.03.526990 (2023) doi:10.1101/2023.02.03.526990.

24. Galipeau, J. & Sensébé, L. Mesenchymal Stromal Cells: Clinical Challenges and Therapeutic Opportunities. Cell Stem Cell 22, 824–833 (2018).

25. Ball, L. M. et al. Multiple infusions of mesenchymal stromal cells induce sustained remission in children with steroid-refractory, grade III–IV acute graft-versus-host disease. Br J Haematol 163, 501–509 (2013).

26. Lanzoni, G. et al. Umbilical cord mesenchymal stem cells for COVID-19 acute respiratory distress syndrome: A double-blind, phase 1/2a, randomized controlled trial. Stem Cells Transl Med 10, 660 (2021).

27. FDA Briefing Document Oncologic Drugs Advisory Committee (ODAC) Meeting Session on Product Characterization (AM Session). (2020).

28. Wilson, A., Hodgson-Garms, M., Frith, J. E. & Genever, P. Multiplicity of mesenchymal stromal cells: Finding the right route to therapy. Front Immunol 10, 1112 (2019).

29. Galipeau, J. et al. International Society for Cellular Therapy perspective on immune functional assays for mesenchymal stromal cells as potency release criterion for advanced phase clinical trials. Cytotherapy 18, 151–159 (2015).

30. Chinnadurai, R. et al. Potency Analysis of Mesenchymal Stromal Cells Using a Combinatorial Assay Matrix Approach. Cell Rep 22, 2504–2517 (2018).

31. Li, H., Dai, H. & Li, J. Immunomodulatory properties of mesenchymal stromal/stem cells: The link with metabolism. J Adv Res (2022) doi:10.1016/J.JARE.2022.05.012.

32. Maughon, T. S. et al. Metabolomics and cytokine profiling of mesenchymal stromal cells identify markers predictive of T-cell suppression. Cytotherapy 24, 137–148 (2022).

33. Liu, Y. & Ma, T. Metabolic regulation of mesenchymal stem cell in expansion and therapeutic application. Biotechnol Prog 31, 468–481 (2015).

34. Liu, Y., Yuan, X., Muñoz, N., Logan, T. M. & Ma, T. Commitment to Aerobic Glycolysis Sustains Immunosuppression of Human Mesenchymal Stem Cells. Stem Cells Transl Med 8, 93–106 (2019).

35. Salazar-Noratto, G. E. et al. Understanding and leveraging cell metabolism to enhance mesenchymal stem cell transplantation survival in tissue engineering and regenerative medicine applications. Stem Cells 38, 22–33 (2020).

36. Jimenez, A. C., Heist, C. A., Navaei, M., Yeago, C. & Roy, K. Longitudinal two-dimensional gas chromatography mass spectrometry as a non-destructive at-line monitoring tool during cell manufacturing identifies volatile features correlative to cell product quality. Cytotherapy 24, 1136–1147 (2022).

37. Sengsayadeth, S., Savani, B. N., Oluwole, O. & Dholaria, B. Overview of approved CAR-T therapies, ongoing clinical trials, and its impact on clinical practice. EJHaem 3, 6–10 (2022).

38. Tyagarajan, S., Spencer, T. & Smith, J. Optimizing CAR-T Cell Manufacturing Processes during Pivotal Clinical Trials. Mol Ther Methods Clin Dev 16, 136 (2020).

39. Feng, K. et al. Chimeric antigen receptor-modified T cells for the immunotherapy of patients with EGFR-expressing advanced relapsed/refractory non-small cell lung cancer. Sci China Life Sci 59, 468–479 (2016).

40. Mueller, K. P. et al. Production and characterization of virus-free, CRISPR-CAR T cells capable of inducing solid tumor regression. J Immunother Cancer 10, e004446 (2022).

41. Morotti, M. et al. Promises and challenges of adoptive T-cell therapies for solid tumours. British Journal of Cancer 2021 124:11 124, 1759–1776 (2021).

42. Zhang, M. et al. Optimization of metabolism to improve efficacy during CAR-T cell manufacturing. Journal of Translational Medicine 2021 19:1 19, 1–11 (2021).

43. Gattinoni, L. et al. A human memory T cell subset with stem cell-like properties. Nat Med 17, 1290–1297 (2011).

44. Wang, R. et al. The transcription factor Myc controls metabolic reprogramming upon T lymphocyte activation. Immunity 35, 871–882 (2011).

45. Frauwirth, K. A. et al. The CD28 signaling pathway regulates glucose metabolism. Immunity 16, 769–777 (2002).

46. Cattley, R. T., Lee, M., Boggess, W. C. & Hawse, W. F. Transforming growth factor β (TGF-β) receptor signaling regulates kinase networks and phosphatidylinositol metabolism during T-cell activation. J Biol Chem 295, 8236 (2020).

47. Sommermeyer, D. et al. Chimeric antigen receptor-modified T cells derived from defined CD8+ and CD4+ subsets confer superior antitumor reactivity in vivo. Leukemia 30, 492–500 (2016).

48. Tang, N. et al. TGF-β inhibition via CRISPR promotes the long-term efficacy of CAR T cells against solid tumors. JCI Insight 5, (2020).

49. Marchesi, F., Vignali, D., Manini, B., Rigamonti, A. & Monti, P. Manipulation of Glucose Availability to Boost Cancer Immunotherapies. Cancers (Basel) 12, 1–16 (2020).

50. Jalota, A. et al. Host metabolome predicts the severity and onset of acute toxicities induced by CAR T-cell therapy. Blood Adv (2022) doi:10.1182/BLOODADVANCES.2022007456.

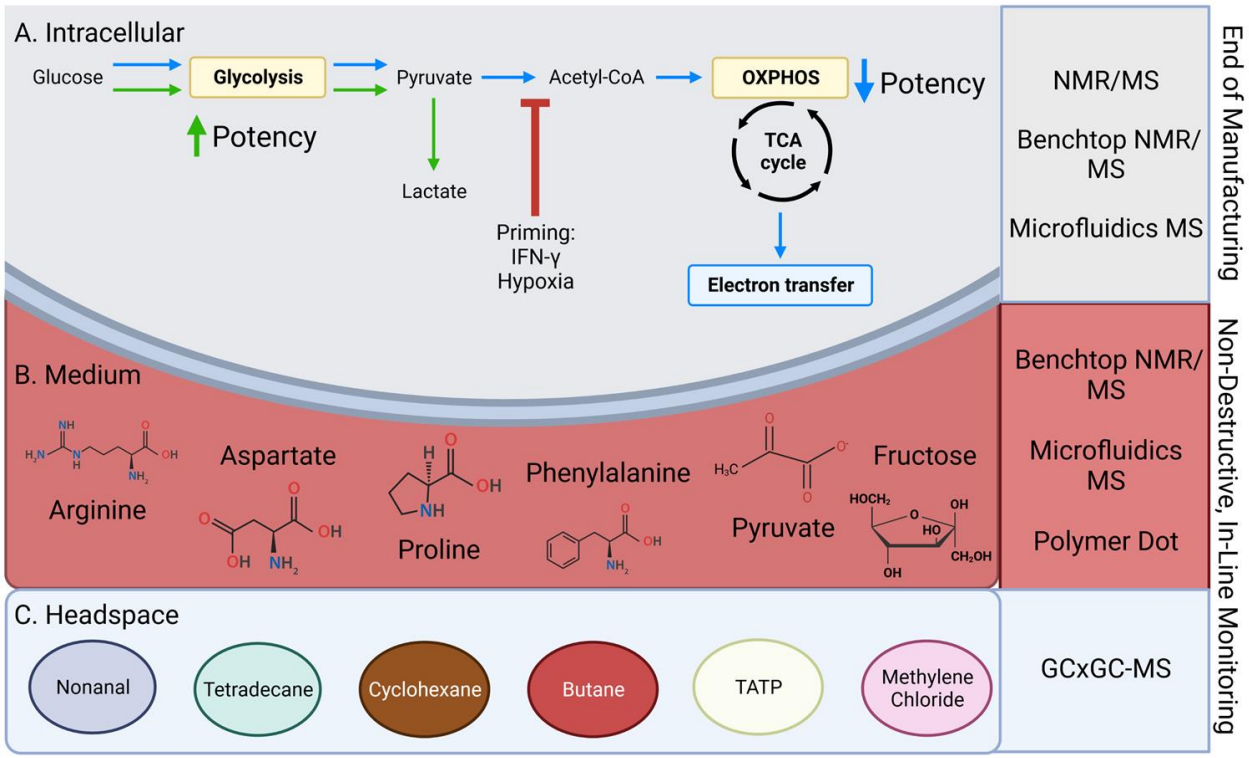

Figure 5.1. MSC Manufacturing. Metabolite measurement integration for monitoring (A) intracellular, (B) medium, and (C) headspace metabolites for MSC potency prediction at the end of manufacturing and in-process. Created with BioRender.com

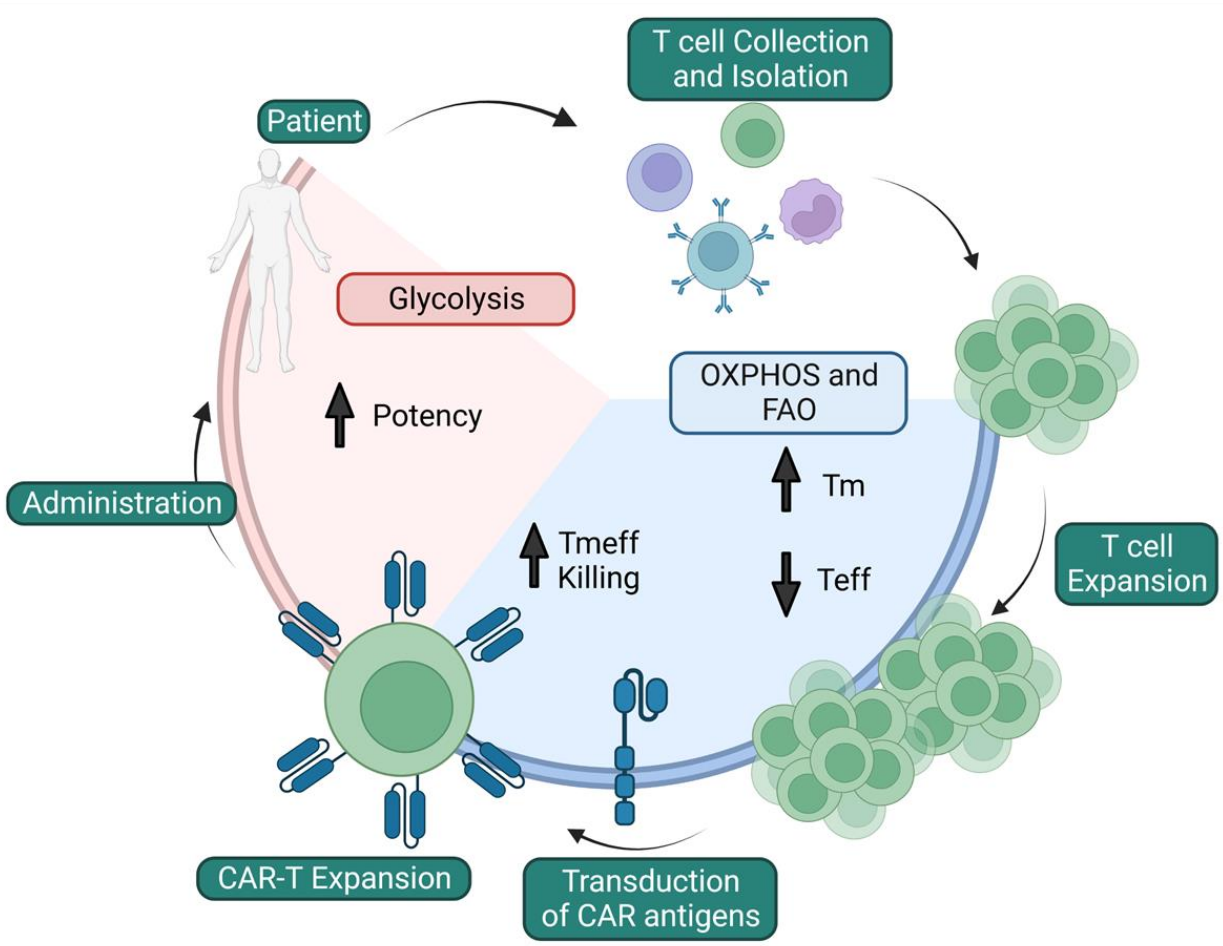

Figure 5.2. CAR-T Manufacturing. CAR-T energy metabolism during manufacturing for increased potency. Oxidative phosphorylation, OXPHOS. Fatty acid oxidation, FAO. Memory T-cell, Tm. Effector T-cell, Teff. Created with BioRender.com

CHAPTER 6

CONCLUSION AND FUTURE DIRECTIONS

6.1 CONCLUSION

The goal of this dissertation was to find robust markers that could be used as candidate critical quality attributes (CQAs) predictive of MSC immunomodulation. To account for the multiple mechanisms by which MSCs modulate the immune system, multiple predictive markers are needed to better predict potency. Determining what to measure both in-process and at the end of manufacturing can better ensure a potent MSC therapy. To achieve this, Chapter Two identified several intracellular markers that predicted MSC function for three cell lines over several passages. A composite functional score was also created to better encompass the multitude of mechanisms of MSC immunomodulation and to account for variability of different PBMC donors. Chapter Three built on Chapter Two by adding six more MSC lines and a repeat line for a more robust metabolite screening. Chapter Three also analyzed in-process metabolites that could be used to predict a composite functional score in early stages of expansion. More robust modeling was performed by comparing several models, and the important predictors identified from each model were cross validated to obtain a list of consensus metabolites. These consensus metabolites (both in-process and intracellular) were highly predictive of MSC function, and several pathways were highly correlated with these markers that were considered candidate CQAs. In the context of potency, the same three MSC lines investigated in Chapter Two and Three had similar results with a low, medium, and high potency donor. For predictive markers, phosphatidylcholines (PC) were found to be predictive markers, but no other lipids or

small polar molecules were found to be predictive in Chapter Two unlike Chapter Three. This could be due to two reasons; First, different mass spectrometry techniques were used when analyzing the data resulting in a larger data set in Chapter Three. Second, the data filtering strategy that was used in Chapter Two was different from Chapter Three. The top twenty-five linear regressed features, both known and unknown, were used in the model for Chapter Two while all the known features were used in the modeling for Chapter Three.

6.2 THE ROLES OF IDENTIFIED METABOLIC PATHWAYS IN MSC POTENCY

In Chapter Two and Three, we identified several lipids and metabolites that were predictive of MSC immunomodulation that we considered candidate CQAs. Further analysis of these lipids and metabolites found several significant pathways that could play a role in the potential potency of MSCs. One of the limitations of these studies is that these candidate CQAs and pathways were not investigated for their role in MSC immunomodulation, only correlated. The subsequent paragraphs discuss several significant pathways and their role in MSC potency.

Autophagy

In Chapter Three, we found that several phosphatidylethanolamines (PEs) and the amino acids, arginine and proline, were predictive of MSC immunomodulation. Intracellular levels of PEs have been shown to positively regulate autophagy in mammalian cells, and arginine and proline concentrations in MSCs are directly affected by autophagy.[1,2] Autophagy is an important factor in balancing energy sources by degrading damaged or unwanted proteins, organelles, and other cellular compounds.[3] By adding the precursor of PEs, ethanolamine, mammalian cells in culture will increase the amount of intranuclear PEs, increase autophagic flux, and improve cellular longevity.[1] Furthermore, both rapamycin and 3-methyladenine (3-MA) have been shown to positively and negatively regulate autophagy in MSCs.[2,4,5] MSCs treated with rapamycin had a

significant increase in arginine and proline levels while MSCs treated with 3-MA had a significant decrease in arginine and proline levels when compared to the control. Similarly, MSCs treated with either rapamycin or 3-MA had a significant increase and decrease in CD4+ T-cell proliferation, respectively.[4]

Sphingolipid Metabolism

Chapter Three also identified several sphingomyelins (SM) and ceramides (Cer) that were predictive of MSC immunomodulation. These two lipids are closely related to one another via the sphingolipid metabolic pathway. Cer is not only the precursor to SMs, but also several other molecules such as sphingosine and ceramide-1-phosphate (C1P), and it is a substrate in the production of sphingosine-1-phosphate (S1P).[6] Treatment of MSCs with C1P increased proliferation of adipose and bone marrow MSCs, and treatment with S1P increased osteogenic differentiation.[7] S1P plays a role in the proliferation, migration, and differentiation of MSCs, and inhibiting S1P receptor 2 with JTE013 significantly increases MSC proliferation, migration, and differentiation into osteoblasts and adipocytes.[8] Treatment of MSCs using young vs aged serum extracellular vesicles (EVs) showed higher Cer levels in the aged serum Evs which induced greater MSC senescence.[9] In terms of immunomodulation, increased levels of acyl chain ceramides in MSCs was associated with decreased indoleamine 2,3-dioxygenase (IDO) activity.[6]

Ammonia Recycling/Urea Cycle

The amino acids arginine and aspartate were found to be predictive of MSC function through media analysis in Chapter Three. It was found that both ammonia recycling and the urea cycle were significantly enriched pathways. When proteins and amino acids are broken down, ammonia is produced as a byproduct. Ammonia is then converted into urea through the urea cycle which includes arginine and aspartate as intermediates.[10,11] Ammonia build up can be

harmful to cells, but increased autophagy via rapamycin treatment leads to greater ureagenesis.[11] Alternatively, ammonia is involved in amino acid biosynthesis. Glutamine is the most common amino acid metabolized from ammonia which is synthesized by the glutamine synthetase with glutamate.[12] In MSCs, high levels of ammonia promoted the glutamine synthetase which led to higher proliferation. Blocking glutamine synthetase using methionine sulfoxomine led to lower proliferation rates.[13] Further investigation into how this affects MSC immunosuppression is needed to better determine if autophagy, ammonia recycling/urea cycle, or both are involved.

GPI Anchors and MSC Surface Markers

Currently, the surface markers used for identifying MSCs (e.g. CD73, CD90, and CD105) do not indicate MSC potency.[14] Therefore, identifying surface markers that relate potency could be used to screen for potent donors. In Chapter Three, phosphatidylinositol (PI) were predictive of MSC immunomodulation. PIs are a precursor for glycosylphosphatidylinositol (GPI) anchors.[15] These GPI anchors are critical components of several surface markers including CD157. CD157 has been shown to aid in immunomodulation, self-renewal, migration, and mitochondrial transfer in MSCs.[16–18] Another surface marker, CD146, has also been used as a marker for potentially identifying high and low potency MSCs. MSCs expressing high levels of CD146 were found to have higher secretory capacity based on total secreted molecules over time and greater production of anti-inflammatory proteins such as transforming growth factor beta (TGF-β) and IL-10 compared to MSCs expressing low levels of CD146. The high CD146-expressing MSCs also exhibited greater functional capacity (i.e. potency) in terms of M1 to M2 macrophage polarization in vivo.[19]

6.3 PROPOSED FUTURE STUDIES

Pathway Inhibition

Given the relationship between the pathways that were found significant and the predictive markers in Chapter Three, a study can be envisioned to experimentally investigate their relationship with MSC potency and the candidate CQAs identified. By culturing potent and less potent MSCs with different inhibitors, it can be determined which pathways (autophagy, ammonia recycling, urea cycle, sphingolipid metabolism) play a significant role in MSC function by running a T-cell suppression assay and analyzing the effects of each inhibitor compared to non-inhibited MSCs. Molecules that upregulate these pathways were also discussed, and adding these molecules could help improve the potency of MSCs. Using T-cell suppression as a potency measurement, it would be of interest to see if less potent MSCs could be "rescued" during expansion. It is important that targeted metabolomics on the media and intracellular metabolites are also performed based on the candidate CQAs found in Chapter Three. Monitoring the changes in the candidate CQAs will help further validate their importance for predicting potency. Lastly, surface marker characterization also has the potential for predicting and screening potent MSCs. Markers such as CD157 and CD146 have been discussed for their potential role in MSC immunomodulation, and screening for these markers could help determine potent and non-potent MSC lines. Heterogeneity within MSC lines could also be assessed by sorting MSCs based on these markers. Functional differences as well as metabolic differences could be measured using the positive and negative populations following cell sorting.

Scale Up Manufacturing for CQA Discovery

The pipeline that was developed in this thesis for identifying candidate CQAs can also be implemented in the scale up manufacturing of MSCs. In Chapters Two and Three, all the MSCs

were grown in flasks, but for therapeutic demand, scaling up manufacturing to bioreactors is necessary. Depending on the therapeutic application, the number of cells per dose could vary between tens of millions to billions.[20] Therefore, determining the effects on the candidate CQAs identified in this work when scaling up to a bioreactor is of great interest. In vivo, MSC metabolic energy demand is met through glycolysis, but this energy demand shifts to oxidative phosphorylation (OXPHOS) once placed in the nutrient rich cell culture environment. This metabolic shift is further accentuated when scaling up MSC expansion which leads to higher clonal heterogeneity, reduced stress resistance, and reduced immunomodulation.[21] Understanding how the candidate CQAs and MSC potency changes when scaling up manufacturing may give more insight into other metabolic changes that are occurring and could lead to strategies to prevent loss of potency. Besides cell yields, another advantage of bioreactors is the ability to incorporate in line monitoring systems.[22] In Chapter Three, sampling of media during expansion only occurred every 24hrs. Many metabolites significantly changed between day one and two, but then returned back to day one levels at day three. As mentioned in Chapter Five, incorporating in line monitoring tools such as benchtop NMR machines or MS microfluidics would allow for continuous monitoring of media metabolites to better understand the metabolic changes that occur during scaled up expansion.[23,24]

MSC Metabolic Response in PBMC Co-culture

The candidate CQAs identified in Chapters Two and Three were from MSCs being grown in basal media conditions, but the metabolic response to inflammatory signals was not measured. MSCs respond to stimuli by altering their transcriptome, metabolism, morphology, and secretory profile (Klinker 2017, Chinnadurai 2018, Liu 2019).[14,25,26] Additionally, MSCs treated with pro-inflammatory stimuli found significant changes in the lipid composition of phosphatidylcholine

(PC), phosphatidylserine (PS), PE, and SM.[27] All of these lipids were found to be predictors of MSC function in Chapter Three. Amino acids also play an important role in MSC inflammatory responses.[28] For example, arginine was identified in Chapter Three as a predictor of MSC function and plays an important role in the urea cycle. Arginine can also be oxidized into nitric oxide (NO) by the nitric oxide synthase.[28] Arginine is required for T-cell activation and proliferation, and one mechanism in which MSCs suppress T-cell proliferation is by depleting arginine through increased NOS activity.[29,30] By comparing potent MSCs and non-potent MSCs in a PBMC co-culture, differences in the inflammatory MSC metabolism could help shed further light on their mechanism of action by analyzing upregulated and downregulated pathways. These pathways could have a relationship with important pathways identified during expansion and inform manufacturers to promote or inhibit pathways to enhance/ensure potency. Furthermore, information could be learned about the PBMC donors as well. Chapters Two and Three had multiple PBMC donors that were used, and all of them had different responses to dynabead stimulation and MSC treatment. Measuring the PBMCs in this co-culture could also give better understanding into patient responses to MSC therapies. Currently, there are large groups of non-responders to MSC therapies in clinical trials. Understanding differences in donor PBMC metabolism during treatment may inform strategies for tuning MSCs for treating various diseases and lead to more potent MSC therapies.[31]

In-process CQAs for MSC EV Therapies

One mechanism in which MSCs modulate the immune system is through the secretion of EVs.[32] Chapter Four discussed the challenges in characterizing MSC EVs for therapeutics. Most of the characterization and identification is performed on EVs post isolation. Although extremely important for release criteria, this does not allow for any in-process manufacturing changes to

occur.[33] The cargo of EVs is highly dependent on the origin cell state and environment of the cells, and the culture system and growth environment (i.e. nutrients) also play a major role in this.[34] Priming MSCs with factors such as IFN-γ or low pH can also alter MSC EV cargo (i.e. proteins and miRNA) and enhance potency (i.e. T-cell suppression and T-reg formation).[35,36] The pipeline developed in Chapter Three could be used to help monitor and establish in-process CQAs during the process of deriving EVs. This would be advantageous since it requires minimal sample and won't disturb EV yields downstream. CQAs could be found that predict EV cargo and function, and allow manufacturers to better optimize EV growth conditions through cell expansion and priming conditions.

6.4 SUMMARY OF POTENTIAL EXPERIMENTS FOR FUTURE DIRECTIONS

Based on the information presented in this chapter, here are four recommend experiments (Figure 6.1) to build on the work done throughout this dissertation:

1. Pathway Interrogation: This study will investigate several pathways that were significantly related to the candidate CQAs in Chapter Three. Based on the information presented earlier in this chapter, the following pathways should be chosen to investigate: autophagy, sphingolipid metabolism, and ammonia recycling/urea cycle. In addition to these, MSC surface markers should be assessed of determining high potency MSCs. Using a cell line of high and low potency, these three pathways can be blocked and enhanced during culture based on the inhibitors and promotors mentioned in the metabolic pathways section of this chapter. In-process media and cells could be collected following expansion to analyze the effect on the consensus metabolites from Chapter Three when compared to the control MSCs (no treatment). MSC potency assays (T-cell suppression and IDO activity) could be performed to determine the effects on MSC potency. Lastly, quantifying the abundance of the surface markers, CD146 and

CD157, on the MSCs and sorting for positive and negative populations could determine their effect on MSC immunomodulation. These markers can be used to better screen for high potency donors, or sort for high potency MSCs within a given line before cell expansion.

2. Scale Up CQA Discovery: Scaling up MSC manufacturing is important for translating these therapies to the clinic. A comparison of the metabolites from several MSC lines of varying potency could be performed by expansion in both a flask and bioreactor. Media could be collected at various time points (depending on sampling capabilities i.e. a person or auto-sampling) during the expansion for metabolite analysis, and harvested cells analyzed for both potency and end of expansion metabolomics. Comparing the potency, in-process metabolites, and end of expansion metabolites of the flask and bioreactor MSC lines one could explore functional and metabolic differences. By identifying consensus markers from the flask group and the bioreactor group individually, a comparison of these consensus markers could indicate if the markers are manufacturing dependent or if there are important metabolites specifically for MSCs. Pathway analysis should also be performed to determine if there are overlapping pathways that are enriched in a given manufacturing environment. These pathways should then be interrogated to determine strategies for maintaining MSC potency while scaling up manufacturing.

3. MSC: PBMC Metabolism: A better understanding of how high and low potency MSCs respond to inflammation would help with identifying better CQAs based on their mechanism of action. Here, one could investigate the changes in the metabolites and lipids of MSCs when exposed to an inflammatory environment (stimulated T-cells) based on the T-cell suppression assay. First, scaling up to a larger well format (48, 24, 12, or 6 well) is important to ensure that there are enough cells and media for metabolite analysis. Next, optimization of the co-culture is

necessary to determine if the MSCs, PBMCs, and dynabeads are easily separated or if a trans well plate is needed. Next, I would choose cell lines of varying potency to use in the co-culture. Separating the MSCs and PBMCs following the PBMC assay would allow for a comparison of the metabolism of all groups (resting MSCs vs co-culture MSCs, high potency MSCs vs low potency MSCs, Stimulated vs unstimulated vs MSC treated PBMCs) using NMR and MS followed by pathway analysis. These pathways could further inform manufacturing decisions through enhancing or inhibiting MSC pathways, and give insight into patient responders vs non-responders based on their metabolic response to treatment.

4. CQA Discovery for MSC EVs: MSC EVs are also being investigated as an alternative therapy, and most of the quality attributes are measured downstream on the EVs specifically. Developing in-process CQAs for MSC EVs based on the consensus modeling pipeline could help inform manufacturing strategies. By manufacturing EVs from several cell lines of differing potencies (potency could be based on T-cell suppression, T-reg formation, or microglia activation) with different priming conditions (IFN-γ, low pH), the media metabolites could be analyzed to distinguish important CQAs. To achieve this, media could be collected at multiple time points during cell expansion and priming. Following EV isolation, potency assays as well as downstream EV characterization (size, yield, proteins, miRNAs) can be used as the outcomes in the consensus modeling pipeline. Pathway analysis should then be performed based on the CQAs to help develop strategies for improving potent EV manufacturing.

6.5 REFERENCES

1. Rockenfeller, P. et al. Phosphatidylethanolamine positively regulates autophagy and longevity. Cell Death & Differentiation 2015 22:3 22, 499–508 (2015).

2. Sun, Y. et al. Metabolic profiling associated with autophagy of human placenta-derived mesenchymal stem cells by chemical isotope labeling LC−MS. Exp Cell Res 372, 52–60 (2018).
3. Glick, D., Barth, S. & Macleod, K. F. Autophagy: cellular and molecular mechanisms. J Pathol 221, 3 (2010).
4. Gao, L. et al. Autophagy Improves the Immunosuppression of CD4+ T Cells by Mesenchymal Stem Cells Through Transforming Growth Factor-β1. Stem Cells Transl Med 5, 1496–1505 (2016).
5. Jakovljevic, J. et al. Modulation of autophagy as new approach in mesenchymal stem cell-based therapy. Biomedicine & Pharmacotherapy 104, 404–410 (2018).
6. DeVeaux, S. A. et al. Characterizing human mesenchymal stromal cells' immune-modulatory potency using targeted lipidomic profiling of sphingolipids. Cytotherapy 24, 608–618 (2022).
7. Marycz, K. et al. The effect of the bioactive sphingolipids S1P and C1P on multipotent stromal cells-new opportunities in regenerative medicine. Cell Mol Biol Lett 20, 510–533 (2015).
8. Price, S. T. et al. Sphingosine 1-Phosphate Receptor 2 Regulates the Migration, Proliferation, and Differentiation of Mesenchymal Stem Cells. Int J Stem Cell Res Ther 2, (2015).
9. Khayrullin, A. et al. Very Long-Chain C24:1 Ceramide Is Increased in Serum Extracellular Vesicles with Aging and Can Induce Senescence in Bone-Derived Mesenchymal Stem Cells. Cells 8, (2019).

10. Tapiero, H., Mathé, G., Couvreur, P. & Tew, K. D. I. Arginine. Biomedicine & Pharmacotherapy 56, 439–445 (2002).

11. Soria, L. R. et al. Enhancement of hepatic autophagy increases ureagenesis and protects against hyperammonemia. Proc Natl Acad Sci U S A 115, 391–396 (2018).

12. Eelen, G. et al. Role of glutamine synthetase in angiogenesis beyond glutamine synthesis. Nature 561, 63–69 (2018).

13. Liu, Y. et al. Ammonia promotes the proliferation of bone marrow-derived mesenchymal stem cells by regulating the Akt/mTOR/S6k pathway. Bone Research 2022 10:1 10, 1–14 (2022).

14. Klinker, M. W., Marklein, R. A., lo Surdo, J. L., Wei, C. H. & Bauer, S. R. Morphological features of IFN-γ-stimulated mesenchymal stromal cells predict overall immunosuppressive capacity. Proc Natl Acad Sci U S A 114, E2598–E2607 (2017).

15. Hooper, N. M. Glycosyl-phosphatidylinositol anchored membrane enzymes. Clinica Chimica Acta 266, 3–12 (1997).

16. Katoh, M. & Katoh, M. CD157 and CD200 at the crossroads of endothelial remodeling and immune regulation. Stem Cell Investig 6, (2019).

17. Li, J. et al. CD157 in bone marrow mesenchymal stem cells mediates mitochondrial production and transfer to improve neuronal apoptosis and functional recovery after spinal cord injury. Stem Cell Res Ther 12, 1–14 (2021).

18. Ortolan, E., Augeri, S., Fissolo, G., Musso, I. & Funaro, A. CD157: From immunoregulatory protein to potential therapeutic target. Immunol Lett 205, 59–64 (2019).

19. Bowles, A. C. et al. Signature quality attributes of CD146 + mesenchymal stem/stromal cells correlate with high therapeutic and secretory potency. Stem Cells 38, 1034–1049 (2020).

20. Olsen, T. R., Ng, K. S., Lock, L. T., Ahsan, T. & Rowley, J. A. Peak MSC-Are we there yet? Frontiers in Medicine vol. 5 Preprint at https://doi.org/10.3389/fmed.2018.00178 (2018).

21. Yuan, X., Logan, T. M. & Ma, T. Metabolism in human mesenchymal stromal cells: A missing link between HMSC biomanufacturing and therapy? Frontiers in Immunology vol. 10 977 Preprint at https://doi.org/10.3389/fimmu.2019.00977 (2019).

22. ROBB, K. P., FITZGERALD, J. C., BARRY, F. & VISWANATHAN, S. Mesenchymal stromal cell therapy: progress in manufacturing and assessments of potency. Cytotherapy 21, 289–306 (2019).

23. Grootveld, M. et al. Progress in low-field benchtop NMR spectroscopy in chemical and biochemical analysis. Anal Chim Acta 1067, 11–30 (2019).

24. Chilmonczyk, M. A., Kottke, P. A., Stevens, H. Y., Guldberg, R. E. & Fedorov, A. G. Dynamic mass spectrometry probe for electrospray ionization mass spectrometry monitoring of bioreactors for therapeutic cell manufacturing. Biotechnol Bioeng 116, 121–131 (2019).

25. Chinnadurai, R. et al. Potency Analysis of Mesenchymal Stromal Cells Using a Combinatorial Assay Matrix Approach. Cell Rep 22, 2504–2517 (2018).

26. Liu, Y., Yuan, X., Muñoz, N., Logan, T. M. & Ma, T. Commitment to Aerobic Glycolysis Sustains Immunosuppression of Human Mesenchymal Stem Cells. Stem Cells Transl Med 8, 93–106 (2019).

27. Campos, A. M. et al. Lipidomics of Mesenchymal Stromal Cells: Understanding the Adaptation of Phospholipid Profile in Response to Pro-Inflammatory Cytokines. J Cell Physiol 231, 1024–1032 (2016).

28. Li, H., Dai, H. & Li, J. Immunomodulatory properties of mesenchymal stromal/stem cells: The link with metabolism. J Adv Res (2022) doi:10.1016/J.JARE.2022.05.012.

29. Bronte, V. & Zanovello, P. Regulation of immune responses by L-arginine metabolism. Nat Rev Immunol 5, 641–654 (2005).

30. Chiu, M., Taurino, G., Bianchi, M. G. & Bussolati, O. The Role of Amino Acids in the Crosstalk Between Mesenchymal Stromal Cells and Neoplastic Cells in the Hematopoietic Niche. Front Cell Dev Biol 9, 1748 (2021).

31. Caplan, A. I. Cell-Based Therapies: The Nonresponder. Stem Cells Transl Med 7, 762 (2018).

32. Nagaishi, K. et al. Mesenchymal stem cell therapy ameliorates diabetic nephropathy via the paracrine effect of renal trophic factors including exosomes. Sci Rep 6, 1–16 (2016).

33. Théry, C. et al. Minimal information for studies of extracellular vesicles 2018 (MISEV2018): a position statement of the International Society for Extracellular Vesicles and update of the MISEV2014 guidelines. J Extracell Vesicles 7, (2018).

34. Wiest, E. F. & Zubair, A. C. Challenges of manufacturing mesenchymal stromal cell–derived extracellular vesicles in regenerative medicine. Cytotherapy vol. 22 606–612 Preprint at https://doi.org/10.1016/j.jcyt.2020.04.040 (2020).

35. Andrews, S., Maughon, T., Marklein, R. & Stice, S. Priming of MSCs with inflammation-relevant signals affects extracellular vesicle biogenesis, surface markers,

and modulation of T cell subsets. J Immunol Regen Med 100036 (2021) doi:10.1016/j.regen.2020.100036.

36. Cheng, A. et al. Human multipotent mesenchymal stromal cells cytokine priming promotes RAB27B-regulated secretion of small extracellular vesicles with immunomodulatory cargo. Stem Cell Res Ther 11, 1–14 (2020).

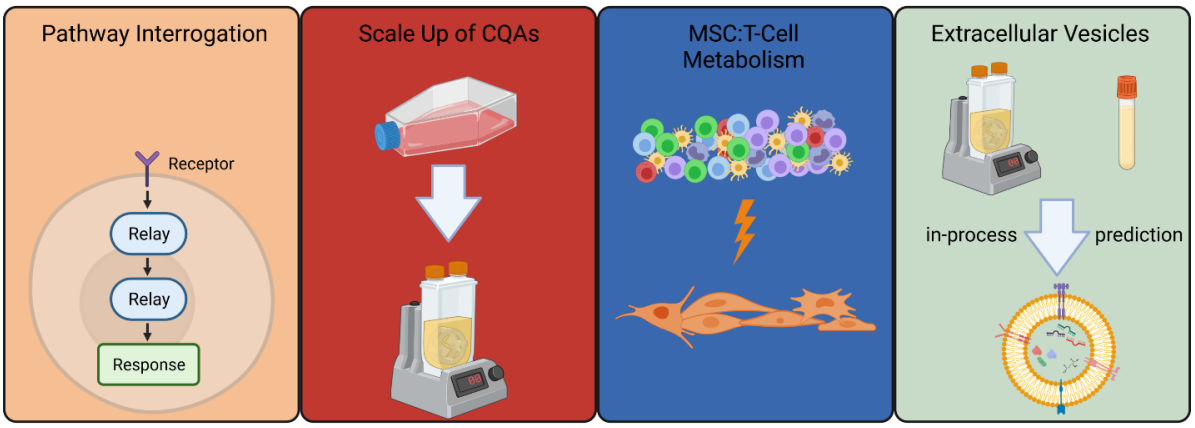

Figure 6.1. Proposed Future Directions.